

# **EFFECT OF SUPPORT CONDITIONS ON STEEL BEAMS EXPOSED OF FIRE**

**By  
Jenny Seputro**

**Supervisor  
Assoc. Professor Andrew H. Buchanan**

**Associate supervisor  
Assoc. Professor Peter J. Moss**

A research project report presented as partial fulfilment of the requirements for  
the degree of Master of Engineering in Fire Engineering

**Department of Civil Engineering  
University of Canterbury  
Christchurch, New Zealand**



## **Abstract**

The performance of steel structures at elevated temperature is determined by many factors. This report describes the analytical investigation of a single span steel beam using the non-linear finite element program, SAFIR. Four support conditions and additional axial spring were used to model structural elements with various level of axial and flexural restraint.

Different fires were applied and the effect of the applied load, number of fire-exposed sides and location of the line of support were analysed in terms of the midspan deflection, bending moment distribution and axial force in the axially restraint beams. It was found that beams with axial restraint, especially those with rotational restraint are very sensitive to the stress-strain relationship of the steel at elevated temperatures.

This research is intended to be a preliminary study leading to the detailed behaviour of complex steel frames such as those tested at Cardington. Some important aspects that could not be included in this project need further investigation in future research.



## **Acknowledgements**

First of all, I would like to gratefully thank a large number of people who have been supporting me in many ways throughout the completion of this project:

Assoc. Professor Andy Buchanan, my supervisor who has guided me in my research and provided endless helps all the way.

Assoc. Professor Peter Moss, my associate supervisor who has given me lots of ideas of what to look for and explanations of what was going on, as well as proof reading this report.

Linus Lim, who has great understanding of structural behaviour and SAFIR program in particular, for the guidance in using SAFIR program and in how to tackle the problems.

Richard Welsh, who has given me a lot of explanations on the structural behaviour.

Zisong Zhen, who has provided a lot of help with the figures in this report.

Dr. Charles Fleischmann and Mr. Michael Spearpoint, the other lecturers in Fire Engineering, and all my other classmates, for making this year such a great and wonderful time.

My parents and grandma, who has financially and spiritually supported me and make my study in Canterbury possible and enjoyable.

Other people, who in various ways have contributed in making this research and report possible.



# Contents

LIST OF FIGURES.....	i
LIST OF TABLES.....	iv
NOMENCLATURE .....	v
<b>1. INTRODUCTION .....</b>	<b>1</b>
1.1 GENERAL.....	1
1.2 ABOUT THE PROJECT .....	2
1.3 OBJECTIVES .....	2
1.4 SCOPE AND ORGANISATION .....	3
<b>2. LITERATURE SURVEY .....</b>	<b>4</b>
2.1 INTRODUCTION.....	4
2.2 THERMAL PROPERTIES OF STEEL.....	5
2.2.1 <i>Thermal elongation</i> .....	5
2.2.2 <i>Thermal conductivity</i> .....	6
2.2.3 <i>Specific heat</i> .....	7
2.3 MECHANICAL PROPERTIES OF STEEL.....	8
2.3.1 <i>Components of strain</i> .....	8
2.3.2 <i>Stress-strain relationship</i> .....	9
2.3.3 <i>Ultimate and yield strengths</i> .....	11
2.3.4 <i>Modulus of elasticity</i> .....	15
2.4 STRUCTURAL STEEL DESIGN .....	17
2.4.1 <i>Steel design at ambient condition</i> .....	17
2.4.2 <i>Steel design at elevated temperature</i> .....	18
2.4.3 <i>Design fires</i> .....	23
2.5 BEHAVIOUR OF REDUNDANT STRUCTURES IN FIRE.....	27
2.5.1 <i>Thermal expansion</i> .....	27
2.5.2 <i>Thermal buckling</i> .....	29
2.5.3 <i>Thermal bowing</i> .....	31
2.6 FIRE RESISTANCE.....	32
2.6.1 <i>Failure criteria</i> .....	33
2.6.2 <i>Fire resistance rating</i> .....	34

2.6.3 <i>Methods of protection</i> .....	36
2.7 FIRE TESTS .....	41
2.7.1 <i>General</i> .....	41
2.7.2 <i>Cardington fire test</i> .....	42
<b>3. SAFIR PROGRAM.....</b>	<b>45</b>
3.1 GENERAL .....	45
3.2 ANALYSIS PROCEDURE.....	46
3.2.1 <i>Thermal analysis</i> .....	47
3.2.2 <i>Structural analysis</i> .....	49
3.3 CAPABILITIES OF SAFIR.....	51
3.4 COMMON FEATURES IN ALL ANALYSES .....	52
3.5 SIGN CONVENTIONS .....	52
3.6 MATERIAL PROPERTIES .....	52
3.7 CONVERGENCE CRITERIA .....	53
<b>4. METHODS OF ANALYSIS.....</b>	<b>54</b>
4.1 THE STEEL BEAM.....	54
4.2 THERMAL ANALYSIS .....	56
4.2.1 <i>Discretisation</i> .....	56
4.2.2 <i>Applied fires</i> .....	58
4.3 STRUCTURAL ANALYSIS .....	61
4.3.1 <i>Discretisation</i> .....	61
4.3.2 <i>Loading</i> .....	61
4.3.3 <i>Supports</i> .....	62
4.3.4 <i>Introduction of springs</i> .....	64
4.4 SUMMARY .....	65
<b>5. ANALYSIS OF RESULTS FOR FOUR SUPPORT CONDITIONS .....</b>	<b>66</b>
5.1 DEFLECTION OF THE BEAMS .....	67
5.2 BEAM WITH PIN-ROLLER SUPPORTS .....	70
5.3 BEAM WITH PIN-PIN SUPPORTS .....	74
5.4 BEAM WITH FIX-FIX SUPPORTS .....	78
5.5 BEAM WITH FIX-SLIDE SUPPORTS .....	84
5.6 COMPARISON WITH CRITICAL BUCKLING.....	88
5.7 CONCLUSIONS.....	90
5.7.1 <i>Simply supported beams</i> .....	90

5.7.2 <i>Moment resisting supported beams</i> .....	91
<b>6. EFFECT OF A SPRING AT THE SUPPORT .....</b>	<b>92</b>
6.1 SPRING STIFFNESS BETWEEN 0 AND 1 .....	92
6.2 SPRING STIFFNESS BETWEEN 0 AND 0.1 .....	94
6.3 SPRING STIFFNESS BETWEEN 0.1 AND 0.2 .....	96
<b>7. COMPARISON BETWEEN DIFFERENT APPLIED FIRES .....</b>	<b>98</b>
7.1 LINEAR HEATING RATES .....	98
7.2 ISO FIRE.....	101
7.3 PARAMETRIC FIRE .....	105
7.4 THREE AND FOUR SIDED HEATING .....	109
<b>8. COMPARISON OF DIFFERENT APPLIED LOADS.....</b>	<b>113</b>
<b>9. COMPARISON OF VARIOUS LINE OF THRUST LOCATIONS .....</b>	<b>116</b>
<b>10. PROBLEMS.....</b>	<b>121</b>
<b>11. CONCLUSIONS AND RECOMMENDATIONS.....</b>	<b>122</b>
11.1 GENERAL BEHAVIOUR .....	122
11.2 EFFECT OF SPRING .....	123
11.3 EFFECT OF DIFFERENT APPLIED FIRES .....	123
11.4 EFFECT OF DIFFERENT APPLIED LOADS .....	124
11.5 EFFECT OF THE LINE OF THRUST LOCATION .....	124
<b>12. RECOMMENDATIONS FOR FUTURE RESEARCH.....</b>	<b>125</b>
<b>13. REFERENCES .....</b>	<b>126</b>
<b>APPENDIX .....</b>	<b>129</b>



## List of figures

Figure 2.1 Thermal elongation of steel as a function of temperature (EC3, 1995)	5
Figure 2.2 Thermal conductivity of steel as a function of temperature (EC3, 1995)	6
Figure 2.3 Specific heat of steel as a function of temperature (EC3, 1995)	7
Figure 2.4 Creep strain of steel tested in tension (Kirby and Preston, 1988)	9
Figure 2.5 Stress strain curve for typical hot-rolled steel at elevated temperature (Harmathy, 1993)	9
Figure 2.6 Stress strain relationship of grade 460 steel at elevated temperature (EC3, 1995)	10
Figure 2.7 Stress-strain relationship for steel at elevated temperature (EC3, 1995)	11
Figure 2.8 Scatter of yield strength and ultimate strength of hot-rolled steel (Harmathy, 1993)	13
Figure 2.9 Yield strength and proof strength of steel (Buchanan, 2000)	13
Figure 2.10 Reduction factors for stress-strain relationship of steel (EC3, 1995)	14
Figure 2.11 Modulus of elasticity for 1 structural, 2 prestressing and 3 reinforcing steel (Harmathy, 1993)	15
Figure 2.12 Relative value of the MOE compared with that of the yield strength (Buchanan, 2000)	16
Figure 2.13 Behaviour of beams with different support conditions (Buchanan, 2000)	20
Figure 2.14 Moment redistribution at elevated temperature (Buchanan, 2000)	21
Figure 2.15 Flexural enhancement by axial restraint (Buchanan, 2000)	22
Figure 2.16 Standard fire curves (Buchanan, 2000)	24
Figure 2.17 Eurocode reference decay rate (EC1, 1994)	25
Figure 2.18 Heat release rate for t-squared fire	26
Figure 2.19 Fixed ended beam subjected to thermal expansion and bowing (Rotter and Usmani, 2000)	31
Figure 2.20 Fire resistance furnace at New Zealand Building Research Association (Buchanan, 1994)	32
Figure 2.21 Protected and unprotected steel temperatures exposed to a parametric fire (Buchanan, 2000)	36
Figure 2.22 Light steel frame wall system (Buchanan, 2000)	37
Figure 2.23 Concrete encasement for steelwork protection (Buchanan, 2000)	39
Figure 2.24 Concrete filled hollow steel section (Buchanan, 2000)	39
Figure 2.25 Concrete filling between the flanges of I-section (Buchanan, 2000)	40
Figure 2.26 General view of the structural frame at the Cardington test (British Steel, 1999)	43
Figure 3.1 Steps and files of the analyses (Franssen et al, 2000)	46
Figure 3.2 Diamond 2000 output for the thermal analysis	48
Figure 3.3 Diamond 2000 output for the structural analysis	50
Figure 4.1 Floor plan of the Telecom Building in Auckland (Clifton, 1999)	54
Figure 4.2 Discretisation of the steel beam cross section	57
Figure 4.3 Linear heating rates	58
Figure 4.4 Standard ISO 834 fire	59
Figure 4.5 Realistic parametric fire	60

<i>Figure 4.6 Discretisation of the beam for the structural analysis</i>	61
<i>Figure 5.1 Midspan deflection of the beams throughout heating</i>	67
<i>Figure 5.2 Midspan deflection for all beams at early stage of the fire</i>	68
<i>Figure 5.2 Failure mechanism of pin-roller beam</i>	70
<i>Figure 5.3 Midspan deflection of pin-roller beam</i>	71
<i>Figure 5.4 Midspan moment of pin-roller beam</i>	72
<i>Figure 5.5 Top flange stresses of pin-roller beam</i>	72
<i>Figure 5.6 Bottom flange stresses of pin-roller beam</i>	72
<i>Figure 5.7 Moment distribution along the pin-roller beam</i>	73
<i>Figure 5.8 Failure mechanism of pin-pin beam</i>	74
<i>Figure 5.9 Midspan deflection of pin-pin beam</i>	76
<i>Figure 5.10 Midspan moment of pin-pin beam</i>	76
<i>Figure 5.11 Axial force of pin-pin beam</i>	76
<i>Figure 5.12 Top flange stresses of pin-pin beam</i>	77
<i>Figure 5.13 Bottom flange stresses of pin-pin beam</i>	77
<i>Figure 5.14 Moment distribution along the pin-pin beam</i>	77
<i>Figure 5.15 Failure mechanism of fix-fix beam</i>	78
<i>Figure 5.16 Midspan deflection of fix-fix beam</i>	81
<i>Figure 5.17 Midspan moment of fix-fix beam</i>	81
<i>Figure 5.18 End moment of fix-fix beam</i>	81
<i>Figure 5.19 Moment distribution along the fix-fix beam</i>	82
<i>Figure 5.20 Axial force of fix-fix beam</i>	82
<i>Figure 5.21 Top flange stresses of fix-fix beam</i>	82
<i>Figure 5.22 Bottom flange stresses of fix-fix beam</i>	83
<i>Figure 5.23 Failure mechanism of fix-slide beam</i>	84
<i>Figure 5.24 Midspan deflection of fix-slide beam</i>	85
<i>Figure 5.25 Midspan moment of fix-slide beam</i>	86
<i>Figure 5.26 End moment of fix-slide beam</i>	86
<i>Figure 5.27 Moment distribution along the fix-slide beam</i>	86
<i>Figure 5.28 Top flange stresses of fix-slide beam</i>	87
<i>Figure 5.29 Bottom flange stresses of fix-slide beam</i>	87
<i>Figure 5.30 Comparison between the axial load and the critical buckling load</i>	89
<i>Figure 6.1 Midspan deflection with spring stiffness between 0 and 1</i>	92
<i>Figure 6.2 Midspan moment with spring stiffness between 0 and 1</i>	93
<i>Figure 6.3 Axial force with spring stiffness between 0 and 1</i>	93
<i>Figure 6.4 Midspan deflection with spring stiffness between 0 and 0.1</i>	94

Figure 6.5 Midspan moment with spring stiffness between 0 and 0.1	94
Figure 6.6 Axial force with spring stiffness between 0 and 0.1	95
Figure 6.7 Midspan deflection with spring stiffness between 0.1 and 0.2	96
Figure 6.8 Midspan moment with spring stiffness between 0.1 and 0.2	96
Figure 6.9 Axial force with spring stiffness between 0.1 and 0.2	97
Figure 7.1 Midspan deflection of pin-pin beam with respect to temperature	99
Figure 7.2 Midspan deflection of pin-pin beam under various linear heating rates	99
Figure 7.3 Midspan moment of pin-pin beam under various linear heating rates	99
Figure 7.4 Axial force of pin-pin beam under various linear heating rates	100
Figure 7.6 Comparison of midspan deflection of pin-pin beam	102
Figure 7.7 Midspan deflection of pin-pin beam exposed to 10° C/minute heating and ISO fire	102
Figure 7.8 Midspan moment of pin-pin beam exposed to 10° C/minute heating and ISO fire	103
Figure 7.9 Axial force of pin-pin beam exposed to 10° C/minute heating and ISO fire	103
Figure 7.10 Top flange stresses of pin-pin beam exposed to ISO fire	104
Figure 7.11 Bottom flange stresses of pin-pin beam exposed to ISO fire	104
Figure 7.12 Midspan deflection of all beams subjected to a parametric fire	106
Figure 7.13 Midspan moment of all beams subjected to a parametric fire	106
Figure 7.14 Deflection of pin-pin beam subjected to ISO and Parametric fires	107
Figure 7.15 Midspan moment of pin-pin beam subjected to ISO and Parametric fires	107
Figure 7.16 Axial force of pin-pin beam subjected to ISO and Parametric fires	108
Figure 7.17 Midspan deflection of all beams exposed to ISO fire on 3 and 4 sides	109
Figure 7.18 Midspan moment of pin-pin beam heated on 3 and 4 sides	111
Figure 7.19 Midspan moment of fix-fix beam heated on 3 and 4 sides	111
Figure 7.20 Midspan moment of fix-slide beam heated on 3 and 4 sides	112
Figure 7.21 Axial force of pin-pin beams heated on 3 and 4 sides	112
Figure 7.22 Axial force of fix-fix beams heated on 3 and 4 sides	112
Figure 8.1 Midspan deflection of fix-fix beam under different loading	114
Figure 8.2 Midspan moment of fix-fix beam under different loading	114
Figure 8.3 Endspan moment of fix-fix beam under different loading	114
Figure 8.4 Axial load of fix-fix beam under different loading	115
Figure 9.1 Lines of thrust for several support conditions (Buchanan, 2000)	116
Figure 9.2 Midspan deflection of pin-pin beam with different lines of thrust	118
Figure 9.3 Midspan moment of pin-pin beam with different lines of thrust	118
Figure 9.4 Axial force of pin-pin beam with different lines of thrust	119
Figure 9.5 Top flange stresses of pin-pin beam supported ¼ down from mid height	119
Figure 9.6 Bottom flange stresses of pin-pin beam supported ¼ down from mid height	120

# List of tables

*Table 2.1 Reduction factors for stress-strain relationship of steel at elevated temperature (EC3, 1995)*\_\_\_\_\_14

*Table 4.1 The steel beam profiles for the analyses (BHP catalogue)*\_\_\_\_\_54

*Table 4.2 Summary of different analyses in the project* \_\_\_\_\_ 64

*Table 5.1 Time line of events in pin-roller beam* \_\_\_\_\_ 69

*Table 5.2 Time line of events in pin-pin beam* \_\_\_\_\_ 73

*Table 5.3 Time line of events in fix-fix beam* \_\_\_\_\_ 77

*Table 5.4 Time line of events in fix-slide beam* \_\_\_\_\_ 83

## Nomenclature

$A_g$	: gross area of cross section ( $\text{mm}^2$ )
$A_s$	: tensile stress area of section ( $\text{mm}^2$ )
$A_t$	: total area of compartment ( $\text{m}^2$ )
$A_v$	: area of opening ( $\text{m}^2$ )
$b_f$	: width of flange (mm)
$c_s$	: specific heat of steel (J/kg.K)
$d$	: depth of section (mm)
$d_1$	: depth between flanges (mm)
$E$	: tangent modulus of steel (MPa)
$E_T$	: total energy content of fuel (MJ)
$e_t$	: fuel load per total surface area ( $\text{MJ}/\text{m}^2$ )
$F$	: yield force (N)
$F_{\text{ref}}$	: reference value of opening factor ( $\sqrt{m}$ )
$F_v$	: opening factor ( $\sqrt{m}$ )
$f_y$	: yield stress (MPa)
$G$	: nominal dead load (kN/m)
$H_v$	: height of opening (m)
$I$	: second moment of area of a cross section ( $\text{mm}^4$ )
$I$	: thermal inertia, $k\rho c_s$ ( $\text{W}^2\text{s}/\text{m}^4\text{K}^2$ )
$I_{\text{ref}}$	: reference value of $\sqrt{k\rho c_s}$ ( $\text{Ws}^{0.5}/\text{m}^2\text{K}$ )
$k$	: growth constant for t-squared fire ( $\text{s}\sqrt{MW}$ )
$k$	: relative stiffness of the spring to that of the beam
$K$	: stiffness of member (N/m)
$l$	: effective length of member (m)
$L$	: span or member length (m)
$M^*$	: design bending moment (kN.m)
$M_n$	: maximum calculated elastic moment capacity (kN.m)

$M_p$  : maximum calculated plastic moment capacity (kN.m)  
 $P$  : axial force (kN)  
 $P_{cr}$  : critical buckling load (kN)  
 $Q$  : nominal live load (kN/m)  
 $r$  : radius of gyration (mm)  
 $r_1$  : root radius (mm)  
 $S$  : plastic section modulus (mm<sup>3</sup>)  
 $T_s$  : temperature of steel (°C)  
 $t_f$  : thickness of flange (mm)  
 $t_w$  : thickness of web (mm)  
 $W$  : self weight (kN/m)  
 $w$  : uniformly distributed design load (kN/m)  
 $Z$  : elastic section modulus of steel (mm<sup>3</sup>)  
 $\alpha$  : thermal expansion coefficient (°C<sup>-1</sup>)  
 $\Delta$  : deflection (mm)  
 $\varepsilon$  : strain  
 $\lambda_s$  : thermal conductivity of steel (W/mK)  
 $\nu_s$  : steel Poisson's ratio  
 $\rho_s$  : density of steel (kg/m<sup>3</sup>)  
 $\sigma_y$  : yield strength of steel (MPa)

# 1. Introduction

## 1.1 General

Structural steel has been widely used throughout the world. It is one of a designer's best options in view of its advantages over other materials. Steel is available in a range of discrete size, and its ductile behaviour allows plastic deformation upon yielding, therefore avoiding brittle failures. In reinforced concrete structures, steel enhances the concrete strength by carrying the tensile forces. It is also commonly used to reinforce timber constructions.

In spite of its advantages, steel on its own is vulnerable in fire. Elevated temperatures in the steel cause reduction in its strength and stiffness which eventually leads to failure due to excessive deformations. This is crucial in steel in compared with concrete or timber members as steel conducts heat very well and often comes in thin or slender elements.

In structural design, there are a few functional requirements such as those stated in Clause C4 of the New Zealand Approved Document (BIA, 1992):

*“Buildings shall be constructed to maintain structural stability during fire to:*

- a. Allow people adequate time to evacuate safely,*
- b. Allow fire service personnel adequate time to undertake rescue and fire fighting operations, and*
- c. Avoid collapse and consequential damage to adjacent household units or other property.”*

There are a lot of different methods for protecting structural steel to maintain its strength and stability in fire, but little is known about the true behaviour of the steel members under various support conditions and heating patterns. The recommended fire resistance to be applied to the steel structures is usually determined based on furnace tests on single elements such as a beam or a column.

Contrary to popular belief, an unprotected steel element that is a part of a large complex structure may have a sufficiently high level of fire resistance to perform well in fire. This is

due to the ability of the overall structure to redistribute loads from the heated area to the cooler neighbouring elements. The lack of understanding of the true behaviour of steel elements in fire leads to inefficient and uneconomical design. To assess the overall performance of steel frames, it is important to understand the detailed behaviour of a single beam with several support conditions that represent various elements in a complex structure.

## **1.2 About the project**

The new finite element program, SAFIR, has been made available as a powerful engineering tool to model the behaviour of structures in fires. Using the SAFIR program, it is possible to investigate the behaviour of steel beams with different support types.

The I-section beam used for this research was a BHP universal beam 610UB101 with yield strength of 430 MPa and elastic modulus of 210 GPa. This is a fairly high strength steel and the analysis results may not apply directly to structural beams which have lower strength and are supported somewhat in between the ones investigated in this project. However, the main purpose of this project is to understand the responses from different end conditions that will lead into appropriate design to avoid catastrophic failures of structures during fire exposure.

## **1.3 Objectives**

The primary objectives of this research are:

- ♣ To analyse and explain the detailed behaviour of steel beams at elevated temperatures under different support conditions and heating rates.
- ♣ To provide preliminary study as a basis for future research on complex structural steel frames.

## **1.4 Scope and organisation**

This report concentrates on structural steel beams, and those aspects of behaviour relevant to design and fire protection. Several chapters investigate the behaviour of steel beams under elevated temperature when restrained by different end conditions.

Chapter 2 summarises the relevant material from the available literature. Information on the SAFIR program used, including its capabilities, common features and assumptions in the analyses as well as the input and output files are laid out in chapter 3. Chapter 4 describes the methods of analysis in this project. This includes the input data for SAFIR analyses such as the beam parameters, applied fires, and various end restraints.

The base case results from SAFIR involving 4 support conditions are discussed in detail in chapter 5. Variation from the base case including the introduction of springs at the ends of the beams, different fires, loading, and locations of line of thrust, are discussed separately in chapters 6-9 respectively.

Some of the problems encountered during the research project due to limitations of the SAFIR program and other causes are summarised in chapter 10. Conclusions from the project are outlined in chapter 11, while chapter 12 discusses recommendations that could be useful for future research.

## **2. Literature survey**

### **2.1 Introduction**

This chapter summarises the theoretical background for this research available in the literature. The materials include the steel properties and the impact of fire that causes deterioration of the steel properties. The information on the thermal and mechanical properties of steel are extracted from the Eurocode3 (EC3, 1995).

Structures in general are designed to carry loads and survive the environmental conditions at ambient temperatures. The fire protection will then be applied according to the functional requirements of the buildings. There are several ways to protect structural steel elements with a wide range of costs, which are introduced in section 2.6.3. Most of the materials in the structural design and the fire resistance sections are summarised from the discussion by Buchanan (2000).

Steel elements that are part of a more complex structure showed much better performance in real fires. This is due to the redundancy of the structure allowing redistribution of the load to stronger parts that are not much exposed to the heat. Section 2.5 outlines the behaviour of redundant structures in fire that was presented by Rotter et al. (1999) and the fire tests, including the Cardington test, are introduced in section 2.7 in accordance with the publication by the British Steel (1999).

The general features on the SAFIR program used in this research are laid out in chapter 3, describing the analysis procedure, the program capabilities and the common assumptions in the analyses.

## 2.2 Thermal properties of steel

### 2.2.1 Thermal elongation

The thermal elongation of steel is determined by the Eurocode 3 formulae as a function of the steel temperature and illustrated in Figure 2.1.

For  $20^{\circ}\text{C} \leq T_s < 750^{\circ}\text{C}$

$$\Delta l/l = 1.2 \times 10^{-5} T_s + 0.4 \times 10^{-8} T_s^2 - 2.416 \times 10^{-4} \quad [2.1]$$

For  $750^{\circ}\text{C} \leq T_s < 860^{\circ}\text{C}$

$$\Delta l/l = 1.1 \times 10^{-2} \quad [2.2]$$

For  $860^{\circ}\text{C} \leq T_s < 1200^{\circ}\text{C}$

$$\Delta l/l = 2 \times 10^{-5} T_s - 6.2 \times 10^{-3} \quad [2.3]$$

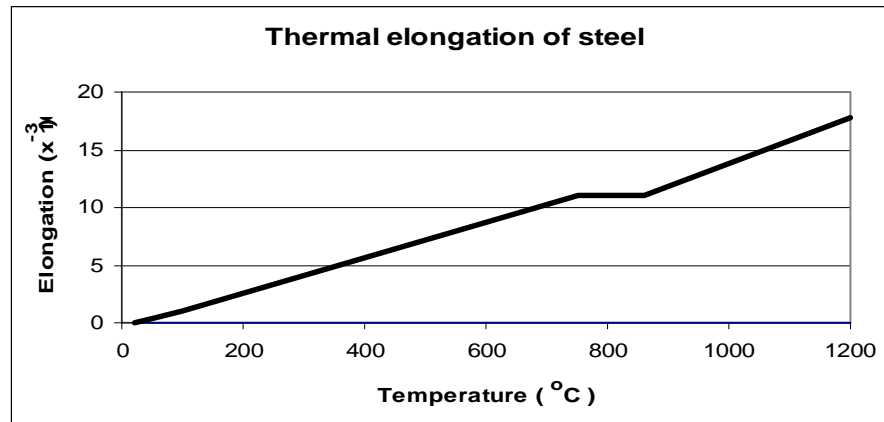


Figure 2.1 Thermal elongation of steel as a function of temperature (EC3, 1995)

In simple calculation models, assuming the thermal elongation to have constant relationship with the temperature of the steel, the elongation can be taken as:

$$\Delta l/l = 14 \times 10^{-6} (T_s - 20) \quad [2.4]$$

## 2.2.2 Thermal conductivity

The variation of the thermal conductivity of steel can also be determined from the following Eurocode formulae and is illustrated below:

For  $20^{\circ}\text{C} \leq T_s < 800^{\circ}\text{C}$

$$\lambda_s = 54 - 3.33 \times 10^{-2} T_s \quad [2.5]$$

For  $800^{\circ}\text{C} \leq T_s < 1200^{\circ}\text{C}$

$$\lambda_s = 27.3 \quad [2.6]$$

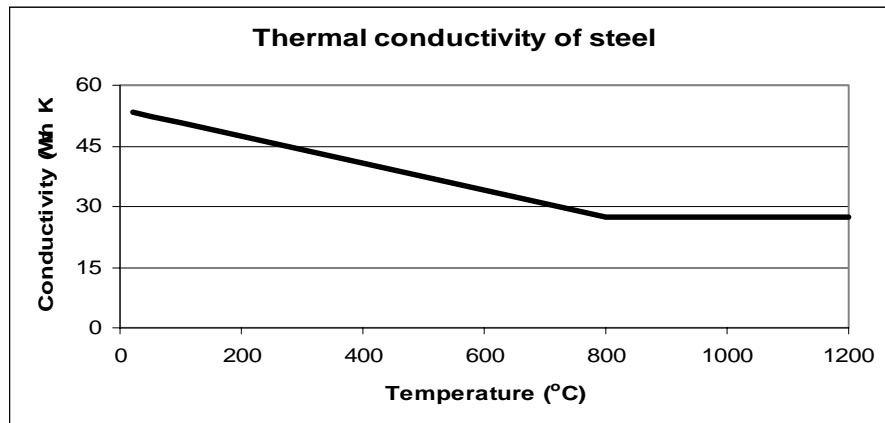


Figure 2.2 Thermal conductivity of steel as a function of temperature (EC3, 1995)

Thermal conductivity of steel with temperature greater than  $1200^{\circ}\text{C}$  is not defined in the Eurocode 3 as most structural steel members can hardly survive such heat. The value of 27.3 W/mK is taken for  $T > 1200^{\circ}\text{C}$  if such case needs to be considered as dealt with in the SAFIR thermal analysis.

For simple calculation models that are independent of the temperature, the value of 45 W/mK can be adopted.

### 2.2.3 Specific heat

The specific heat of steel is defined and illustrated as follows:

For  $20^{\circ}\text{C} \leq T_s < 600^{\circ}\text{C}$

$$c_s = 425 + 7.73 \times 10^{-1} T_s - 1.69 \times 10^{-3} T_s^2 + 2.22 \times 10^{-6} T_s^3 \quad [2.7]$$

For  $600^{\circ}\text{C} \leq T_s < 735^{\circ}\text{C}$

$$c_s = 666 + \frac{13002}{738 - T_s} \quad [2.8]$$

For  $735^{\circ}\text{C} \leq T_s < 900^{\circ}\text{C}$

$$c_s = 545 + \frac{17820}{T_s - 731} \quad [2.9]$$

For  $900^{\circ}\text{C} \leq T_s < 1200^{\circ}\text{C}$

$$c_s = 650 \quad [2.10]$$

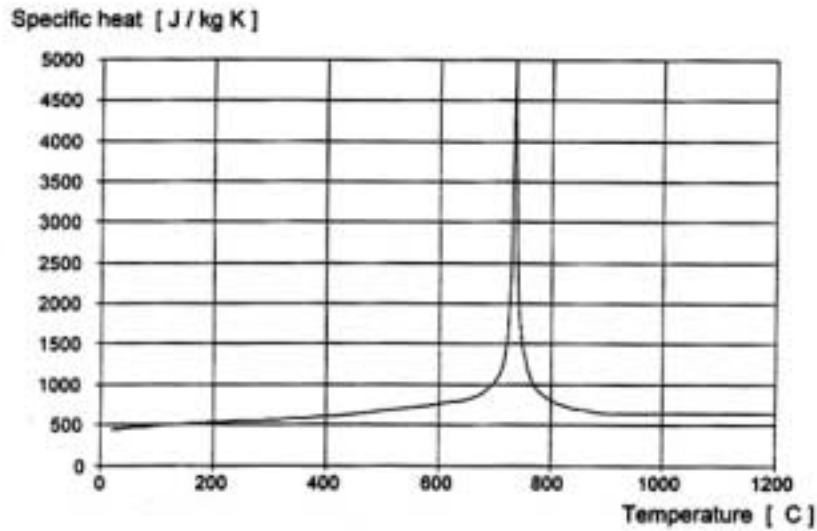


Figure 2.3 Specific heat of steel as a function of temperature (EC3, 1995)

Simple calculation models take the specific heat of steel as 600 J/kgK, independent of the temperature of the steel. For temperature greater than 1200°C, the specific heat is taken as 650 J/kgK.

## 2.3 Mechanical properties of steel

### 2.3.1 Components of strain

Strain is the measure of elongation of an element with respect to its original length. The change in strain with temperature is defined as:

$$\Delta\varepsilon = \varepsilon_{th}(T) + \varepsilon_{\sigma}(\sigma, T) + \varepsilon_{cr}(\sigma, T, t) \quad [2.11]$$

where  $\Delta\varepsilon$  is the change in strain;

$\varepsilon_{th}$  is the thermal strain;

$\varepsilon_{\sigma}$  is the stress-related strain;

$\varepsilon_{cr}$  is the creep strain.

The thermal strain is the elongation of the material due to heat, and is commonly referred to as thermal expansion as described by Rotter (1999) and is summarised in section 2.5.1. It is a very important aspect especially in larger structures with the elements restrained by the adjacent members.

The stress-related strain is obtained from steady state tests at certain temperatures or derived from transient test results. More of the stress-strain relationship is discussed in the next section.

Creep strain is not a problem at ambient condition but becomes very crucial at temperatures above 400°C. Kirby and Preston (1988) gives the creep strain of steel with different strength subjected to 10°C/minute heating rate tested in tension as shown in Figure 2.4.

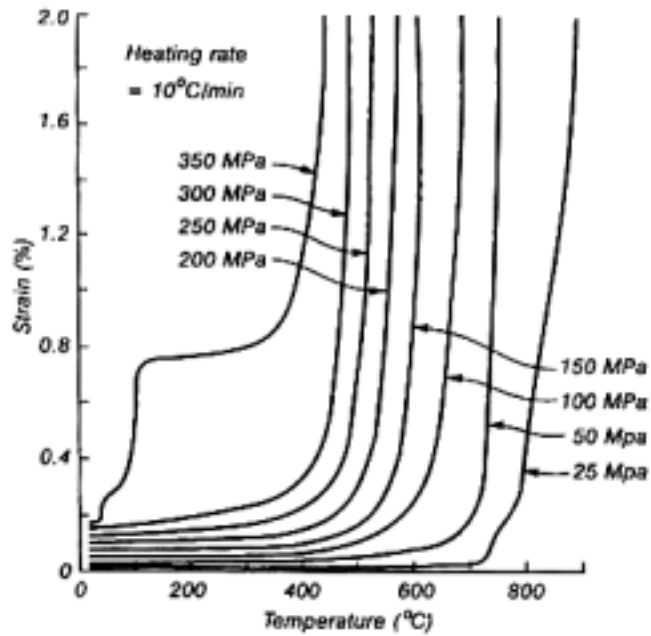


Figure 2.4 Creep strain of steel tested in tension (Kirby and Preston, 1988)

### 2.3.2 Stress-strain relationship

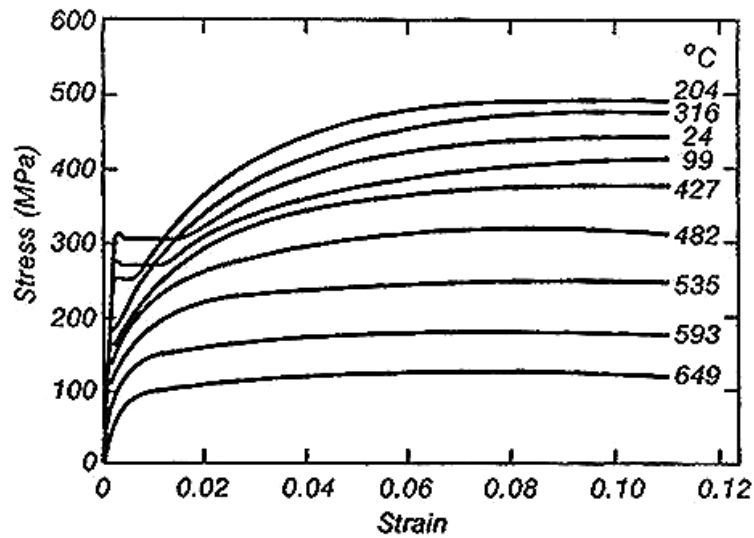


Figure 2.5 Stress strain curve for typical hot-rolled steel at elevated temperature (Harmathy, 1993)

The typical stress-strain curve for common hot-rolled steel at high temperature is given by Harmathy (1993) and shown in Figure 2.5. It shows that the yield strength plateau becomes less obvious with the rise of temperature and eventually disappears. The yield stress increases at the start of heating and gradually decreases with temperature.

The Eurocode 3 suggests similar charts for the stress strain relationship with temperature for various steel grades as adopted by the SAFIR program. Figure 2.6 shows a stress-strain chart for grade 460 steel, not including strain hardening.

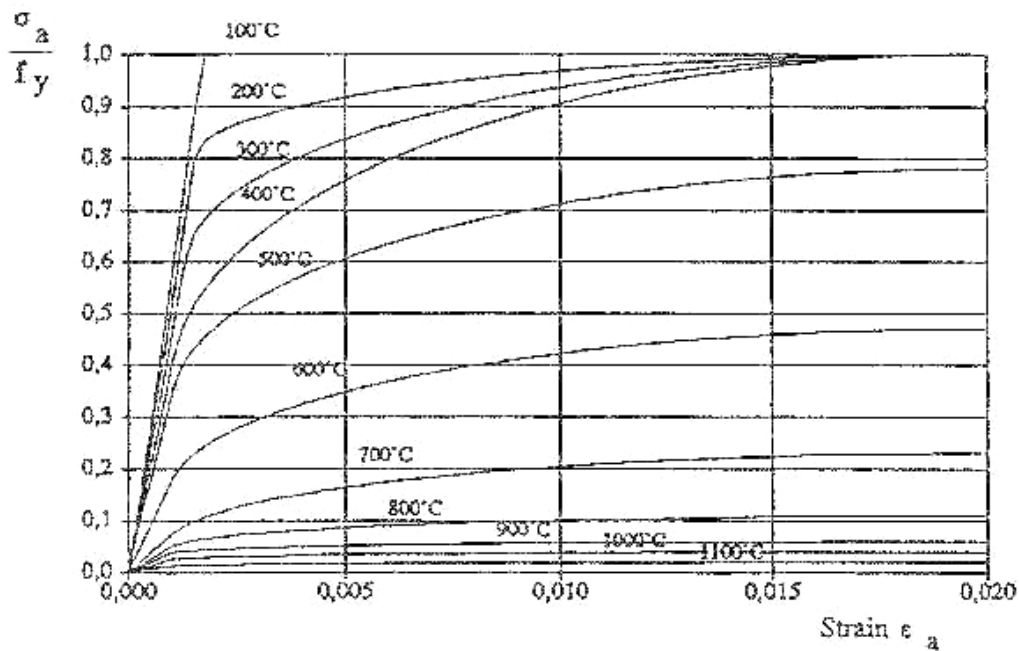


Figure 2.6 Stress strain relationship of grade 460 steel at elevated temperature (EC3, 1995)

### 2.3.3 Ultimate and yield strengths

The generalised stress-strain relationship is described in the Eurocode 3 and is shown in Figure 2.7. It is used to obtain the strength and deformation properties of steel to determine the resistance to tension, compression, moment or shear. This holds for heating rates between 2-50°C/min.

An alternative approach for temperatures below 400°C is to extend the stress-strain relationship by strain hardening provided that the restraints are adequate to prevent buckling.

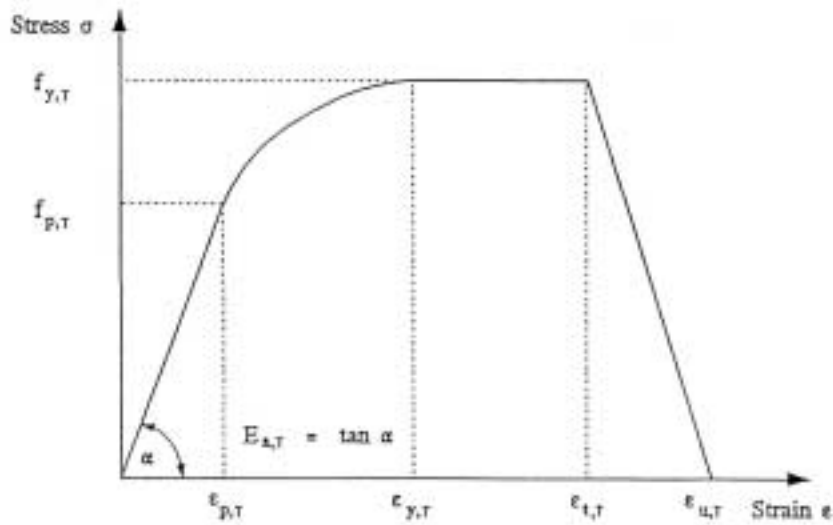


Figure 2.7 Stress-strain relationship for steel at elevated temperature (EC3, 1995)

where  $f_{p,T}$  is the proportional limit;

$f_{y,T}$  is the effective yield strength;

$E_{a,T}$  is the slope of the linear elastic range;

$\epsilon_{p,T}$  is the strain at the proportional limit;

$\epsilon_{y,T}$  is the yield strain;

$\epsilon_{t,T}$  is the limiting strain for yield strength;

$\epsilon_{u,T}$  is the ultimate strain.

The Eurocode 3 assumes that at ambient temperature, the stress-strain relationship is bilinear and the proportional limit  $f_p$ , which is the end point of the linear-elastic portion of the stress-strain curve, is equal to the yield strength,  $f_y$ . It also assumes no strain hardening. The first yield moment  $M_y$  can be obtained from:

$$M_y = f_p Z \quad [2.12]$$

where  $Z$  is the elastic section modulus.

At elevated temperature, the stress-strain relationship becomes linear elliptical. The initial elastic portion is linear up to the proportional limit and becomes non-linear in the trend of an ellipse up to the yield strength,  $f_y$ . Thereafter it becomes a plateau. The plastic moment  $M_p$  can be obtained from:

$$M_p = f_y S \quad [2.13]$$

where  $S$  is the plastic section modulus.

As shown by Harmathy (1993) in Figure 2.5 the decreased yield strength at elevated temperature is not clearly defined. Various researches suggest different values and the scatter in published results is shown in Figure 2.8. The dotted straight lines are the recommended design values by the Institution of Structural Engineers (ISE, 1978).

The use of the 1% proof strength is recommended by Kirby and Preston (1988) as the effective yield strength as defined and illustrated by Buchanan (2000) in Figure 2.9. It was chosen based on Figure 2.4 that shows a runaway situation once the strain exceeds 1%. However, the level of proof strain and the steel temperature are adjustable for particular conditions and requirements.

The reduction factors relative to the appropriate value at ambient condition for the stress-strain relationship of steel are defined by the Eurocode 3 as functions of temperature and are tabulated in Table 2.1 and illustrated in Figure 2.10. Linear interpolation is acceptable for intermediate steel temperatures.

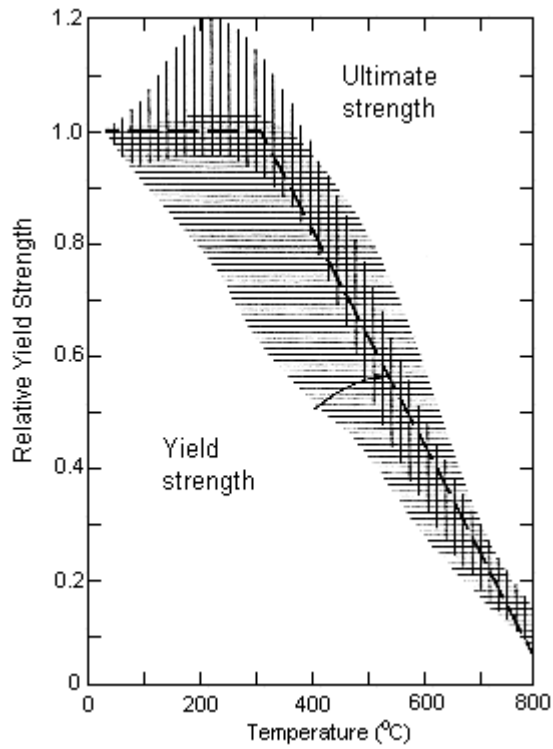


Figure 2.8 Scatter of yield strength and ultimate strength of hot-rolled steel (Harmathy, 1993)

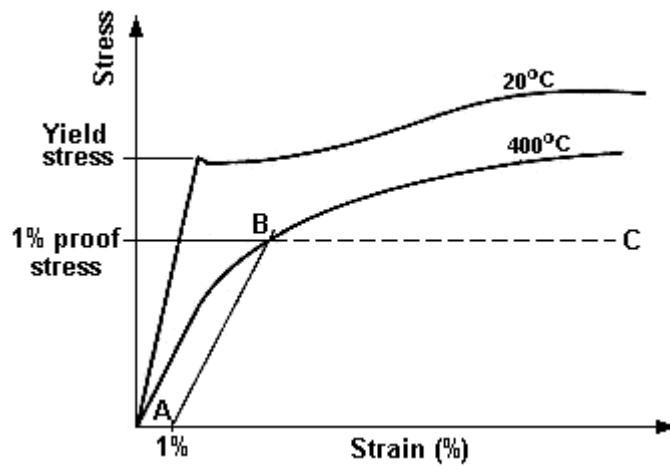
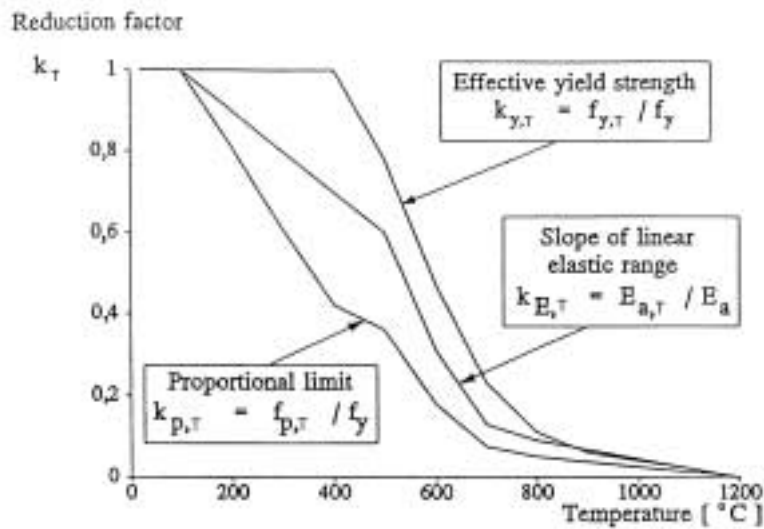


Figure 2.9 Yield strength and proof strength of steel (Buchanan, 2000)

**Table 2.1 Reduction factors for stress-strain relationship of steel at elevated temperature (EC3, 1995)**

Steel temperature $T_s$	Reduction factors at temperature T relative to the value of $f_y$ or $E_s$ at 20°C		
	Reduction factor (relative to $f_y$ ) for effective yield strength	Reduction factor (relative to $f_y$ ) for proportional limit	Reduction factor (relative to $E_a$ ) for the slope of the linear elastic range
	$k_{y,T} = f_{y,T} / f_y$	$k_{p,T} = f_{p,T} / f_y$	$k_{E,T} = E_{s,T} / E_s$
20°C	1.000	1.000	1.000
100°C	1.000	1.000	1.000
200°C	1.000	0.807	0.900
300°C	1.000	0.613	0.800
400°C	1.000	0.420	0.700
500°C	0.780	0.360	0.600
600°C	0.470	0.180	0.310
700°C	0.230	0.075	0.130
800°C	0.110	0.050	0.090
900°C	0.060	0.0375	0.0675
1000°C	0.040	0.0250	0.0450
1100°C	0.020	0.0125	0.0225
1200°C	0.000	0.0000	0.0000



**Figure 2.10 Reduction factors for stress-strain relationship of steel (EC3, 1995)**

### 2.3.4 Modulus of elasticity

As the temperature increases, the modulus of elasticity of the steel decreases as shown below for different types of construction. The curves labelled 1, 2 and 3 are for structural steel, prestressing steel and reinforcing steel respectively as summarised by Harmathy (1993). It can be seen that with an increase in temperature, structural steel tends to maintain its elasticity more than reinforcing or prestressing steel by a considerable amount, especially at higher temperatures.

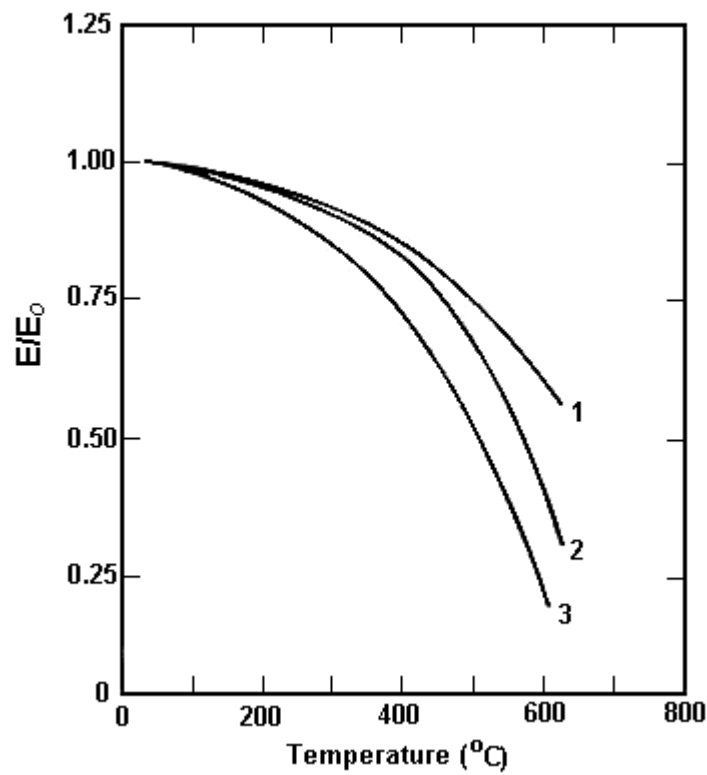
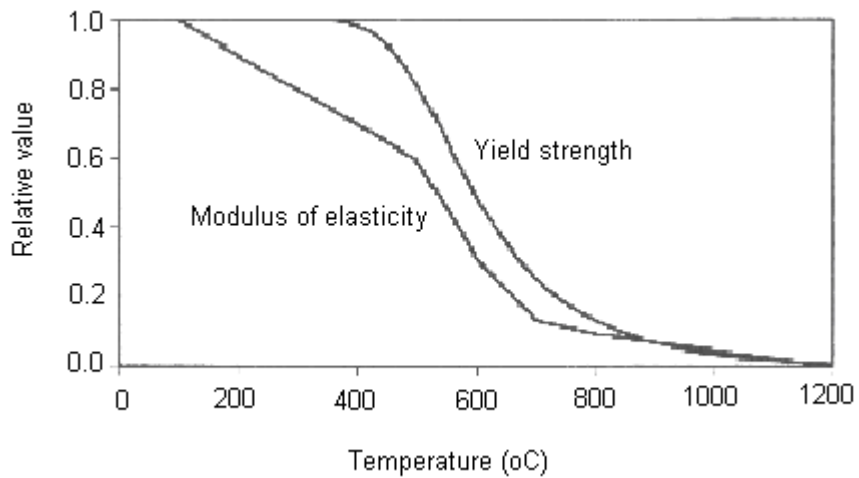


Figure 2.11 Modulus of elasticity for 1 structural, 2 prestressing and 3 reinforcing steel (Harmathy, 1993)

The reduction in the modulus of elasticity is crucial in buckling calculations. The Australian Code AS 4100 and the New Zealand Standard NZS 3404 give the equation for the ratio of the modulus of elasticity at elevated temperature to that at ambient condition as follows:

$$\begin{aligned}
 K_{E,T} &= 1.0 + T / [2000 \ln (T/1100)] \quad \text{for } 0 < T < 600^{\circ}\text{C} \\
 &= 690 (1-T/1000) / (T-53.5) \quad \text{for } 600^{\circ}\text{C} < T < 1000^{\circ}\text{C}
 \end{aligned}
 \tag{2.14}$$

Figure 2.12 illustrates the ratio of the modulus of elasticity at temperatures up to 1200°C compared with the ratio for the reduction in the yield strength.



**Figure 2.12 Relative value of the MOE compared with that of the yield strength (Buchanan, 2000)**

## 2.4 Structural steel design

### 2.4.1 Steel design at ambient condition

This section is to briefly review structural design in the cold conditions where thermal effects are not taken into consideration. Design at normal temperature ensures that the structure is able to resist the applied loading by nominating certain sizes for the members that have sufficient strength and stiffness. The loads applied depend on the functional requirements and the geographical location of the building.

The functional requirements determine the dead loads, which are always present such as the self weight of the structures and permanent fixtures, and the live loads which may vary from time to time such as the weight of people and non-permanent goods. Depending on the location of the building, snow load, wind load and seismic load may need to be considered.

Buchanan (2000) describes some design formats that are commonly used in construction. The traditional *working stress* or *allowable stress* design compares the permissible safe stresses under long term condition with the expected loading in service. Modern design considers the *ultimate strength*, which is comparing the most likely *characteristic load* with the *characteristic strength*, which is the strength of the weakest likely material under short term condition. This design is also known as the limit state design. It considers the serviceability limit state which is associated with the structure being usable for service, and the ultimate limit state which is only concerned about the collapse of the building.

In the ultimate strength design, a strength reduction factor  $\Phi$  is used for the design capacity as a safety factor. Steel is observed to have the same tension and compression properties and behaves elastically up to a certain yield point and in a very ductile manner thereafter. Gorenc et al. (1996) provides a complete steel design at ambient temperatures for different members exposed to bending, tension or compression stresses as well as the connection design.

### 2.4.2 Steel design at elevated temperature

There are a few modifications to be considered when designing structures for fire conditions although the concepts are similar to those for the ambient condition. Most of the material properties change with temperature, the strength is reduced upon heating and thermal expansion may induce internal forces that lead to structural failure with various mechanisms depending on the type of supports, connections and structural arrangements.

Instability failure also needs to be considered even though the structure still has adequate strength. The applied loads for fire design are less due to very low probability of the event occurring when the structure is fully loaded at its maximum capacity, therefore a smaller safety factor is acceptable.

The actual load at a given time as a proportion of the load that would cause collapse of the structure is often referred to as the *load ratio*. Most constructions have a load ratio of 0.5 or less. Smaller load ratio means greater fire resistance as the reduction of strength of any member will not necessarily cause collapse of the structure.

#### **Failure mechanisms**

The failure of a beam is reached when its strength is exceeded at one or more particular points termed *plastic hinges*, depending on the way it is supported. Figure 2.13 is the illustration by Buchanan (2000), showing the bending moment, deflected shape and the failure mechanism for different end conditions.

The development of plastic hinges shows ductile behaviour as energy is dissipated at these points. It allows the growth of deflection without sudden collapse of the structure. A simply supported beam fails when one plastic hinge is formed at midspan, while a continuous beam with moment resisting connections fails when three plastic hinges are developed, one at midspan and one at each support.

An end span beam can be thought of as a beam with continuous support at one end and simply supported at the other end, in which case two plastic hinges are required to form a failure mechanism, one at the continuous end and one at midspan.

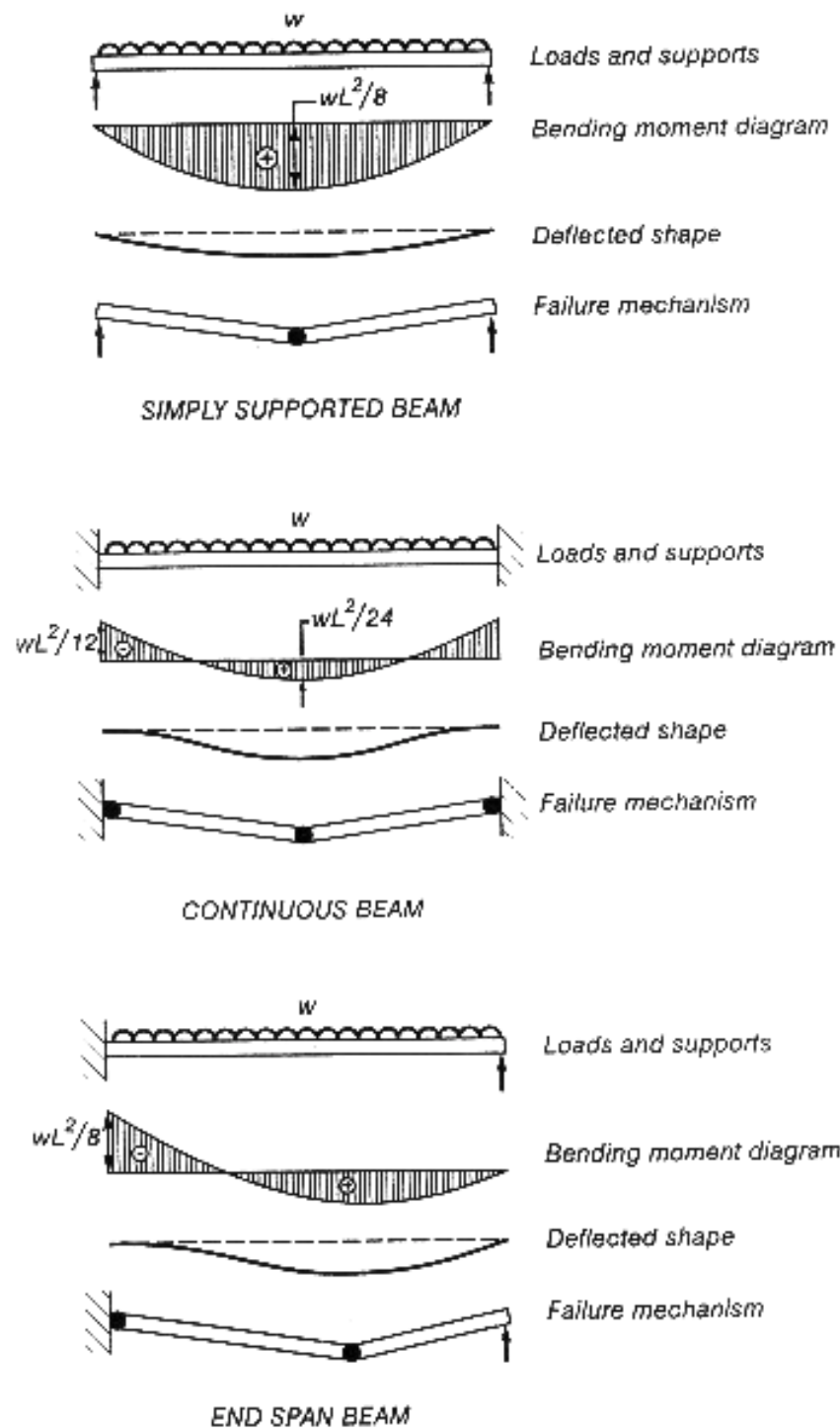


Figure 2.13 Behaviour of beams with different support conditions (Buchanan, 2000)

**Moment redistribution**

Moment redistribution is one of the significant phenomena occurring in a heated continuous beam that is very beneficial in terms of sustaining the section capacity to carry the imposed loading. In Figure 2.14, the solid line shows the bending moment of the beam under uniformly distributed loading at ambient condition. The  $M^*_{fire}$  line is the bending moment of the same beam under fire conditions with reduced load as discussed earlier.

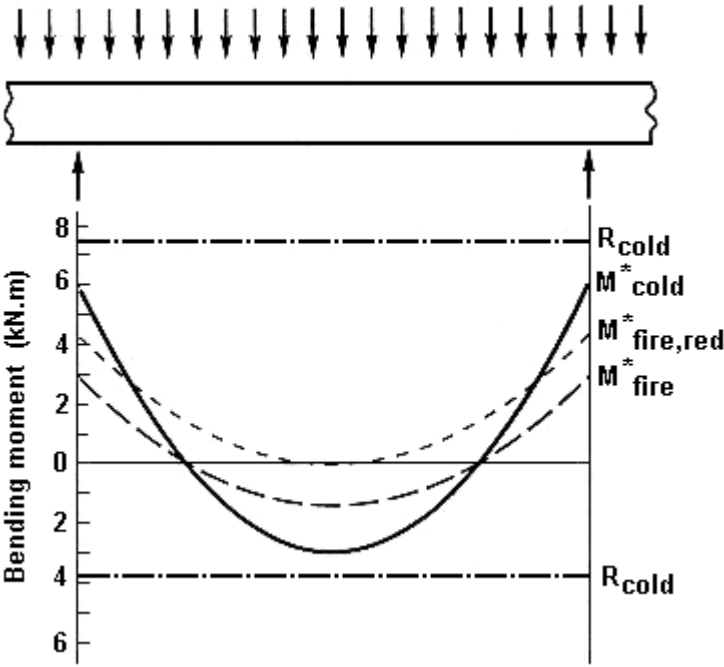


Figure 2.14 Moment redistribution at elevated temperature (Buchanan, 2000)

$R_{cold}$  is the flexural strength of the section that decreases upon heating due to reduction of section capacity. In sections as shown in Figure 2.14, the top fibre has higher strength than the bottom fibre. Moment redistribution allows decrease in the midspan moment and it is compensated by the increase in the moment at the ends of the span denoted by the curve  $M^*_{fire,red}$ . Therefore the beam would not fail at midspan due to the lack of flexural strength.

### The effect of axial restraint

When a beam with rigid end supports is heated, the thermal expansion induces some axial load along the beam due to the axial restraint provided by the supports. This axial restraint is found to be very useful especially in reinforced, prestressed or composite slabs where it compensates the loss of steel strength due to high temperature.

Figure 2.15 shows the axial force  $T$  develops in a beam that is axially restrained but is free to rotate, which in this report is termed ‘pin-pin’ condition. The eccentricity  $e$  is the distance from the line of action of the thermal thrust to the centroid of the compression block near the top of the beam in reinforced concrete member, or to the centroid of the top flange in I-section steel assuming only the top flange is in compression. This eccentricity enhances the moment capacity as:

$$R_f = M_f + T.e \quad [2.15]$$

where  $R_f$  is the total flexural resistance;

$M_f$  is the moment capacity in fire;

$T$  is the axial thrust in the beam;

$e$  is the eccentricity.

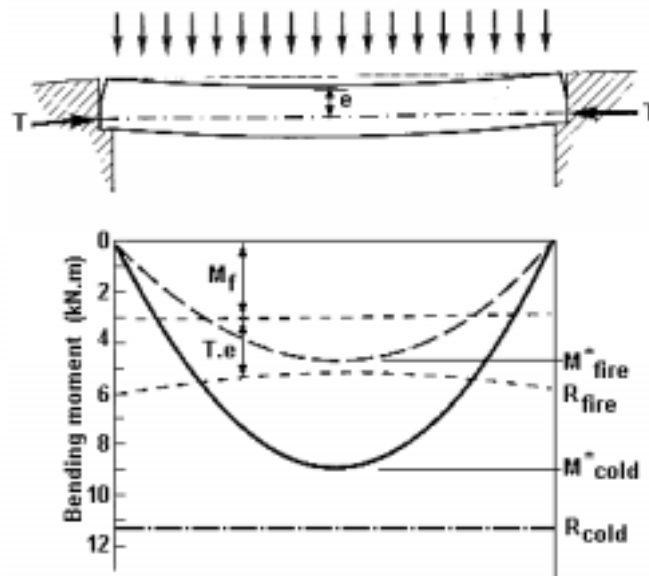


Figure 2.15 Flexural enhancement by axial restraint (Buchanan, 2000)

### 2.4.3 Design fires

Information below is the summarised description of the available design fires commonly used in fire tests and computer modelling as laid out by Buchanan (1994, 2000). The design fire is one of the main assumptions in the design and one of the required inputs in almost all fire growth computer analyses. It is usually specified as a heat release rate which varies over time for specific fuel burning in the open air. Some standard fires such as ISO fire and Eurocode parametric fire are defined by temperature varying over time.

#### ISO fire

The ISO834 is the international standard of time-temperature curve, which is defined by:

$$T = 345 \log_{10}(8t + 1) + T_o \quad [2.16]$$

where  $t$  is the time in minutes and  $T_o$  is the ambient temperature in degree Celsius.

This curve is very similar to the one from ASTM119, which is approximated by:

$$T = 750 [1 - e^{(-3.79553\sqrt{t})}] + 170.41\sqrt{t} + T_o \quad [2.17]$$

where  $t$  is the time in hours.

Figure 2.16 shows the similarity between these two curves as well as the comparison with the Eurocode design fires (EC1, 1994) for hydrocarbon and structural members outside a burning compartment, which are defined by Equations 2.18 and 2.19 respectively.

$$T = 1080 (1 - 0.325 e^{(-0.167t)} - 0.675 e^{(-2.5t)}) + T_o \quad [2.18]$$

$$T = 660 (1 - 0.687 e^{(-0.32t)} - 0.313 e^{(-3.8t)}) + T_o \quad [2.19]$$

where  $t$  is the time in minutes for both cases.

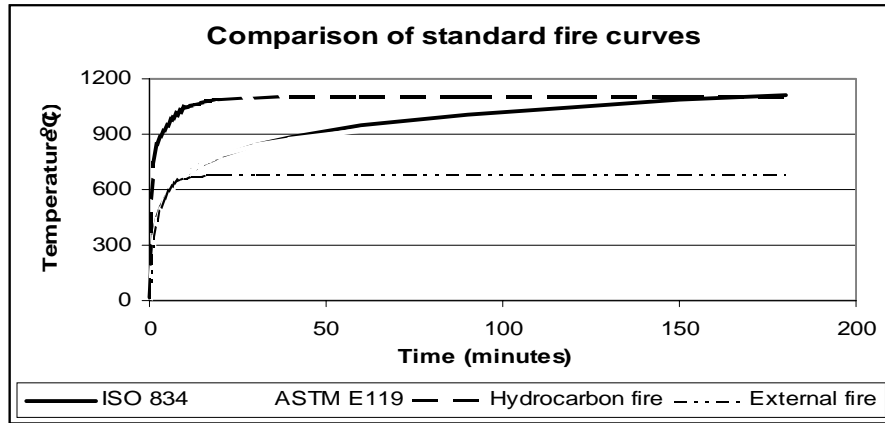


Figure 2.16 Standard fire curves (Buchanan, 2000)

### Eurocode parametric fire

The parametric fire curves as defined in EC1 (1994) allow different combinations of fuel load, ventilation factor and wall lining material to be incorporated. The temperature is specified as:

$$T = 1325(1 - 0.324e^{-0.2t^*} - 0.204e^{-1.7t^*} - 0.472e^{-19t^*}) \quad [2.20]$$

where  $t^*$  is the fictitious time in hours defined by:

$$t^* = \Gamma t \quad [2.21]$$

with  $t$  being the time in hours and

$$\Gamma = \frac{(F_v / F_{ref})^2}{((\sqrt{k\rho c_s}) / I_{ref})^2} \quad [2.22]$$

The opening factor  $F_v$  is given by:

$$F_v = A_v \sqrt{H_v} / A_t \quad [2.23]$$

where  $A_v$  is the area of the opening;

$H_v$  is the height of the opening;

$A_t$  is the total area of the compartment;

$F_{ref}$  and  $I_{ref}$  are the reference values for opening factor and thermal inertia respectively.

The opening factor gives the amount of ventilation with respect to the size of the compartment. This determines how hot the temperature inside the compartment can become.

Higher opening factor results in hotter temperature but shorter burning time. Thermal inertia indicates how fast energy is emitted or absorbed through a surface. The values of 0.04 for typical small windows and 1160 for typical concrete insulation are adopted for  $F_{ref}$  and  $I_{ref}$  respectively in the Eurocode standard. For a special case for  $\Gamma = 1$ , i.e. when  $F_v = F_{ref}$  and  $\sqrt{k\rho c_s} = I_{ref}$ , the Eurocode curve (Equation 2.20) is a very good approximation to the standard ISO 834 fire up to 1300°C.

The duration of the burning period is governed by the amount of fuel available in the compartment and is defined in the Eurocode as:

$$t_d = 0.00013 e_t / F_v \quad [2.24]$$

$$= 0.00013 E / (A_v \sqrt{H_v}) \quad [2.25]$$

where  $e_t$  is the fuel load per total surface area (MJ/m<sup>2</sup>);

$E$  is the total energy content in the fuel (MJ).

The reference decay rate from the Eurocode parametric fire suggests that for a burning period up to 30 minutes, the decay rate be taken as 625°C per hour. Longer burning time results in proportionally slower decay up to 120 minutes with 250°C per hour rate and stays constant thereafter as illustrated in Figure 2.17.

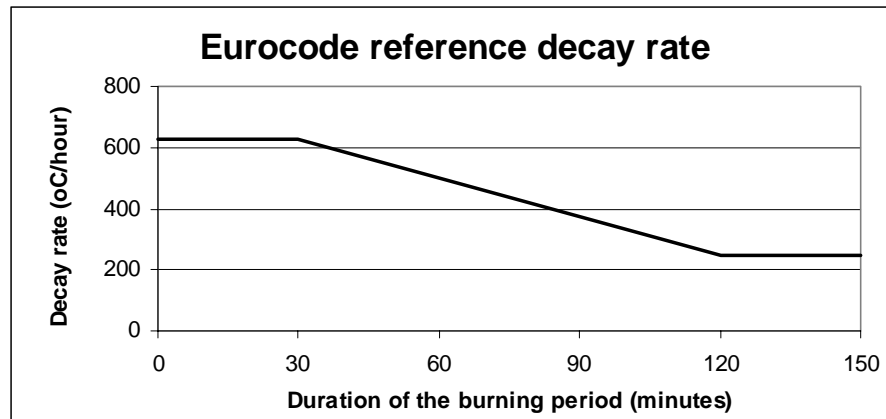


Figure 2.17 Eurocode reference decay rate (EC1, 1994)

## T-squared fire

A common way of expressing the rate of heat release during the growth period is by defining it as proportional to the time squared up to a certain peak, which depends on the available fuel and ventilation. It then either levels off to indicate constant burning or starts to decay. The decay period is only important when assessing the structural stability. When life safety is the only priority, this phase is normally ignored.

Buchanan (2000) described this parabolic curve as a burning object with constant heat release rate such that the fire is spreading in a circular pattern with a constant radial flame spread. The heat release rate for t-squared fire is defined by:

$$Q = (t/k)^2 \quad [2.26]$$

where Q is the heat release rate (MW);

t is the time (s);

k is the growth constant ( $s\sqrt{MW}$ ).

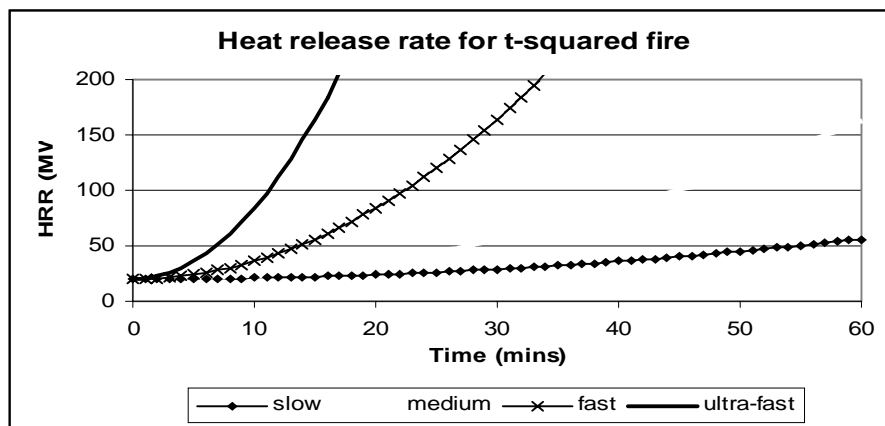


Figure 2.18 Heat release rate for t-squared fire

The value of the growth constant, k is 600, 300, 150 and 75 for slow, medium, fast and ultra-fast fire growth respectively. This value represents the time required for the fire to grow to 1 Megawatt. Typical wooden furniture falls into the medium category and light wooden material such as plywood is considered fast. An ultra-fast fire is usually found in upholstered furniture with plastic foam.

## 2.5 Behaviour of redundant structures in fire

This section is a summary of the findings from the investigation by Rotter et al. (1999) on the performance of redundant structures subjected to local fires. Similar results based on a research by Rotter and Usmani (2000) also describe some phenomena that occur in the structures under thermal effects.

The majority of theories and rules of the structural strength under fire assume an isolated structure, which is not affected by conditions of the surrounding elements. However, real structures consist of a large number of members and are usually highly redundant. Redundancies in the structure offer several alternative load paths, which allow redistribution of loads to relatively stiffer parts. Such interactions within complex structures in fires provide a reserve member capacity and the structures may survive the fire with no severe damage.

On the other hand, disproportionate collapse as described by Buchanan (2000) is the opposite situation where one element failure causes a major collapse of the structure. To avoid such failure, the design should incorporate redundant load paths and provision of some structural toughness.

### 2.5.1 Thermal expansion

Thermal expansion is a very important phenomenon that occurs in heated elements. Beams and slabs are structural members that are designed to carry loads by bending and shear. For slabs and beams which are fully or partially restrained axially, the expansion due to heating can cause high axial force on the surrounding structures. This force can either be an advantage or disadvantage for the structural performance.

Rotter et al. (1999) showed the temperature rise required for a fully restrained beam to yield ( $\Delta T_y$ ) could be calculated by the equation:

$$\Delta T_y = \frac{\sigma_y}{E\alpha} \quad [2.27]$$

where  $\sigma_y$  is the yield strength of the steel,  $E$  is the elastic modulus and  $\alpha$  is the thermal expansion coefficient. This indicates that temperature rise of only 102°C and 142°C are all that is required to yield 250 and 350 grade steel respectively, ignoring any material degradation. This low temperature proves that high stress is most likely developed in real fires even though the axial restraint is only partial.

In fire conditions, the total strain of redundant structures is the sum of the thermal and mechanical strains. The mechanical strain governs the elastic or plastic stress in the structure while the total strain governs the deformed shape. When the beam is unrestrained and there is no external loading, the total strain is equal to the thermal strain which governs the deflection. By contrast, for a fully restrained beam with no external load, the thermal and mechanical strains cancel out and the thermal stress and plastification are due to the mechanical strain.

In most real cases, there is a complex interaction of thermal expansion, restraint, and the applied loading. Extensive plastification results from combined mechanical strains, which far exceed the yield values. Extensive plastic straining occurs on highly restrained beams even though the deflection may be quite small as it depends only on the total strains. Where less restraint exists, larger deflection may develop but the plastic straining will not be too severe and hence reserve the stiffness properties of the material.

### 2.5.2 Thermal buckling

When a structural member, particularly a column, is subjected to an increasing axial load, it will reach a point where the member is no longer able to resist the applied load and fails instantly. This phenomenon is known as *member buckling* or *column buckling*.

The compressive stress developed in the heated, elastic, axially restrained beam may reach the critical buckling load which is defined by the Euler formula as:

$$P_{cr} = \frac{\pi^2 EI}{l^2} = \pi^2 EA \left(\frac{r}{l}\right)^2 \quad [2.28]$$

where  $E$  is the elastic modulus which changes with temperature,  $r$  is the radius of gyration and  $l$  is the effective length of the beam which depends on the restraint conditions. The critical temperature to cause buckling for slenderness of common slabs and beams can be as low as 100 or 200°C, which is very easily reached in real fires.

The axial force in a restrained heated beam is given by:

$$P = E.A.\alpha.L.\Delta T \quad [2.29]$$

where  $L$  is the length of the beam. Buckling will occur when  $P$  is greater than  $P_{cr}$ .

Therefore the temperature rise to cause buckling in an axially restrained beam could be obtained as follows:

$$\Delta T_{cr} = \frac{\pi^2 (r/l)^2}{\alpha L} \quad [2.30]$$

However, it is practically impossible to have a perfectly rigid supports, therefore a beam can only have partial restraint which can be modelled by a linear translational spring of certain stiffness. The critical buckling temperature increment assuming no change in the elastic modulus  $E$  can be expressed as:

$$\Delta T_{cr} = \frac{\pi^2}{\alpha} \left(\frac{r}{l}\right)^2 \left(1 + \frac{EA}{kL}\right) \quad [2.31]$$

where  $k$  is the relative stiffness of the spring and  $L$  is the length of the beam. Rotter et al. (1999) suggested that buckling and post-buckling phenomena can be observed in beams at moderate fire temperature about 300°C, which is very typical in real fires, moreover as the axial stiffness of the member  $\frac{EA}{L}$  is reduced due to reduction in the elastic modulus  $E$ .

As described by Rotter et al. (1999), the axial force induced in the beam under fire condition is merely due to the thermal expansion. Upon buckling, the deflection of the beam increases rapidly and axial shortening is observed through member curvature. There is little alteration in the axial force at post-buckling zone as the greater deflection absorbs the thermal expansion. In this case, buckling can be beneficial for the structure as the limitation in the axial force reduces damage in the adjacent members.

Buckling can also be localised at certain area in a structural member. When a fully fixed beam is subjected to elevated temperature, there will be three plastic hinges form, one at the midspan and one at each end. High compressive stress will be induced at the bottom flange of the ends of the span and the top flange of the midspan, causing these areas to buckle due to bending, known as *local buckling*. This was observed in the Cardington test, as explained by the British Steel (1999), at the connections between the beams and columns.

### 2.5.3 Thermal bowing

Most simple design calculations for fire condition assume the temperature in the members is uniform, which may roughly be the case for small members of unprotected steel. However, more complicated members, depending on the section shape and the material properties may have temperatures that are far from uniform. For constructions with high thermal insulation, such as concrete slabs or walls, the temperature of the fire exposed side can be very different from that of the cool unexposed side causing high thermal gradient across the section. The hotter surface will expand much more than the cooler one and induce bending in the member, which is known as *thermal bowing*.

Figure 2.19 shows a beam that is translationally and rotationally fixed at both ends, subjected to temperature rise and uniform thermal gradient. The internal stresses along the cross section of the beam are also shown. The axial restraint causes a uniform compressive stress and the thermal gradient causes a uniform moment.

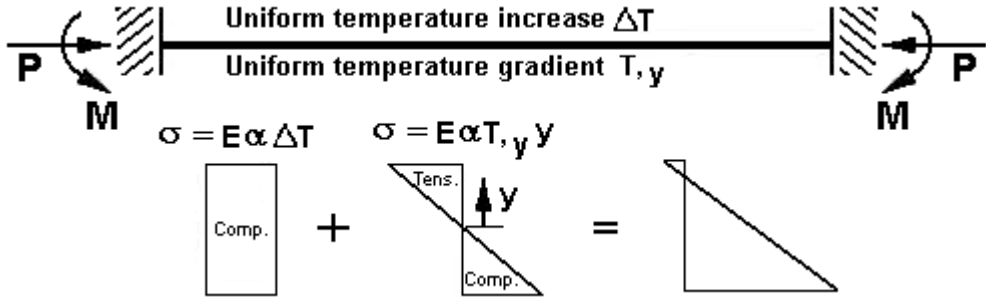
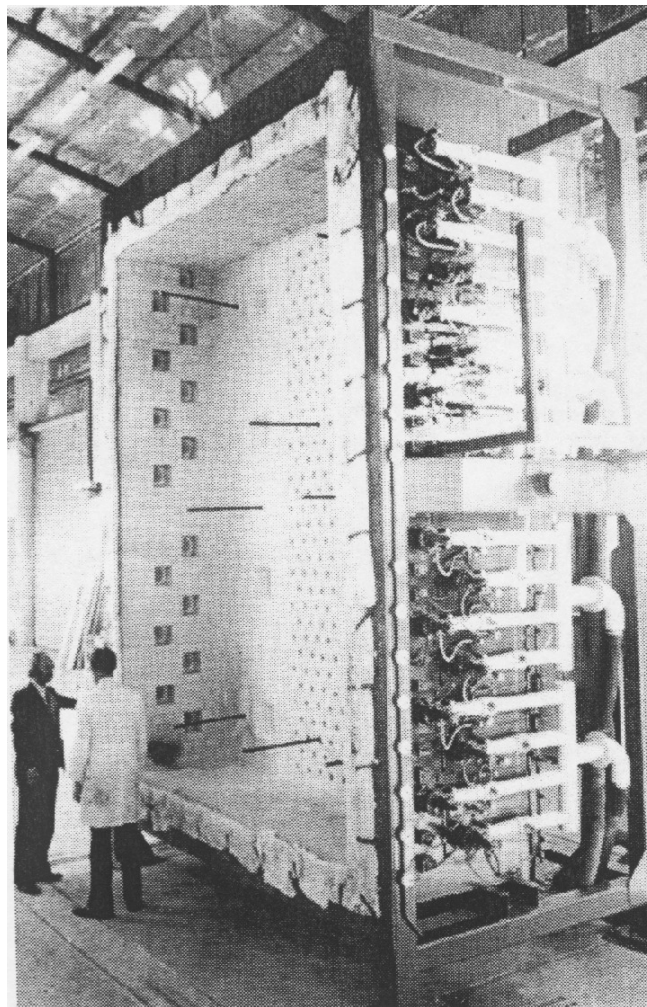


Figure 2.19 Fixed ended beam subjected to thermal expansion and bowing (Rotter and Usmani, 2000)

It can be seen that the bottom of the beam is subjected to very high compressive stress while the top fibre is in either tension or compression. This phenomena were found in the Cardington test (refer to section 2.7.2) where local buckling occurred in the lower flange at the ends of the beam as a result of large flexural rotation.

## 2.6 Fire resistance

Fire resistance is a measure of the ability of a building element to resist a fire. It is usually obtained from standard fire tests as being the time it can maintain certain criteria as discussed in the next section. The fire resistance of an element depends on several factors such as the fire severity, geometry, support condition and the material of the element. Full scale tests are required in many countries to establish the appropriate fire resistance, as smaller tests may not be able to assess potential problems due to deflections, shrinkage, connections or cracks.



**Figure 2.20 Fire resistance furnace at New Zealand Building Research Association (Buchanan, 1994)**

However, full scale tests are very expensive and therefore only considered when necessary. This leads to the development of new calculation methods and computer programs to predict the behaviour of large structures based on the results of full scale fire tests.

There are a few standards that are commonly used for fire resistance tests. ISO 834 (ISO 1975) is used by many countries and some national standards are based on this. Similar standards are used by most European countries, while the British use the BS 476 standard (BSI 1987). The United States use ASTM E119 (ASTM 1988a) which was first published in 1918, while the Canadian standard (ULC 1989) is based on this.

### **2.6.1 Failure criteria**

Building elements that are assigned a fire resistance rating should meet the corresponding failure criteria as follow:

#### **Stability**

The stability of an element is the ability to carry the applied load for the duration of the test without collapse. Limited deflection or rate of deflection can be assigned to prevent the actual failure that would damage the furnace.

#### **Integrity**

Integrity indicates the ability of the structure to contain the fire, smoke and hot gasses. The specimen tested must not develop cracks or fissures that would allow penetration of fire products.

#### **Insulation**

An insulation criterion ensures that the temperature on the cold side of the specimen is not too hot to start ignition. An average increase of 140°C and maximum increase of 180°C at a single point are usually adopted as conservative measures.

### **2.6.2 Fire resistance rating**

Based on the furnace test or some other approval systems, a building element is granted a fire resistance rating to indicate its resistance level. The fire resistance rating is usually expressed in terms of stability/integration/insulation. A typical load bearing wall with 60/60/60 rating means that it is expected to have one hour rating for each criterion. A non-load bearing glazed panel may have -/30/- rating, which means it only has 30 minutes rating for integration.

While full scale tests tend to be very expensive and are infeasible in some cases, expert opinions on whether an assembly will pass a certain test based on observation of similar successful tests have become more common in listing the fire resistance ratings. The ratings obtained from the tests, expert opinions or calculations are listed in various documents in three main categories as laid out by Buchanan (2000) as follow:

#### **Generic ratings**

This category mostly applies to typical material regardless of the manufacturers or detailed specifications. It is very conservative and can be used anywhere, but it has some limitations as it only assumes exposure to the standard fire and it does not take into account the material quality and the arrangement of the structure. An example of this rating is that a certain thickness of concrete is required to protect a steel element, regardless of the quality of the concrete and whether or not reinforcement is present.

#### **Proprietary ratings**

Proprietary ratings depend on particular manufacturers of proprietary products. Accompanied by an approved specification on the material and construction methods, it usually approves the assembly rather than the material. It is also based on the standard fire exposure and the level of loads is not considered, but it is more accurate than the generic listings as it sometimes include reference to the size and shape of the members.

### **Calculation methods**

Calculation methods have become more common in predicting the structural behaviour as it is much more feasible especially when different fire scenarios are considered. These methods should be based on full scale tests or similar assemblies to maintain accuracy. Descriptions on many of these methods are provided by Buchanan (2000).

### 2.6.3 Methods of protection

Steel is vulnerable in fire. Complex structures may survive fires due to redistribution of load to surrounding cooler parts, but local failure can also be disastrous to the whole structure. Buchanan (2000) describes how protected steel has considerably lower temperature and slower heating rate than unprotected steel, even though it takes a longer time for protected steel to cool down.

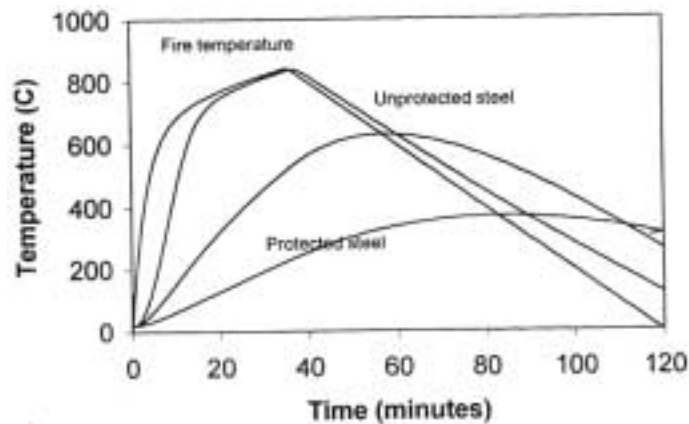


**Figure 2.21 Protected and unprotected steel temperatures exposed to a parametric fire (Buchanan, 2000)**

The top curve in Figure 2.21 is the parametric fire temperature, followed closely by the temperature of the unprotected steel. The bottom two curves show the temperatures of steel protected with 15 and 50 mm thick insulating material.

Several passive protections have been widely used to protect steel elements and avoid rapid increase in the steel temperature. Some of these methods are outlined below.

## Board system

The board protection system is commonly used as the wall lining material in light steel framing constructions as shown in Figure 2.22. Most boards are made of calcium silicate or gypsum plaster.

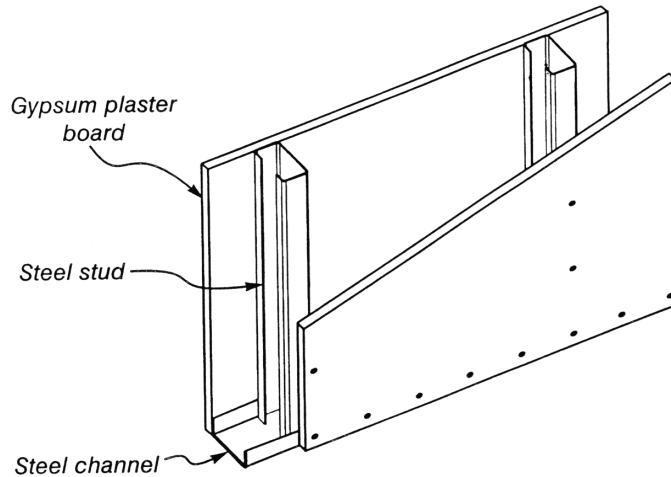


**Figure 2.22 Light steel frame wall system (Buchanan, 2000)**

Calcium silicate is only produced in a few countries and therefore is more expensive in some places. As inert material, the board is designed to remain in place with no damage throughout heating. As for the gypsum board, its performance is enhanced by water of crystallisation, which is driven off during heating. This dehydration process gives time delay at about 100°C but the strength of the board after exposure is very significantly reduced as it turns into powdery form held together by the reinforcing fibre glass and other additives.

The board system is mostly used for clearly visible structures such as columns for aesthetic reasons. Proprietary information on wallboard is available from the manufacturer and there is a range of different thicknesses to suit particular applications.

### **Spray-on system**

A spray-on system is normally the cheapest protection of steel members. It is made of cement-based material held together with some kind of glass or cellulosic fibrous reinforcing. Spray-on protection is usually applied to beams or other steel members that are not very visible as it is not suitable for decorative purposes.

Other disadvantages of this system are that the process is messy and the soft product may require protection if placed in vulnerable locations. The 'stickability' of the material to remain in place during fire exposure has to be approved.

### **Intumescent paint**

This special material looks like a normal paint but it swells up into a thick charry mass upon heating. Even though it is more expensive than board and spray-on system, it does not take much space and can be applied quickly.

Many layers of coating can be applied to obtain the required thickness. Intumescent paint is often used on door frames and the inside of fitting penetrations to provide fire and smoke barrier in the event of fire.

### **Concrete encasement**

The traditional method of steel protection is the poured concrete encasement as shown in Figure 2.23. This system provides excellent protection against corrosion. Some reinforcing steel can be provided in the concrete to hold it in place during fire and it can also be specially designed for composite action of the three materials.

This construction is bulky, expensive and also time consuming. It is a common system used in Japan but not widely used elsewhere.

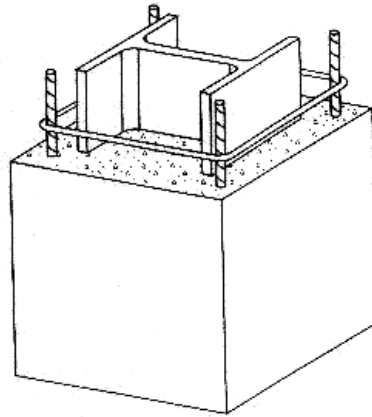


**Figure 2.23 Concrete encasement for steelwork protection (Buchanan, 2000)**

### **Concrete filling**

In contrast with the concrete encasement method, this system protects hollow steel sections by filling concrete in the inside as illustrated in Figure 2.24. The concrete can reduce the steel temperature due to its high heat sink, and/or act as part of the structure by carrying some of the load when the steel is heated.

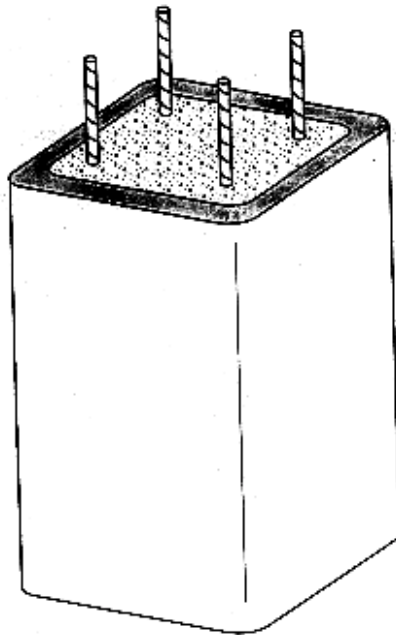


**Figure 2.24 Concrete filled hollow steel section (Buchanan, 2000)**

This type of protection avoids the bulky exterior concrete and the steel can provide excellent confinement to the concrete during ambient conditions or under seismic loading. Vent holes are essential to prevent the steel from exploding due to excessive steam pressure from the concrete upon heating.

I-section members can be protected this way by placing concrete between the flanges as shown in Figure 2.25 with reinforcing steel to hold the concrete in place.

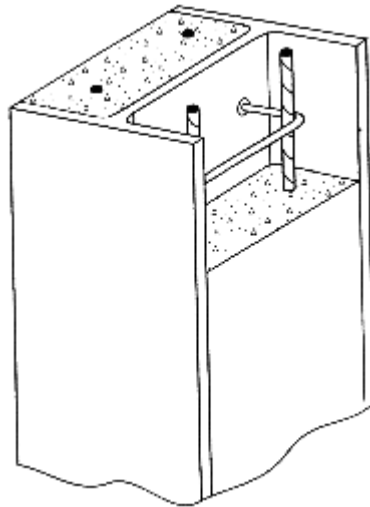


**Figure 2.25 Concrete filling between the flanges of I-section (Buchanan, 2000)**

### **Water filling**

This method is expensive and only used for special structures. The hollow steel section is filled with water to effectively prevent rapid heating. A plumbing system is required as well as additives in the water to prevent freezing at ambient conditions and corrosion of the steel. It is necessary to ensure that there is no excessive pressure when the water is heated.

## **2.7 Fire tests**

### **2.7.1 General**

A publication by the British Steel (1999) introduces steel framed buildings research projects in general as summarised below. Many European countries have undertaken a number of fire resistance tests on steel members. The findings have led to development of new composite floor system and advance in fabrication technology of fire protecting steel frames which reduce the cost significantly.

The British Steel program tried to find the true inherent fire resistance in the steel framed building in order to fully utilise the structural contribution in severe fires. A number of tests with natural fires and realistic environments have been developed to replace the gas fired furnace of a single floor beam as investigations following real fires and analytical models have proven that complete structures perform better in fire than single elements as expected.

With various locations of fire within the structure, different structural restraint and load levels can also be investigated. The common commercial constructions have been tested instead of the idealised conditions to consider the realistic scenarios in both loading and compartment design and layout.

In Australia, the biggest steel maker BHP has also been carrying out research on steel framed buildings for several years. A set of four tests was conducted regarding the 41-storey building on William Street in Melbourne. The tests concluded that there is no protection required to the steel beams or the soffit of the composite slab and the existing light hazard sprinkler system was adequate to provide the required 120 minutes fire resistance (British steel, 1999).

Another example of the fire tests undertaken by BHP is one on Collins Street (British steel, 1999). The objective was to collect data from combustion of furniture in a typical office. The tests showed that the non-fire-rated suspended ceiling was beneficial as it provided an effective fire barrier to protect the steel beams, as most of it remained in place during the fire.

The use of unprotected steel was justified as the temperature of the beams and the external columns were sufficiently low.

### **2.7.2 Cardington fire test**

The Cardington test was undertaken by the Building Research Establishment at the Cardington laboratory at Bedfordshire, UK. Six major tests were carried out between January 1995 and July 1996 including restrained beam, plane frame, corners, and large compartments. Most of the information on this section was obtained from British Steel (1999) and a paper by Rotter et al. (1999) on the Cardington test and the results.

The Cardington test was a full scale fire test on a realistic 8-storey steel framed building as shown in Figure 2.26. It was designed to model the typical modern office in a city centre according to the British Standard, BS 5950 and the Eurocodes, EC3 and EC4. The building had a concrete slab supported on composite steel-concrete beams and steel columns (Sanad et al., 1999).

The primary objective was to obtain data that can aid the understanding of the interactions between different structural mechanisms, which leads to determination of the overall behaviour of composite steel frames in fire. The test was also intended to demonstrate the large scale structure behaviour in fire based on UK building regulations which required such building to have 90 minutes fire resistance.

With this knowledge, it is possible to design steel framed buildings in a more rational design methodology with known inherent degree of fire resistance. If the resistance is not enough to withstand the fire risk, additional means of protection or other active measures such as sprinkler systems should be incorporated in the design.



**Figure 2.26** General view of the structural frame at the Cardington test (British Steel, 1999)

The restrained beam test was carried out using a 305UB40 heated over the middle eight metres out of its nine metre length in order to keep the connection as close to ambient temperature as possible. With  $3\text{-}10^{\circ}\text{C} / \text{minute}$  heating rate, the beam was heated on its three sides up to  $800\text{-}900^{\circ}\text{C}$  through the section profile. It was noticed that runaway deflection did not occur even though the steel strength had reduced to less than 10% of its yield strength at ambient conditions.

Local buckling occurred at both ends of the beam. The lower flange was distorted as it expanded against the column web. Thermal contraction during cooling generated very high tensile forces, which caused fracture at the end-plate connection at both ends. This fracture

occurred over a period of time rather than instantaneously. The other side of the plate retained its integrity and was able to provide shear capacity to the beam.

An important observation from the Cardington tests was that redistribution of load clearly exists, as it was the reason why composite steel frames have higher fire resistance than individual members even though the floor beam was unprotected. Interactions with the cool surrounding structures are extremely beneficial to the heated members. The maximum steel temperature at the Cardington test exceeded 1100°C and no sign of structural collapse was observed.

A large displacement numerical model was developed in a project funded by the Department of the Environment, Transport, and Regions (DETR) in UK through the PIT scheme, led by the University of Edinburgh in collaboration with the British Steel, Imperial college, SCI and BRE (Rotter et al., 1999). The overall objective was to develop analytical tools to adequately model the structural behaviour of composite steel frames in fire.

The redistribution of load was observed using this model based on the data from the Cardington test that was used to validate this model. The computer program SAFIR is a similar modelling tool, which will be discussed further in chapter 3.

As explained by Sanad et al. (1999), the accuracy of the analytical models can be measured by comparing the analysis results with those obtained from the tests. However, there are some parameters from the numerical tool that can not be measured in a fire test. If this information is inseparable from those that are comparable and agree with the test results, the overall behaviour is most likely to be reasonably accurate.

### 3. SAFIR program

#### 3.1 General

There are several computer packages available to model structural behaviour in fires. This section gives an overall description of SAFIR, the new program used for the analyses in this project. The information was extracted from the SAFIR98 user manual (Franssen et al., 2000) and the material from the SAFIR seminar given by Franssen at University of Canterbury (Franssen, 2000). More details of the thermal and structural analysis procedures regarding this research are discussed later in chapter 4.

SAFIR98 is a special purpose computer program for structural analysis under ambient and elevated temperature conditions. It was developed by Jean-Marc Franssen at University of Liege, Belgium, as the second generation of the structural fire codes after CEFICOSS program (Computer Engineering of the Fire design of Composite and Steel Structures), which was also developed in Liege.

Based on the Finite Element Method, SAFIR is able to model the temperature and structural behaviour of one, two, and three dimensional structures under user defined fires through discretisation of the structure, solution, and time. The built-in fire curves in the program are ISO 834, ASTM E119 or ULC S-101. SAFIR is capable of modelling beam, shell, and truss elements. The stress-strain behaviour is incorporated in the element idealisations, calculation procedures, and various material models. A linear-elliptic relationship is generally adopted for steel stress-strain material laws while a non-linear relationship is adopted for concrete.

The analysis, as described by Nwosu et al. (1999) consists of setting up the following matrix equation to solve a large number of simultaneous equations to provide the correct solution.

$$\{ F \} = [ K ] \{ U \}$$

where F is the generalised loads or forces in the structure, K is the stiffness matrix and U is the generalised displacement of the structure.

### 3.2 Analysis procedure

There are two major steps in analysing structures at elevated temperature using the SAFIR program, the thermal analysis and the structural or mechanical analysis. The input files for the earlier version SAFIR98a consist of \*.DAT and \*.STR files for both analyses. These are ASCII files which are either created using a text editor or automatically generated by SAFIR wizard for the thermal analysis as explained in the next section.

The input data file with a \*.DAT extension contains the calculation strategy, applied loads, the \*.STR file name, and the time discretisation. Information contained in the \*.STR file includes the structural parameters such as the node coordinates, the type of finite elements used and the material properties.

For the structural analysis, the \*.STR file also specifies the name of the \*.TEM file which is created during the thermal analysis for a particular cross section and applied fire. Changing this \*.TEM file name allows the user to analyse the same structural elements with various cross section properties and different heating. Figure 3.1 shows the schematic representation of the steps and files incorporated in the analysis of a frame consisting of beams and columns.

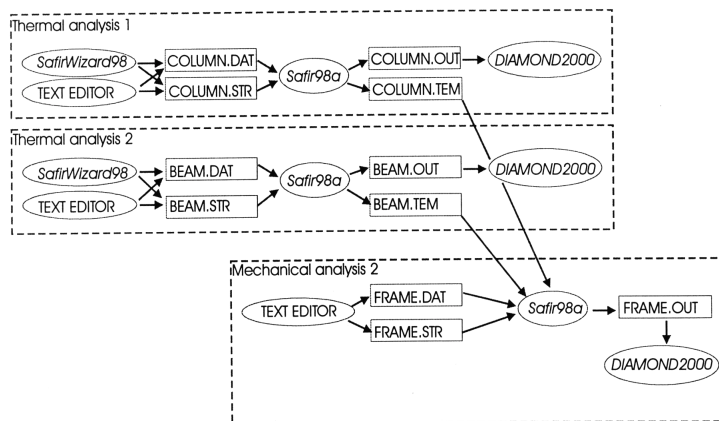


Figure 3.1 Steps and files of the analyses (Franssen et al, 2000)

The newer version SAFIR 2001 only requires one input .IN file. This version has currently been released with shell element analysis and some new features for an improved concrete model to allow for the opening and closing of cracks in concrete. Five user defined thermal materials are also included in the program.

As there are no apparent advantages of SAFIR 2001 on steel analysis over SAFIR98a, the older version is used in this research. The results of both thermal and structural analyses can be viewed graphically using the DIAMOND 2000 post-processor written by Franssen.

### **3.2.1 Thermal analysis**

In the thermal analysis, a cross section specified by the user is subjected to fire and the temperature development across the section is recorded at each time step. It requires the section to be discretised into a finite element mesh where the temperature is calculated at each node. A fine mesh is suitable for materials with a fast heating rate or high thermal gradient, while a coarser mesh can be used for materials with a slower heating rate. Different materials with temperature dependant properties can be assigned to different elements allowing a combination of materials in a section such as in reinforced concrete or other composite sections.

The input files can be manually written or automatically generated by a pre-processor. The SAFIR pre-processor Wizard98 by Franssen is a user interface program to define the cross section material properties and discretisation, the applied fires and protections for the thermal analysis. However, Wizard98a is limited to model only I-sections, either HE, IPE, American or a user defined sections. The pre-processor v0.9 by Mason (2000) is also able to create the required input files, and this pre-processor also allows other profiles apart from I-section to be modelled.

The output files for the thermal analysis are \*.OUT, \*.LOG, and either \*.TEM or \*.TND. The \*.OUT file contains the inputs and the temperature history at each node for each time print

defined. It is also a good place to look at when encountering problems in the analysis as it describes what is missing in the input files or what has caused the termination of the analysis. The \*.TEM file records the temperature of the elements averaged from the surrounding nodes at each time step which is used as the input in the structural analysis.

The \*.LOG file for the thermal analysis does not contain anything and therefore is not of any use in the analysis. The post-processor Diamond 2000 is able to show the graphical representation of the output \*.OUT file. An example of the thermal analysis result is shown below.

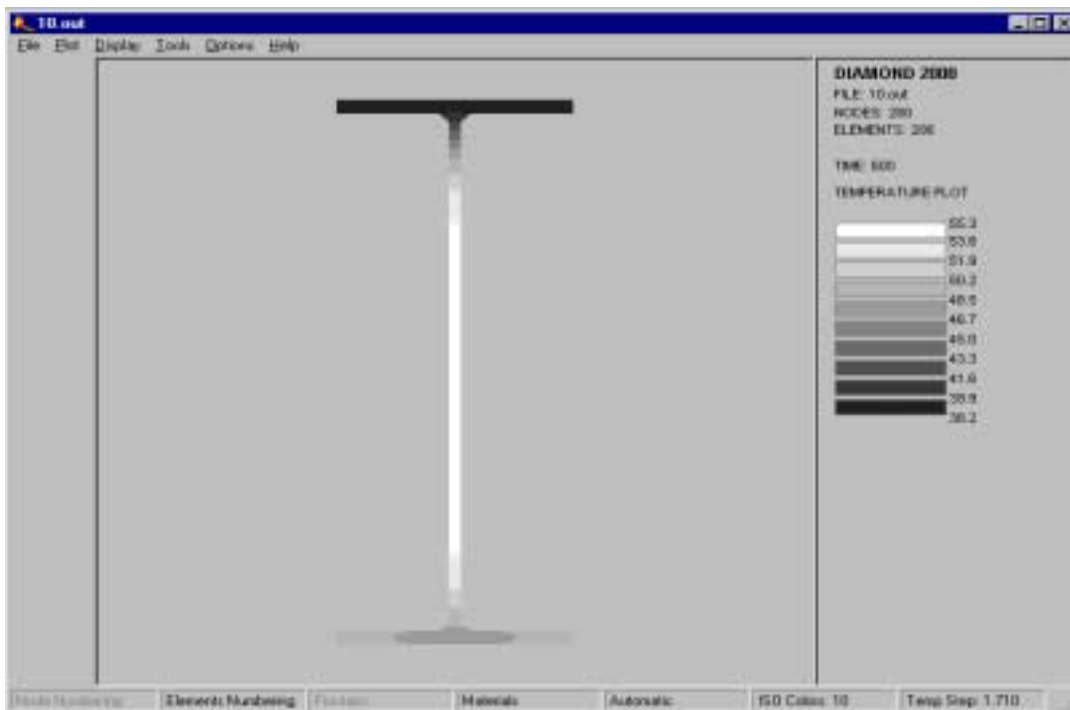


**Figure 3.2 Diamond 2000 output for the thermal analysis**

### 3.2.2 Structural analysis

After the temperature along the cross section has been defined, the whole structure can be analysed based on the temperature history recorded in the \*.TEM file. The structure is discretised into beam, truss or solid elements based on plastic analysis theory. For each time step, the program finds equilibrium between the internal forces and external load by an iterative process by evaluating the stiffness matrix and solving the equations based on the Newton-Raphson method.

Each iteration establishes the displacement at each node, bending moment and axial force at each integration point and all stresses, strains and tangent modulus of each fibre at each integration point. The integration point is described later in section 4.3.1. The program terminates if the convergence criteria is not fulfilled as discussed in section 3.7.

The structural analysis also requires the input \*.DAT and \*.STR files which have to be created by the user. Similar to the thermal analysis, two output files, \*.OUT and \*.LOG are produced from the structural analysis. The \*.OUT file contains all the output information including deflection at each node along the structure, bending moment and axial force. The fibre stresses at each longitudinal integration point can be recorded in this \*.OUT file if required by the user. The \*.LOG file stores the duration of the runs and the loads. It has no significant role in the analysis.

Illustrated below is an example of DIAMOND 2000 representation of the output from the structural analysis, showing the bending moment distribution along the beam with fix-fix end conditions.

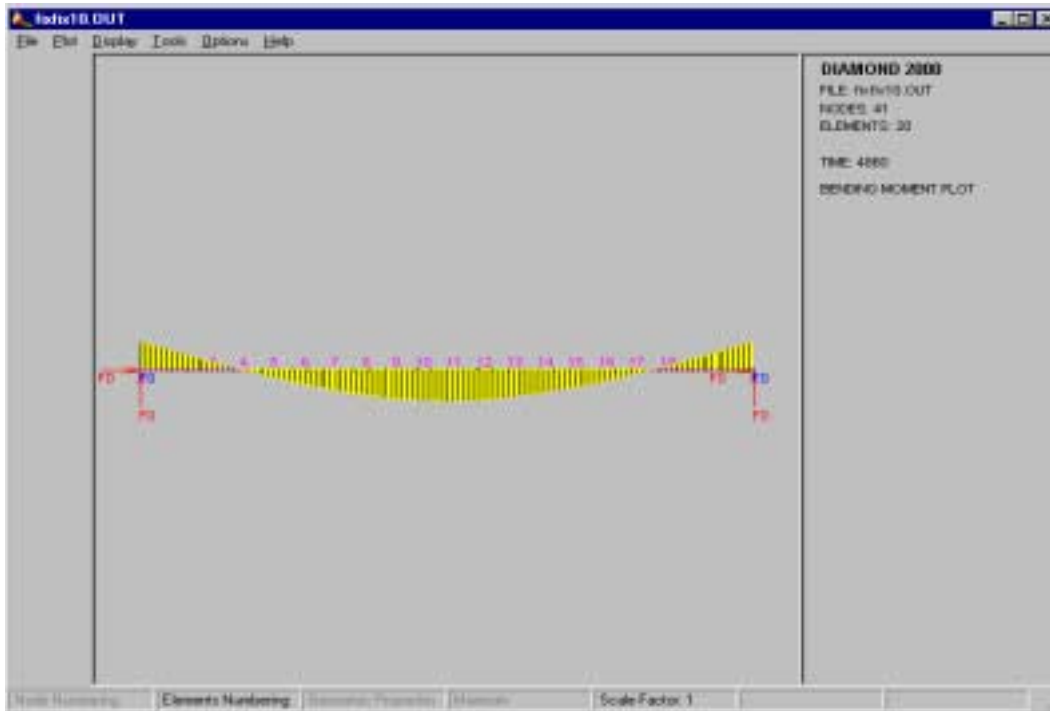


**Figure 3.3 Diamond 2000 output for the structural analysis**

For beam elements as is used in this research, there are several assumptions incorporated in the analysis as set out by Kodur et al. (1999) as follows:

1. A plane section remains plane under bending.
2. As per Bernoulli hypothesis, shear energy is not considered.
3. The plastic strain is not affected by an increase in temperature.
4. Residual stresses are considered by means of initial and constant strains.
5. The non-linear part of the strain is averaged on the length of the elements to avoid locking.
6. In case of strain unloading, material behaviour is elastic with the modulus of elasticity equal to Young's modulus at the origin of the stress-strain curve.
7. Non uniform torsion is taken into account.
8. Plastification is only considered in the longitudinal direction of the member.

### **3.3 Capabilities of SAFIR**

Concerning the thermal analysis, SAFIR is capable of analysing both two and three-dimensional structures. Plane sections are discretised by triangular and quadrilateral elements which virtually represent all cross sectional shapes. Three dimensional structures are discretised by prismatic and non-prismatic solid elements, which virtually represent all structural shapes.

Analyses of elements with different materials are possible as well as those with different fire temperatures and cooling down phases. Variations of material properties with temperature, including moisture evaporation are incorporated. Thermal performance of steel, reinforced concrete, and composite steel-concrete sections can be analysed, as well as other materials with known physical properties at elevated temperatures.

In the structural analysis, SAFIR is also able to analyse plane sections, two and three-dimensional structures, and also prestressed members. Structures are discretised by truss, beam, solid, or shell elements where large displacements can be incorporated in the truss, beam, and shell elements. The effects of thermal strains and thermal restraint are taken into account as well as material properties that are non-linearly temperature dependent. Unloading of material is parallel to the elastic loading branch. Local failure of a member does not lead to overall structural failure, which is handled by an arc length technique. This technique is only applied on large structures to prevent the whole program from crashing due to a small element failure.

Nodal coordinates are introduced in either the Cartesian or cylindrical system. Imposed degrees of freedom can be introduced thus allowing external supports to be inclined at an angle to the global axes. Residual stresses and initial strains can also be accounted for.

### **3.4 Common features in all analyses**

For all SAFIR analyses, there are some common computational features involved as follows:

1. Internal re-numbering of the system equations, which is transparent to users, can be performed by the program in order to optimise the matrix bandwidth to reduce the computer storage and calculation time.
2. Imposing the same temperature or displacement at two different nodes can be done using master-slave relations.
3. Thermal and mechanical properties of steel and concrete according to Eurocode 2, 3, and 4 are embedded in the code and can be used directly.
4. Graphic pre-processing capabilities can be handled by the SAFIR wizard98 or the pre-processor v0.9, and the post-processing by DIAMOND 2000.

### **3.5 Sign conventions**

The global and local axes defining a structure use the Cartesian coordinate system. Deflection and applied loads are positive in the direction of the positive Cartesian coordinates. Positive deflection indicates that the beam is hogging while negative deflection indicates that the beam is sagging. The moment and rotation are positive in the counter-clockwise direction, while the stresses and the axial force, which is the sum of all stresses, are positive in tension.

### **3.6 Material properties**

Various material properties are incorporated in the SAFIR program for different analyses. For simulations under ambient temperatures only, the valid materials may have elastic, bilinear or Ramberg-Osgood properties. For elevated temperatures, Eurocode steel materials are provided for structural steel, reinforcing and prestressing steel. The Eurocode and Schneider's models are used for calcareous and siliceous concrete. Valid materials such as Insulation, C Gypsum, and X Gypsum can be used for non-load bearing structures.

The stress-strain relations of steel and concrete are non-linear and temperature dependent. Materials in heated structures are subjected to initial strains ( $\epsilon_i$ ), thermal effects ( $\epsilon_{th}$ ) and stress

related effects ( $\epsilon_{\sigma}$ ). The stresses are the difference between the total strain ( $\epsilon_{total}$ ), which are obtained from the nodal displacements, and the initial and thermal strains.

### **3.7 Convergence criteria**

To obtain the correct solution, SAFIR uses an iterative procedure of convergence at each time increment. Solutions are obtained at each integration point along the discretised elements which are also specified by the user. The precision specified in the data file, which is a small value dependent on the type of the structure analysed, must be reached in order to fulfil the convergence requirement.

When the program fails to converge to a solution due to physical or numerical instability, the time increment will be halved and the process repeated. The program is terminated if convergence is not reached after the time increment reaches a certain value or when the final run time is reached, both defined by the user, whichever occurs first. The program cannot be terminated by specifying a limiting deflection criterion.

## 4. Methods of Analysis

### 4.1 The steel beam

The analyses are based on investigations of a single span steel beam supported at both ends. The beam is part of a structural steel frame building similar to that of the Telecom building in Auckland, and was chosen because it has similar properties to the one used in the Cardington steel frame tests (Clifton, 1999).

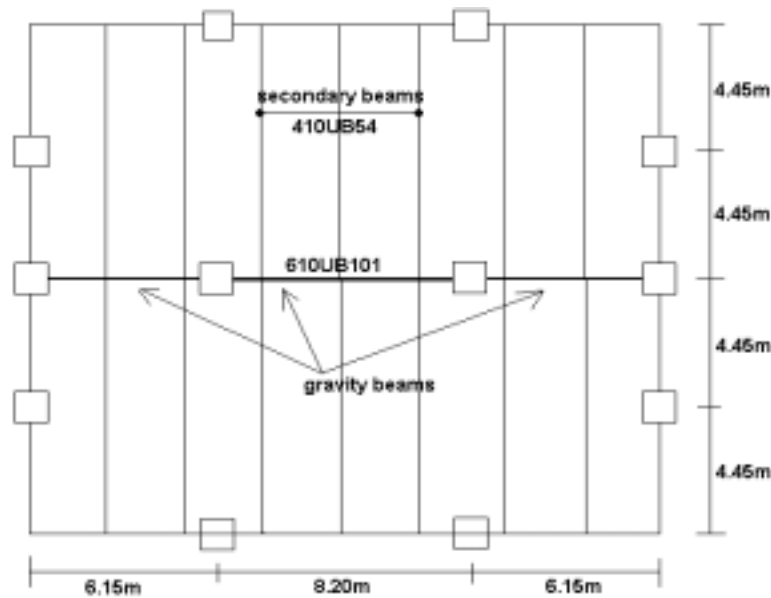


Figure 4.1 Floor plan of the Telecom Building in Auckland (Clifton, 1999)

A span of 8m instead of 8.2m was chosen for simplicity. It is a universal I-beam, 610UB101 with the dimensions and properties laid out in Table 4.1 (BHP catalogue). At ambient conditions, the yield strength and the elastic modulus of the steel are 430 MPa and 210 GPa respectively, with a Poisson's ratio,  $\nu_s$  of 0.3.

This high strength steel may not represent most real steel structures. However, for the purpose of this report, which is to investigate the beam behaviour at elevated temperatures, stronger steel will provide longer exposure time before approaching failure, thus allowing better observation on the sequence of events that are happening in the beam.

**Table 4.1 The steel beam profiles for the analyses (BHP catalogue)**

Type	610UB101
Weight, W	101 kg/m
Depth, D	602 mm
Flange width, $b_f$	228 mm
Flange thickness, $t_f$	14.8 mm
Web thickness, $t_w$	10.6 mm
Root radius, R	14.0 mm
Depth between flanges, $d_1$	572 mm
Gross cross sectional area, $A_g$	13000 mm <sup>2</sup>
Second moment of area, $I_{xx}$	761 x 10 <sup>6</sup> mm <sup>4</sup>
Plastic section modulus, S	2900 x 10 <sup>3</sup> mm <sup>3</sup>

## **4.2 Thermal analysis**

### **4.2.1 Discretisation**

The modelling of thermal response by the SAFIR program requires the cross section to be discretised into small finite elements. This was done using the SAFIR pre-processor wizard98. This pre-processor automatically generates an efficient numbering system to minimise the amount of required memory and the CPU time for calculation, and to ensure the precision of the solution.

The web and the flanges of the steel beam were divided into rectangular elements with coarser mesh on the web due to the almost uniform temperature in the web throughout heating. The roots between the flanges and the web were modelled as triangular finite elements. The temperature was defined at every node and varied linearly in between.

SAFIR computing time can be reduced by modelling only half of the cross section, of large complex sections. This simplifies some analyses but is only possible when the structure has symmetrical geometry, including the supports and initial imperfections, loading, and thermal conditions, and when a non-symmetric failure mode is not expected. Modelling half of symmetrical structures can be done by ensuring the displacements and rotations perpendicular to the plan of symmetry are fixed while the displacements in the plan of symmetry are free.

The beam for this particular research, however, was discretised as a whole due to its simple cross section, as shown in Figure 4.2. The overall mesh consisted of 280 nodes and 206 elements. The applied fires are described in the next section.

For the thermal analysis, time steps of 10 seconds were used throughout the heating. A five seconds time step was applied for the first hour of the structural analysis followed by 10 seconds step up to the end of the runs. Ten seconds is a typical value used in steel section analyses. A small time step is necessary if the element size is small, the elements possess high

thermal conductivity, the solution varies quickly, or when the thermal properties have steep variations such as found in gypsum sections. Numerical failures are likely to occur if the time step used is too long or when the time range in the temperature file is shorter than that in the structural file.

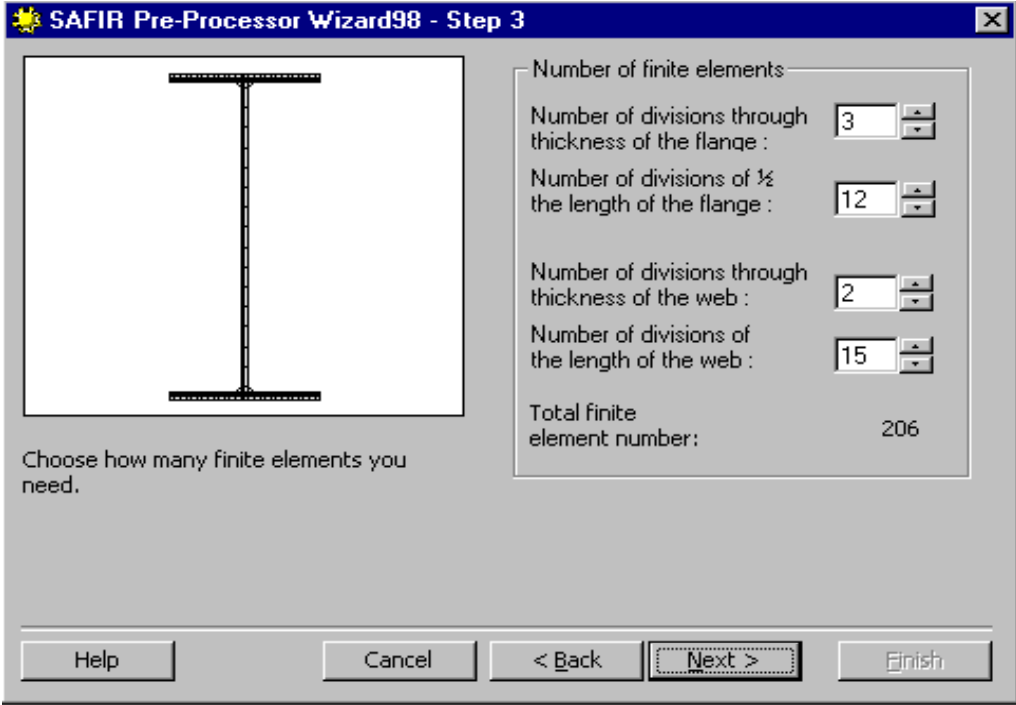


Figure 4.2 Discretisation of the steel beam cross section

## 4.2.2 Applied fires

Different fires and heating rates are used to compare the behaviour of the steel beam under any given condition. The fire was applied to beams having four different support conditions and the behaviour of these beams were compared as described in later chapters.

The incipient phase of the fire was ignored in all cases as is normally assumed in most fire tests. Apart from the built-in fires such as the ISO fire, the temperature function has to be input into the SAFIR program using a separate \*.fct file. It was also assumed that the fire only affect the one beam, meaning the other spans or other parts of the frame were at the ambient conditions. Overall heating in the whole frame structure leads to great complication and was outside the scope of this project.

### Linear heating rates

A linear heating rate of 10°C per minute was used as the base case to analyse the detailed behaviour of differently restrained beams heated on three sides. Faster heating rates of 20 and 30°C per minute were then used to observe any differences in behaviour from the base case. The fire was only applied on three sides of the beam as the top part would be protected by a concrete slab.

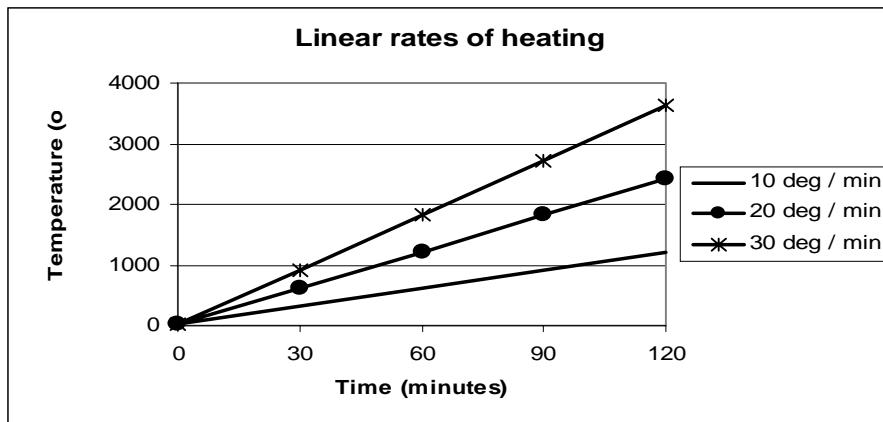


Figure 4.3 Linear heating rates

## Standard ISO fire

The deflections, bending moments, and axial forces from the base case were also compared with those from the analysis when an ISO fire is applied. It is important to investigate ISO fire exposure for comparison, as most fire tests use this standard fire.

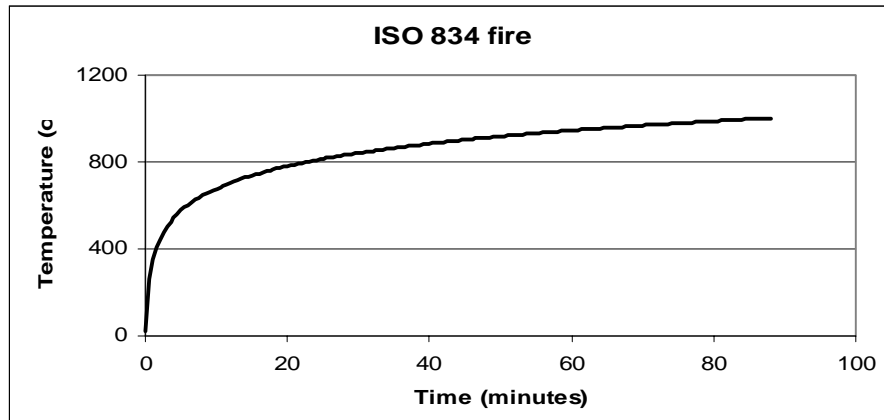
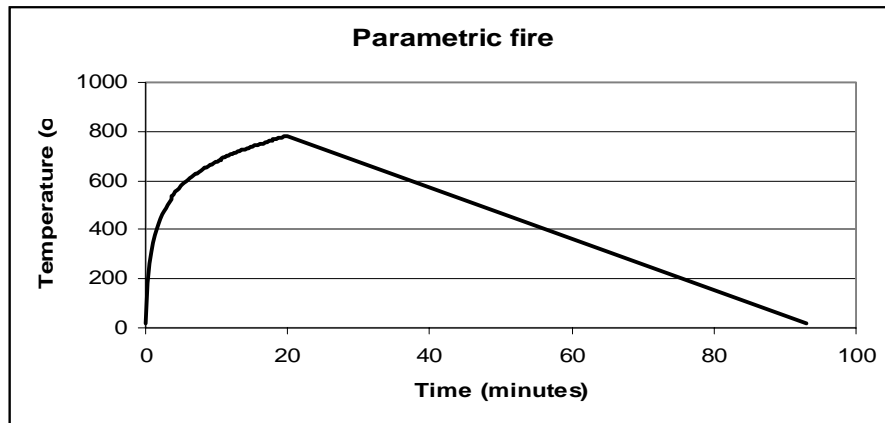


Figure 4.4 Standard ISO 834 fire

## Parametric fire

Using the types of fire described above, the beams are heated up to failure. However, in reality the fire may start to decay before the structural beams fail. The behaviour of the steel beams will then change accordingly. A realistic parametric fire was also applied to investigate these phenomena.

The fire is the special case when  $\Gamma = 1$  (refer to section 2.4.3) and Equation 2.20 represents the ISO fire curve during the burning period at the beginning of the fire. The burning period was taken as 20 minutes which will be verified later in more detail in section 7.3. This represents a fire in a typical compartment 5m x 5 m x 2.5m high with a window of 2m high and 1.4m wide, and a fuel load of 410MJ/m<sup>2</sup> floor area. It then decays linearly back to the ambient condition.



**Figure 4.5 Realistic parametric fire**

The fire was only applied on three sides of the beam as the top part will be protected by the concrete slab. Exposure on four sides of the beam was investigated using the standard ISO fire to observe any similarities and differences from the three-sided case. This is discussed in chapter 7.4.

## 4.3 Structural analysis

### 4.3.1 Discretisation

The 8 metre beam was discretised into 10 beam elements. The elements were joined together by nodes with 3 degrees of freedom, 2 translational and 1 rotational. An additional node was placed in the middle of each element to avoid the beam being too stiff and therefore improve the element performance. This node only had 1 degree of freedom as it could only rotate and was assumed not to carry any load. Therefore, for the structural analysis, the beam was divided into 20 elements with 41 nodes.

Some integration points, also known as Gaussian points, were introduced at each element at some distance from each node. All calculations were done at these points. For the project, two integration points were used at 21% of the element length from each node as illustrated in Figure 4.6. The values of the bending moment and axial force at various locations along the beam can be obtained from these points. The deflection, however, was calculated at each node.

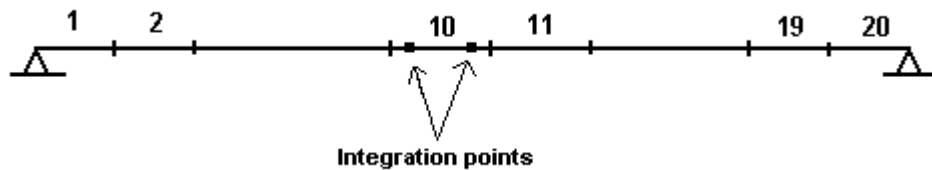


Figure 4.6 Discretisation of the beam for the structural analysis

### 4.3.2 Loading

The actual loading of the steel beam of the Telecom building includes the self weight of the beam, the concrete slab, the secondary beams, and the live load. However as the purpose of the analyses is to investigate the responses of the steel beam alone, an arbitrary load of 25kN/m was taken as the base case. In reality, the beam is able to take higher load than the one modelled as it has some composite action with the concrete slab and the cooler surrounding structures, which is not taken into account in the analysis. The model assumes

that the loading applied to the beam is sitting on top of the beam with no load transferring means of connection, therefore ignoring any composite behaviour that may occur.

### 4.3.3 Supports

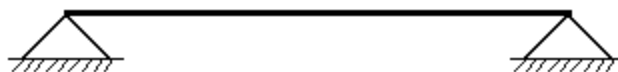
Four different support conditions were modelled in the analyses.

#### Pin-roller supports



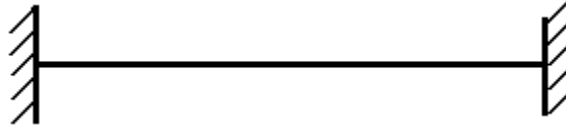
Pin-roller support is a simply supported beam, which means the member forces can be solved using equilibrium alone. At the pin end of this support, the beam is restrained both axially and vertically, while at the roller support, it is free to move axially. There is no bending moment induced at both supports as they are free to rotate. The ideal pin-roller beam is unrealistic. However, it is important to understand the behaviour of a pin-roller beam as the extreme case where there is very little axial restraint provided to the beam.

#### Pin-pin supports



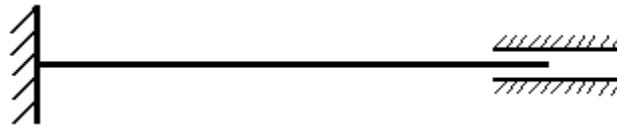
With pins at both ends, the whole beam is axially restrained. Both supports are free to rotate and possess zero moment. An example of this type of supports is the bolted connection between steel elements.

### **Fix-fix supports**



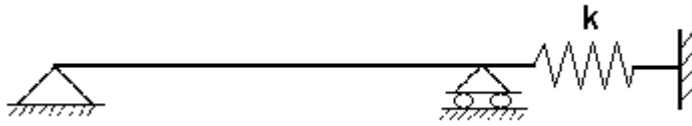
Fix supports indicate that the beam is fully restrained, vertically, axially and rotationally. There is bending moment induced at the supports. This is the case where steel elements are connected by welds or other similar types of very rigid connections.

### **Fix-slide supports**



For this case, one end of the beam is fixed while the other end is free to move axially, but restrained both vertically and rotationally. There is also bending moment developed at both of the supports.

#### 4.3.4 Introduction of springs



Ideal simply supported beams on pins and rollers are very rare in reality. Even though not fully pinned, there is usually some kind of stiffness that makes the structure more restrained than being simply on rollers. A spring was introduced into the analysis in order to model the stiffness induced at the roller support.

The spring is modelled as a one-metre long steel truss member with a single degree of freedom in contrast with the steel beam that possesses three degrees of freedom. In the discussion that follows, the spring stiffness will be denoted by  $k$ , the relative stiffness of the spring to that of the steel beam. When  $k$  is zero, the beam is simply supported, while if  $k$  is equal to infinity, the beam is fully pinned.

The axial stiffness of the beam defined as  $K = \frac{EA}{L}$  is 336.5 kN/m. Taking  $0.01\text{m}^2$  as the constant area of the spring, the elastic modulus of the spring is obtained for each value of  $k$  desired. Elastic material properties are assigned for the spring as it is not to yield prior to the failure of the beam.

## 4.4 Summary

Shown below in Table 4.2 is a summary of different combinations of fire exposure, the support condition and the number of fire-exposed sides used in the analyses undertaken for this research project.

**Table 4.2 Summary of different analyses in the project**

Fire	Exposed sides	Pin-roller	Pin-pin	Fix-fix	Fix-slide	Spring
10°C / minute	3	♣Υ	♣Υ⊗	♣Υ	♣Υ	♣
	4					
20°C / minute	3	♣	♣	♣	♣	
	4					
30°C / minute	3	♣	♣	♣	♣	
	4					
ISO fire	3	♣	♣	♣	♣	
	4	♣	♣	♣	♣	
Parametric fire	3	♣	♣	♣	♣	
	4					

### Legend:

- ♣ : Investigated in the project
- Υ : Various applied loadings were investigated
- ⊗ : Various lines of thrust were investigated

## 5. Analysis of Results for Four Support Conditions

This section describes the general observations of the heated beam characteristics including deflections, bending moments, and axial forces under different support conditions and failure mechanisms. The deflection in general is discussed in section 5.1, while sections 5.2 to 5.5 discuss the behaviour of the beams with different support types.

The bending moment from SAFIR takes into account the P- $\Delta$  effect. At the midspan of a pin-pin beam, the bending moment at all times is given by:

$$M = wL^2 / 8 + P\Delta \quad [5.1]$$

where P is the axial force induced in the member and  $\Delta$  is the deflection. Considerable axial force only exists in the axially restrained beams. Axial force in the beams that are free to elongate is negligible. For beams with supports fixed against rotation, the bending moment will show much greater changes during fire exposure. For symmetrical beams, the differences between end moments and midspan moments will be the value given in equation 5.1, at all times.

As the general trends of the above parameters are very similar for the different values of uniform heating used, the detailed descriptions of the behaviour of the beam are based only on the analysis of the beam heated on three sides at 10°C/minute. Comparisons of behaviour under different fires, loading, locations of line of thrusts, and the effect of spring at one of the supports will be discussed later in separate chapters.

### Sign convention

For the deflection, negative deflection indicates sagging of the beam. For the bending moment, SAFIR convention is opposite to that commonly used in New Zealand. It is still plotted on the tension side, but positive moment is used when the moment is above the beam line and vice versa.

The sign convention adopted in New Zealand is that “negative moment” indicates a hogging moment where there is tension at the topside of the beam, and “positive moment” indicates a sagging moment where tension is on the bottom side of the beam. This convention is adopted in the report apart from the graphs that show the SAFIR convention. For the axial force, it is negative when the beam is in compression.

### 5.1 Deflection of the beams

Deflection criterion is important when assessing failure of the structure. Rapidly increasing deflection indicates imminent collapse. In many severe fires, there will be very large deflections but no collapse, in which case the deflected members can be repaired or replaced after the fire.

Figure 5.1 illustrates the comparison of midspan deflections of beams with four different types of support condition with regards to the steel temperature at the mid height of the web, which was considered to be the hottest place in the cross section.

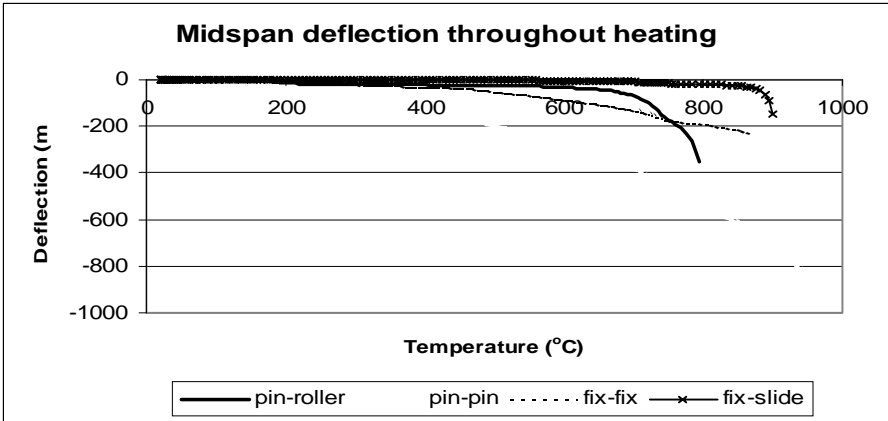


Figure 5.1 Midspan deflection of the beams throughout heating

## Deflection at early stage of the fire

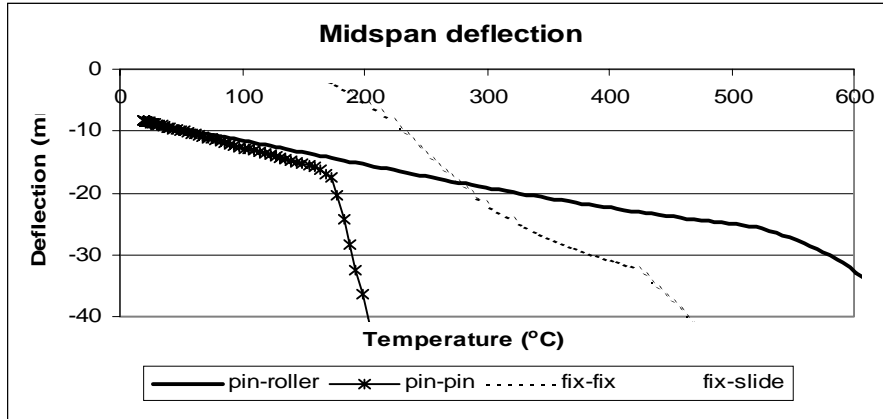


Figure 5.2 Midspan deflection for all beams at early stage of the fire

Figure 5.2 illustrates the same curves as Figure 5.1, considering only the deflection up to 40mm and steel temperature up to 600°C. It can be seen that the simply supported beams, both with pin-roller and pin-pin end conditions had slightly more deflection at the midspan to start with, as they were free to rotate at the supports. On the other hand, the beams with moment resisting supports are restrained from rotation at the ends and therefore produced less deflection at normal conditions.

As the heating progressed, the pin-roller supported beam had constant increase in deflection, while the pin-pin supported beam had slightly more deflection up to approximately 170°C when something happened and the deflection increased dramatically. The beam with fix-slide supports maintained the minimum deflection at the early stage of the fire while the beam with fix-fix end conditions behaved like the one with fix-slide supports up to about 170°C and then underwent rapid deformation. This behaviour is described in more detail below.

### **Pin-roller**

In the pin-roller condition, the beam was free to elongate. There was no effect of thermal expansion and the deflection was purely due to the loading. Upon heating, Figure 5.1 shows that the beam slowly deflects up to approximately 700°C. At this point, the beam had lost most of its strength and the deflection pulled the roller support slightly closer to the pin support. When the beam lost its stiffness, runaway failure started to occur. Failure occurred at 83 minutes after the beginning of the fire.

### **Pin-pin**

The beam with pin-pin supports was not free to expand upon heating. The heat caused the beam to try to elongate and since it was restrained against thermal expansion, it started bowing down at an early stage of the fire, i.e. at about 200°C. It had a much larger displacement than the pin-roller supported beam and eventually failed after 97.5 minutes of exposure.

### **Fix-fix**

Similar to the pin-pin end conditions, the fix-fix supports also provided axial restraint to the beam. However, as the supports were not free to rotate, only slight deflection was observed up to about 400°C, while thereafter the deflection became more apparent even though it did not deflect as far as the beam with the pin-pin supports. This beam failed at 88 minutes.

### **Fix-slide**

Fix-slide supports allowed the beam to undergo thermal expansion. The beam hardly deflected throughout the heating because both ends were not free to rotate, in contrast with the pin-roller supported beam. The very slight deflection was followed by runaway failure at 90.5 minutes due to yielding of both the top and bottom flanges at midspan following the yielding of those at ends of the span shortly before, as explained in detail in section 5.5.

## 5.2 Beam with pin-roller supports

This beam failed when one plastic hinge was formed at the midspan as illustrated in Figure 5.2. As the beam was free to expand, the bending moment along the beam was only due to the imposed load and there was no axial force induced.

The moment distribution was constant throughout the heating as shown in Figure 5.7. There was zero moment at the ends as the beam was free to rotate at its supports, and  $wL^2/8$  at the midspan (Figure 5.4), with  $w$  being the uniformly distributed load and  $L$  being the span length of the beam. The sequence of events throughout the fire exposure is summarised in Table 5.1.

**Table 5.1 Time line of events in pin-roller beam**

No.	Events	Time (minutes)
1	Bottom flange at midspan reached the proportional limit	64
2	Top flange at midspan reached the proportional limit	70
3	Bottom flange at midspan reached yield	81.5
4	Top flange at midspan reached yield	83
5	Failure mechanism achieved (1 plastic hinge)	83

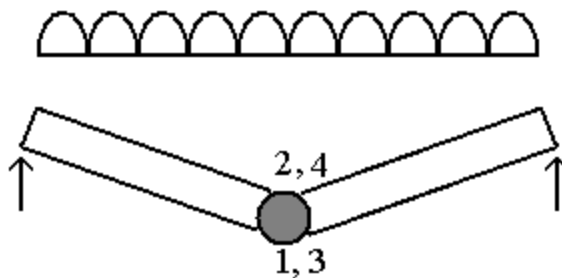


**Figure 5.2 Failure mechanism of pin-roller beam**

The behaviour of the beam can be explained by examining the flange stresses during the fire. Stresses in the top and bottom flanges are shown in Figures 5.5 and 5.6. The top line in each graph is the yield stress, reduced for elevated temperature according to EC3 (1995). The next line is the proportional limit stress, also from EC3.

The bottom flange stress at the midspan reached the proportional limit at 64 minutes, marked (a) on Figure 5.6. The top flange was still elastic and able to carry more stress up to 70 minutes when it reached the proportional limit, indicated by the obvious increase in deflection at point (b) in Figures 5.3 and 5.5.

The bottom flange yielded at 81.5 minutes (point (c) in Figures 5.3 and 5.6) and the section capacity dropped significantly causing runaway deflection, and the top flange yielded at 83 minutes when the failure mechanism formed (point (d) in Figure 5.5)

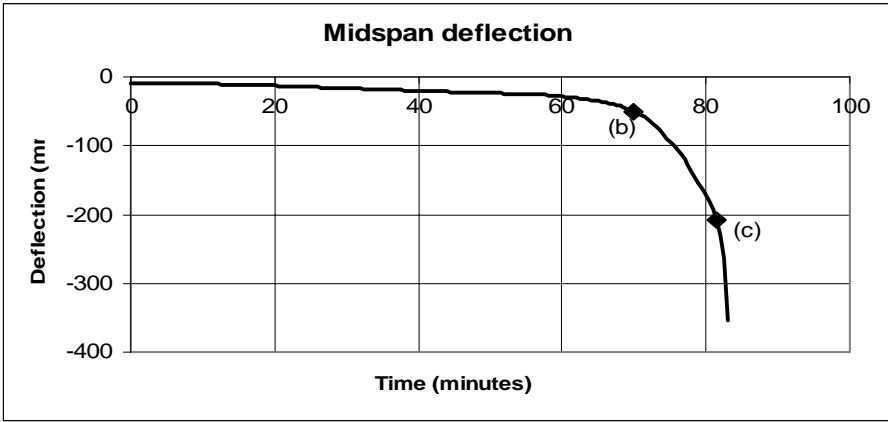
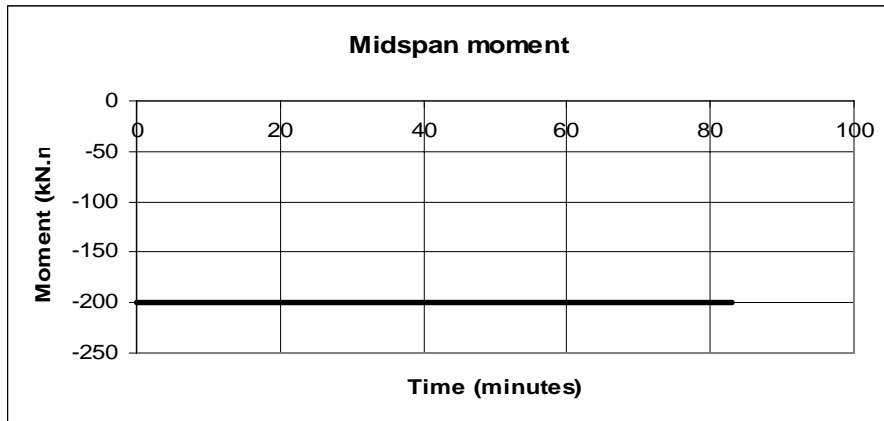
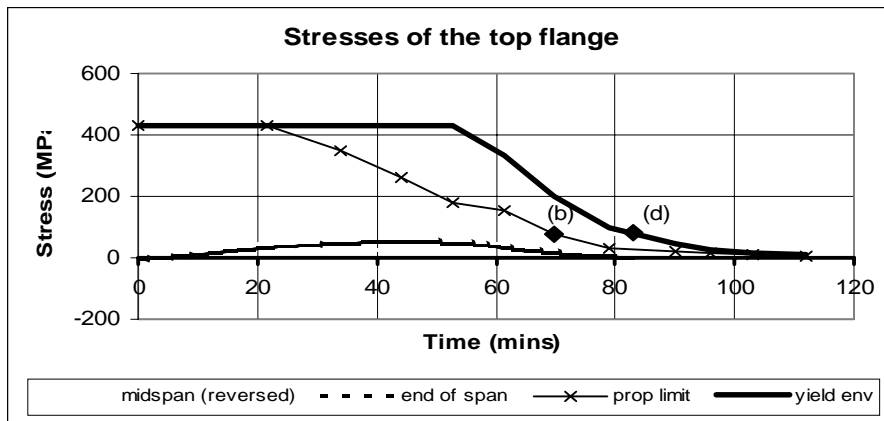


Figure 5.3 Midspan deflection of pin-roller beam



**Figure 5.4** Midspan moment of pin-roller beam



**Figure 5.5** Top flange stresses of pin-roller beam

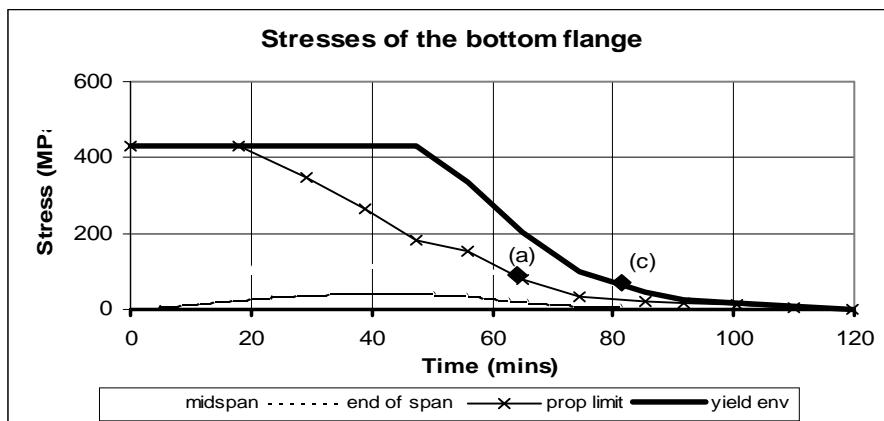


**Figure 5.6** Bottom flange stresses of pin-roller beam

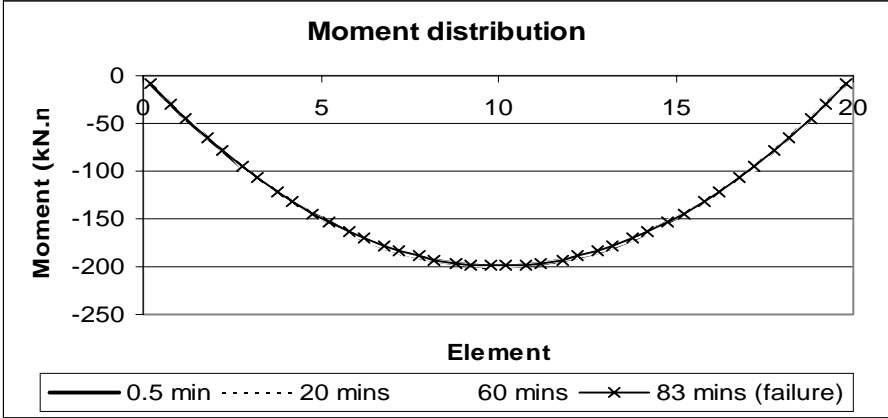


Figure 5.7 Moment distribution along the pin-roller beam

### 5.3 Beam with pin-pin supports

Unlike the straightforward behaviour of the simply supported beam with pin-roller end conditions, the behaviour of the beam supported by pins at both ends was found to be more complicated due to the interactions of the subsequent events as listed in Table 5.2. The behaviour of pin-pin beam was more sensitive to reduction in the elastic and yield limit as shown Figures 5.12 and 5.13, due to the axial restraint as explained below.

**Table 5.2 Time line of events in pin-pin beam**

No.	Events	Time (minutes)
1	Top flange at midspan reached the proportional limit	25
2	Bottom flange at ends of span reached the proportional limit	45
3	Top flange at ends of span reached the proportional limit	49.5
4	Top flange at midspan reached yield	53
5	Bottom flange at midspan reached the proportional limit	53.5
6	Bottom flange at midspan reached yield	74
7	Failure mechanism achieved (1 plastic hinge)	97.5

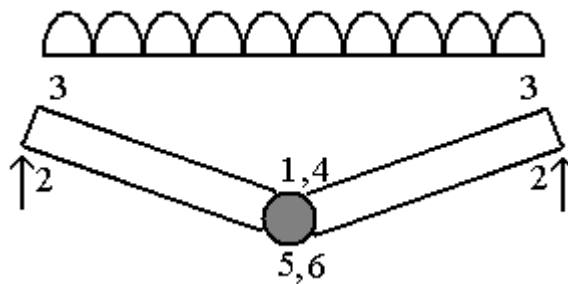


**Figure 5.8 Failure mechanism of pin-pin beam**

Axial force was induced in the beam due to thermal elongation since it was axially restrained. This force increased due to thermal expansion until the beam started to deflect considerably as the top flange reached the proportional limit at 25 minutes, very close to the yield envelope.

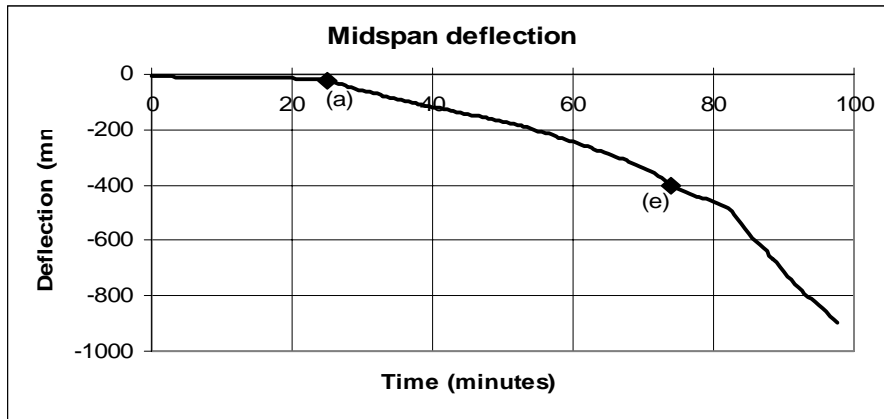
This caused alteration in the stresses at the bottom flange and at the supports. The beam also started to lose its stiffness as the modulus of elasticity was reduced by elevated temperature, which caused a larger deflection. This yielding and lack of stiffness allowed some reduction in the axial load. However, the bending moment, which was governed by the P- $\Delta$  effect, kept on increasing as the increase in deflection was greater than the reduction in the axial force. This is marked as point (a) in Figures 5.9 - 5.12.

The bottom flange and the top flange of the endspan reached the proportional limit at 45 minutes and 49.5 minutes respectively, marked by point (b) and (c) in Figures 5.13 and 5.12. There was no obvious change in the deflection, bending moment or axial force due to these as the beam supports did not resist moment and therefore the beam still maintained its strength.

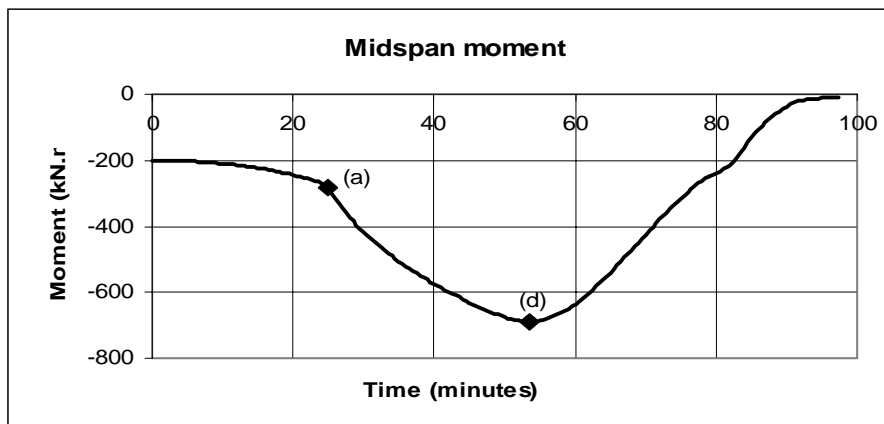
At 53 minutes, the top flange at the midspan yielded, followed by the bottom flange stress at the midspan reaching the proportional limit 30 seconds later. Marked by point (d) in Figures 5.10 - 5.13, the midspan moment started decreasing as the first plastic hinge began to form and the decrease in axial load was greater than the increase in deflection. Seventy four minutes after the start of the fire, indicated by point (e) in Figures 5.9 and 5.13, the bottom flange yielded and the plastic deformation caused larger deflections.

Figure 5.14 illustrates changes in the bending moment along the beam throughout the exposure. There was no moment at the supports that were not rotationally restrained. The midspan moment started with  $WL^2 / 8$  as for simply supported beam and kept increasing at the start, then decreased when the top flange yielded, all due to the P- $\Delta$  effect (Equation 5.1). The increase and decrease of the moment was governed by the change in either the deflection or the axial force, or both.

When both top and bottom flanges have yielded, the beam did not carry much moment as most of the load was transferred to the supports by catenary action when everywhere along the beam was in tension.



**Figure 5.9 Midspan deflection of pin-pin beam**



**Figure 5.10 Midspan moment of pin-pin beam**

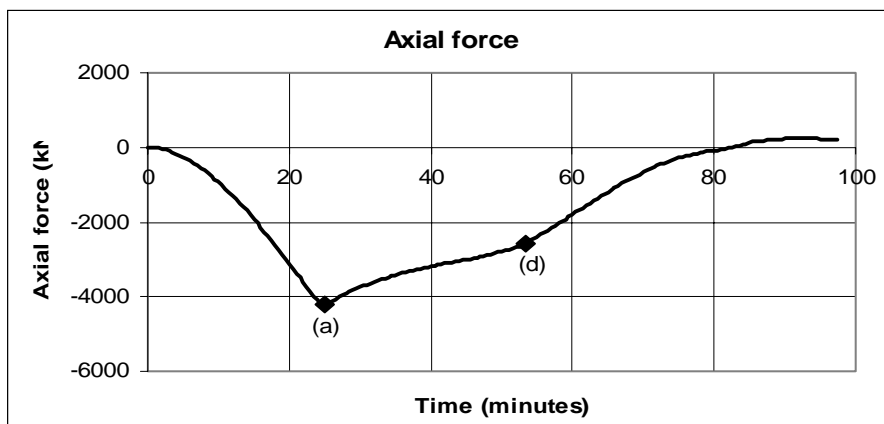


**Figure 5.11 Axial force of pin-pin beam**

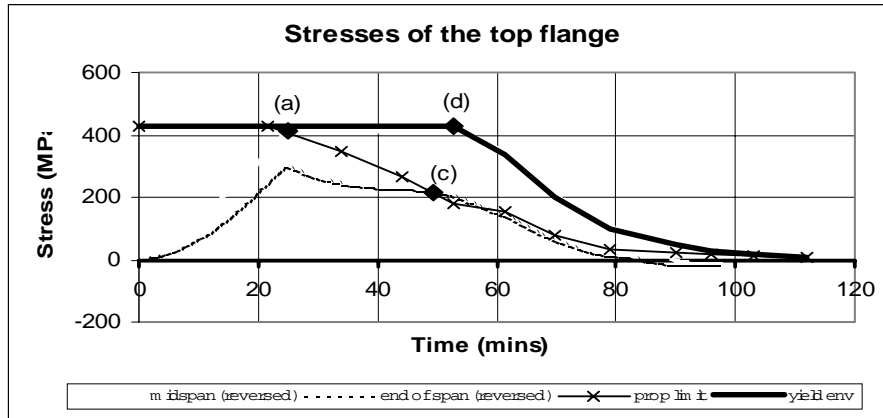


Figure 5.12 Top flange stresses of pin-pin beam

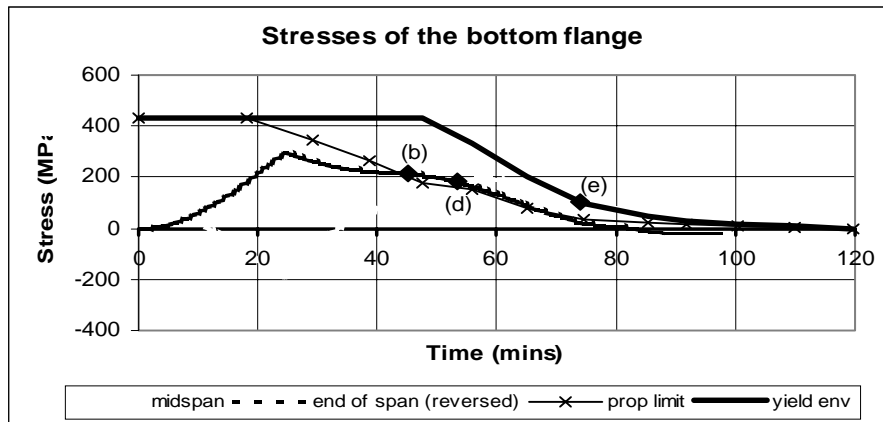


Figure 5.13 Bottom flange stresses of pin-pin beam

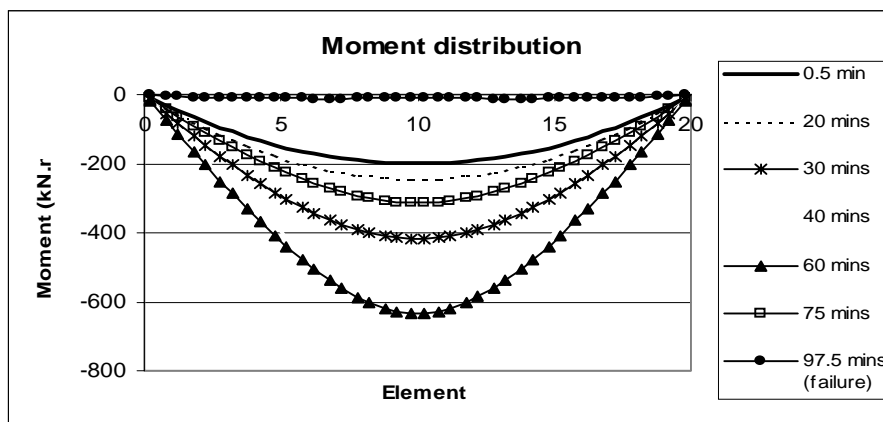


Figure 5.14 Moment distribution along the pin-pin beam

## 5.4 Beam with fix-fix supports

With fully fixed supports at both ends, the beam with fix-fix supports required the development of three plastic hinges to form a failure mechanism as shown in Figure 5.15. The sequence of events is outlined in Table 5.3.

The moment restraint at the supports caused the beam with fix-fix supports to be very sensitive to the stress condition with respect to the proportional limit and the yield that were reduced due to high temperature. This is illustrated in Figures 5.21 and 5.22 that compare the stresses at the top and bottom flanges respectively with the proportional limit and the yield envelope.

**Table 5.3 Time line of events in fix-fix beam**

No.	Events	Time (minutes)
1	Bottom flange at ends of span reached the proportional limit	25
2	Top flange at midspan reached the proportional limit	29.5
3	Bottom flange at midspan reached the proportional limit	37.5
4	Top flange at ends of span reached the proportional limit	48.5
5	Bottom flange at ends of span reached yield	55
6	Top flange at midspan reached yield	63.5
7	Failure mechanism achieved (3 plastic hinges)	88

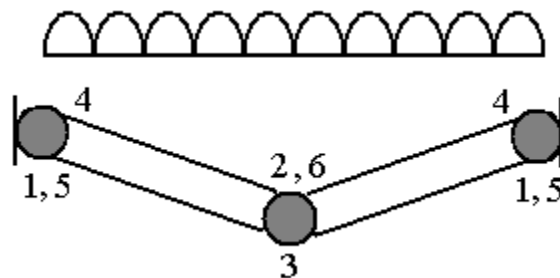


**Figure 5.15 Failure mechanism of fix-fix beam**

Prior to the fire under the given loading, the moments at the midspan and at the ends of the span were  $wL^2 / 24$  and  $wL^2 / 12$  respectively as expected from a static analysis. The beam hardly deflected at the beginning of the fire. Thermal expansion caused development of a compressive axial force and the differential temperature caused a change in the bending moments.

High compressive force caused the bottom flange at the ends of the span to reach the proportional limit at 25 minutes, the beam had more obvious deflection thereafter and the bending moment decreased, marked as point (a) in Figures 5.16 – 5.18, 5.20 and 5.22. As a result, the midspan moment also dropped as it was affected by the compression in the bottom flange.

The neutral axis now shifted up. The web did not carry much of the stresses as it was so thin and heated up very quickly. Most of the stresses would be carried by the flanges which had much bigger thermal mass. Soon the top flange at midspan reached the proportional limit at 29.5 minutes (point (b) in Figure 5.21). The midspan moment grew rather constantly at this point and moment redistribution caused the end moment to compensate for the strength reduction at the midspan indicated by point (b) in Figures 5.17 and 5.18.

When the plastic hinges started to form, the axial force started to drop (point (b) in Figure 5.20) and the deflection continued to increase. The bottom flange at midspan reached the proportional limit at 37.5 minutes but caused no obvious change in the overall behaviour of the beam.

However, when the top flange at the ends of the span reached the proportional limit at 48.5 minutes, the axial load dropped even more and the midspan moment showed a sudden increase as the midspan was carrying more of the load (point (c) in Figure 5.17 and 5.21). The P- $\Delta$  effect was governed by the deflection as the deflection was increasing even though the axial load was reducing (point (c) in Figures 5.16 and 5.20). The pattern observed in the bending

moment plots showed that moment redistribution between the midspan and ends of the span occurred to prevent collapse as long as possible.

The bottom flange at the endspan was the first to yield at 55 minutes after the beginning of the fire, shown in Figure 5.22 as point (d), which slightly altered the endspan moment (point (d) in Figure 5.18). The midspan moment kept on increasing up to 63.5 minutes when the top flange at midspan yielded, indicated as point (e) in Figures 5.17 and 5.21. There was not much strength left in the beam at this stage as three plastic hinges were already developed and the axial force was approaching zero. Unlike the pin-pin case where catenary effect caused the beam to hang in tension, this beam experienced loss of stiffness and strength earlier and failed at 88 minutes.

There was no exact explanation on the moment alterations observed at about 80 minutes apart from that some moment redistribution occurred. It can be seen that the behaviour of the fix-fix beam was very sensitive to the proportional limit and the yield limit of the material.

The moment distribution throughout heating along the beam as illustrated in Figure 5.19 shows that the end moment was always a hogging moment, while the midspan moment was always a sagging moment, except for a brief period about 20 minutes into the fire. The beam started with  $WL^2 / 12$  at the supports and  $WL^2 / 24$  at the midspan as the beam had moment resisting supports, and was changing upon fire exposure due to the P- $\Delta$  effect and thermal bowing.

At failure when three plastic hinges have developed and the axial force is almost zero, the midspan moment was equal to the end moment of  $wL^2 / 16$  as both had the same flexural capacity, with no more contribution from the P- $\Delta$  effect.

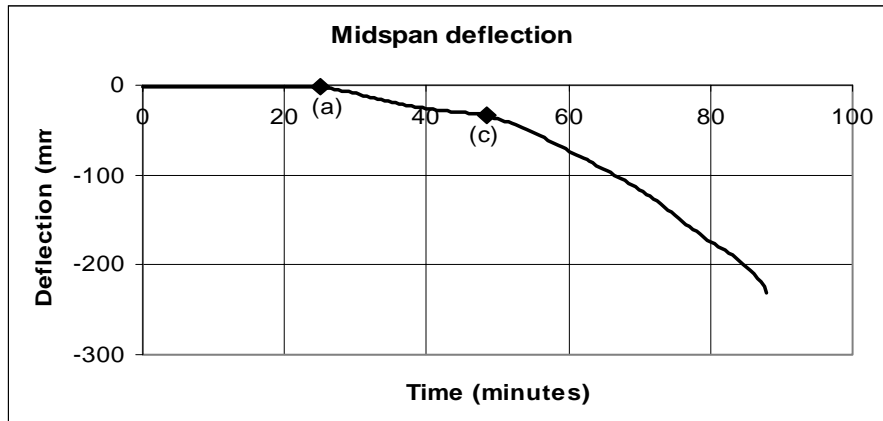


Figure 5.16 Midspan deflection of fix-fix beam

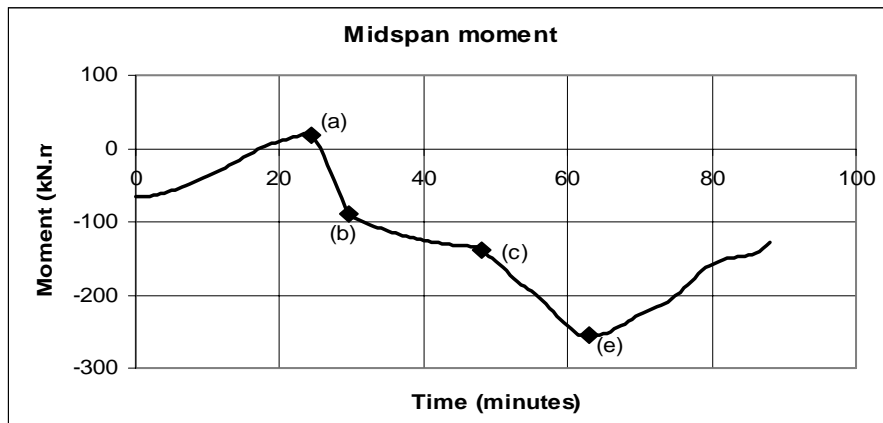


Figure 5.17 Midspan moment of fix-fix beam

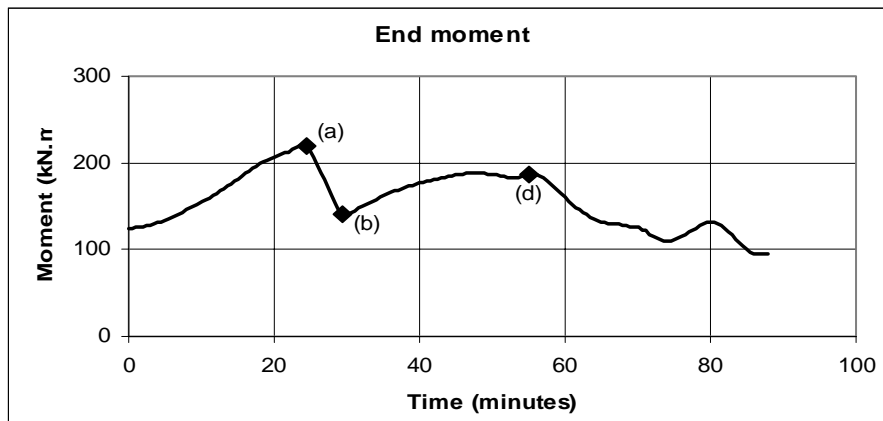


Figure 5.18 End moment of fix-fix beam

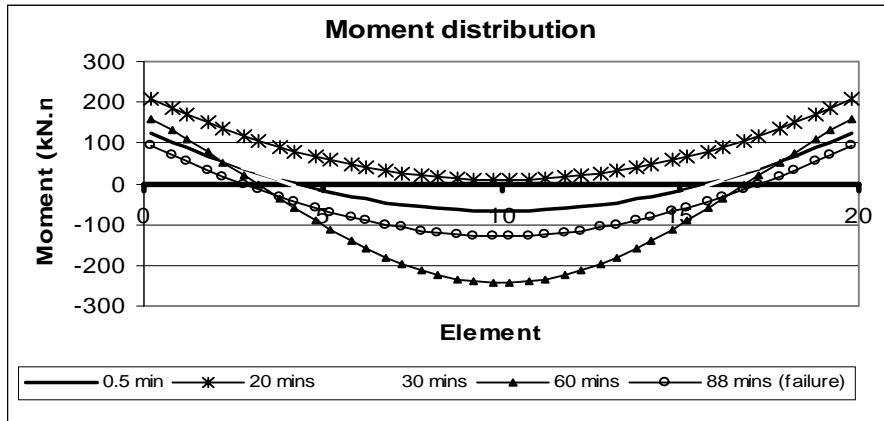


Figure 5.19 Moment distribution along the fix-fix beam

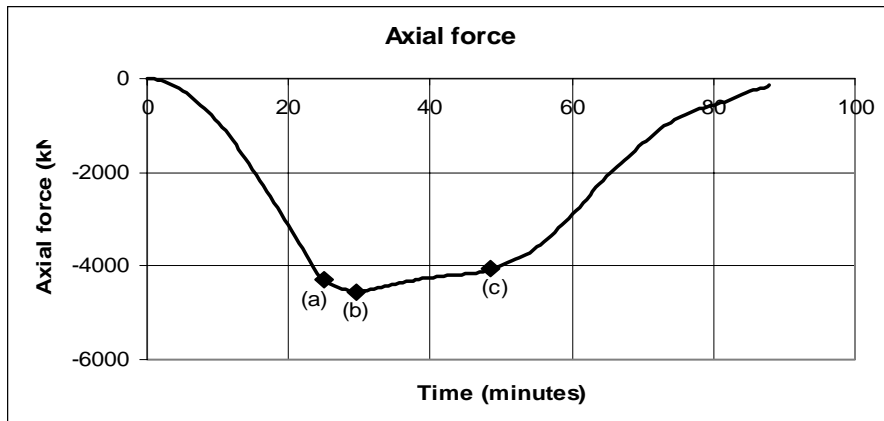


Figure 5.20 Axial force of fix-fix beam

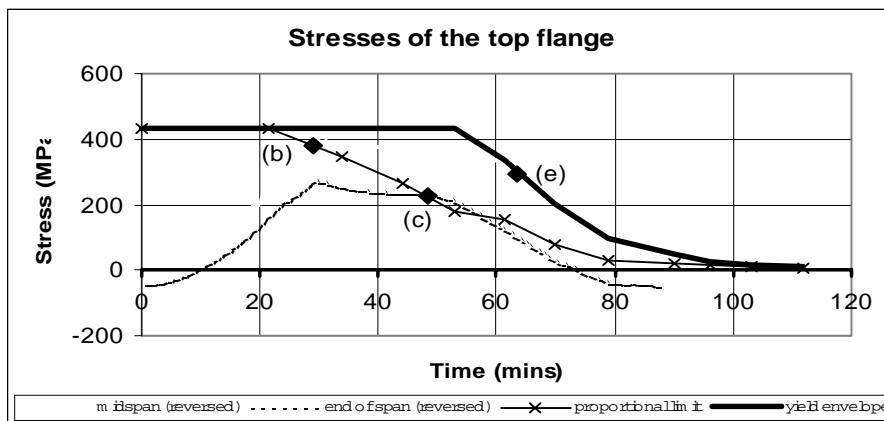
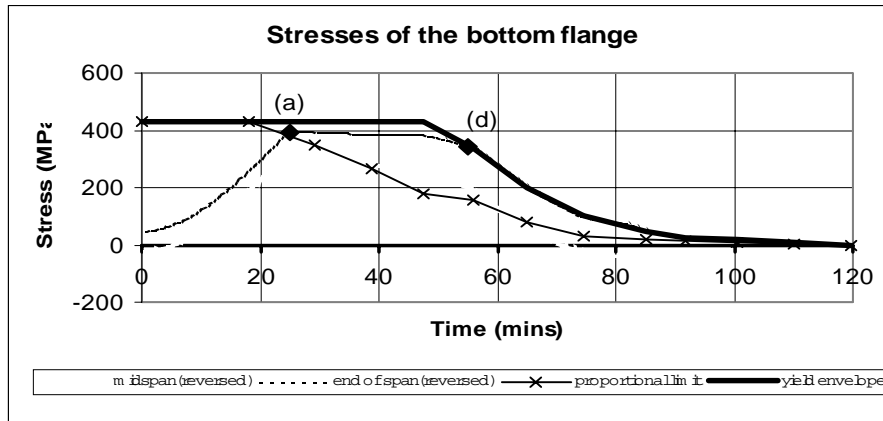


Figure 5.21 Top flange stresses of fix-fix beam



**Figure 5.22 Bottom flange stresses of fix-fix beam**

## 5.5 Beam with fix-slide supports

The beam with fix-slide supports needed three plastic hinges to form a failure mechanism. The beam was free to elongate and therefore there was no axial force induced as a result of thermal expansion as found in the pin-pin and fix-fix cases. For the first hour of fire exposure the beam behaved elastically with minimum deflection. Thereafter a sequence of events as mentioned below occurred consecutively.

**Table 5.4 Time line of events in fix-slide beam**

No.	Events	Time (minutes)
1	Top flange at ends of span reached the proportional limit	66
2	Bottom flange at ends of span reached the proportional limit	69
3	Bottom flange at midspan reached the proportional limit	77
4	Top flange at midspan reached the proportional limit	84
5	Bottom flange at ends of span reached yield	85
6	Top flange at ends of span reached yield	89
7	Top flange at midspan reached yield	90
8	Bottom flange at midspan reached yield	90
9	Failure mechanism achieved (3 plastic hinges)	90.5

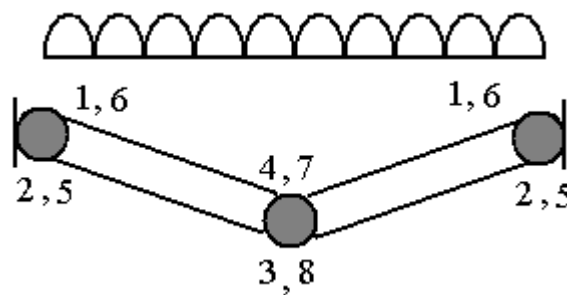


**Figure 5.23 Failure mechanism of fix-slide beam**

Figure 5.27 shows the evolution of the bending moment diagram throughout heating. It can be seen that the overall shape of the bending moment was unchanged. The negative moment at the ends of the beam increased during the first 40 minutes due to thermal bowing. The thermal bowing then decreased as the temperature gradient decreased, causing the end moments to drop. The midspan moment changed accordingly, because the sum of midspan and end moments at any given time must be equal to  $wL^2 / 8$  for any beams without axial forces. At the time of failure, the midspan and end moments were equal to  $wL^2 / 16$  as plastic hinges formed.

At 66 minutes, the top flange at the endspan reached the proportional limit, followed shortly three minutes later by the bottom flange, marked as points (a) and (b) in Figures 5.28 and 5.29 respectively. By this time the deflection started to be noticeable. The bottom flange and the top flange at the midspan reached the proportional limit at 77 and 84 minutes respectively (points (c) and (d) in Figures 5.29 and 5.28).

The bottom flange at the ends of the span yielded at 85 minutes of exposure (point (e) in figure 5.29) and the top flange at 89 minutes (point (f) in Figure 5.28). The elastic modulus of the beam had reduced significantly and when the top and bottom flanges at the midspan yielded at the same time at 90 minutes (point (g) in Figures 5.28 and 5.29), runaway deflection occurred failing the beam 30 seconds later.

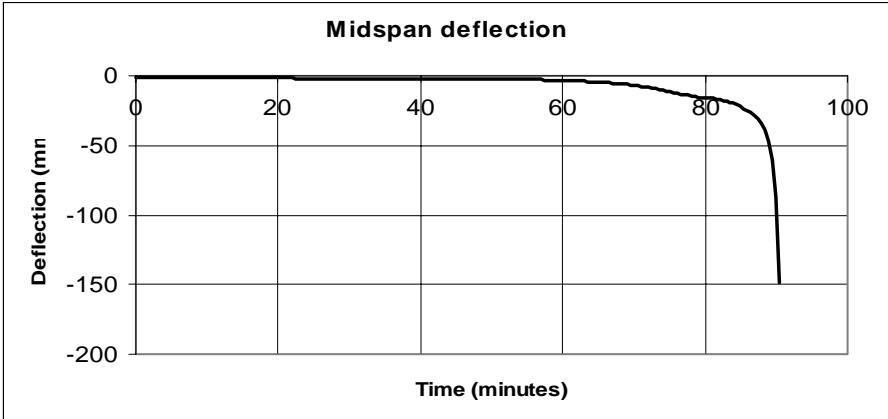


Figure 5.24 Midspan deflection of fix-slide beam

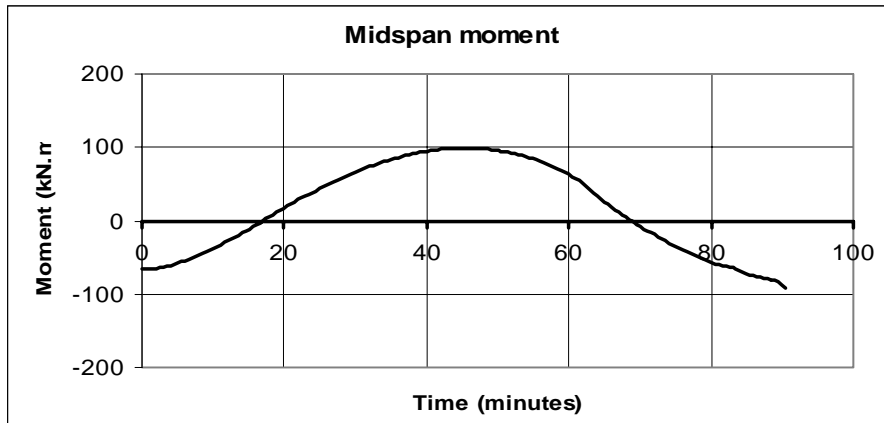


Figure 5.25 Midspan moment of fix-slide beam

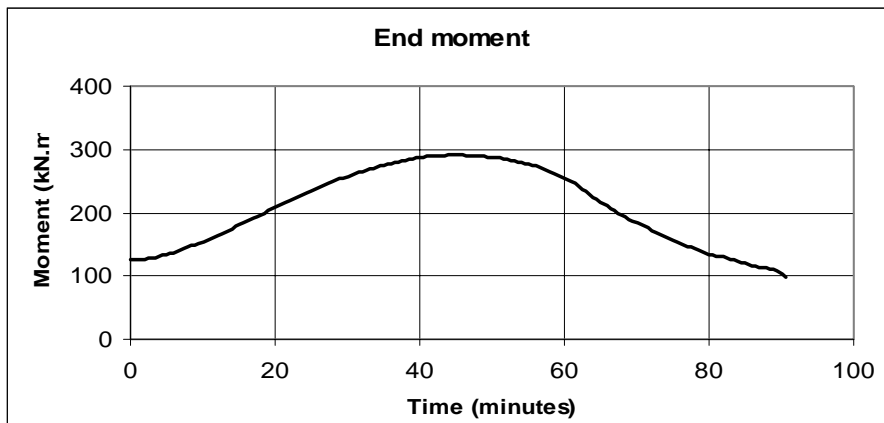


Figure 5.26 End moment of fix-slide beam

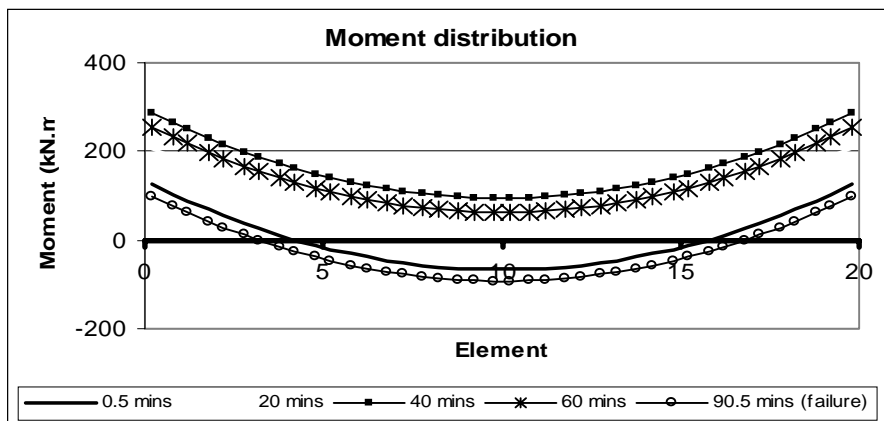
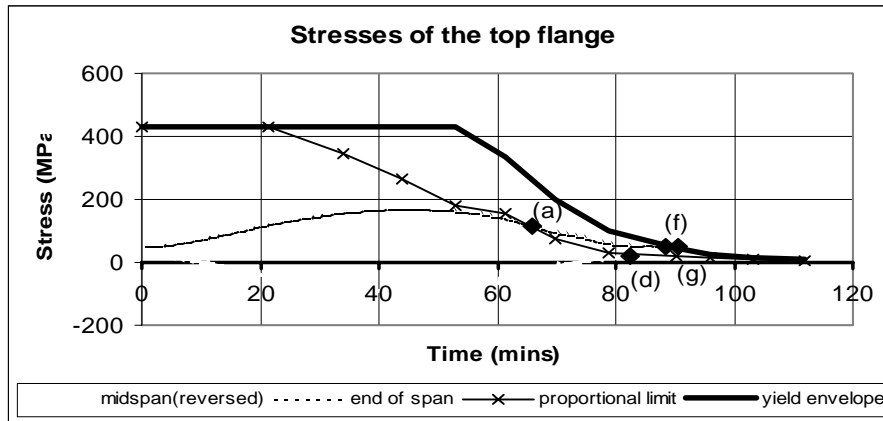
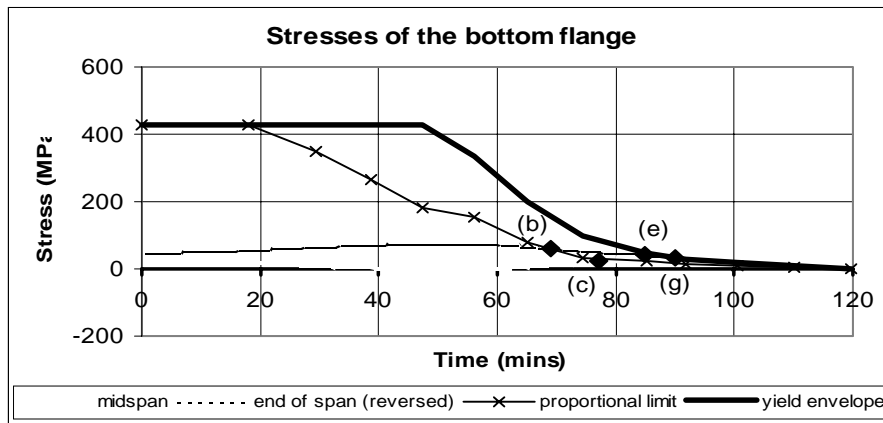


Figure 5.27 Moment distribution along the fix-slide beam



**Figure 5.28 Top flange stresses of fix-slide beam**



**Figure 5.29 Bottom flange stresses of fix-slide beam**

## 5.6 Comparison with critical buckling

The failure mechanism of beams that are sufficiently compact is usually by the forming of plastic hinges at the critical locations. On the other hand, slender beams will buckle under the axial stress before the material reaches its yield stress as explained by Rotter and Usmani (2000). This phenomenon is observed in cases where the beam is axially restrained against thermal expansion such as the beam with the pin-pin end conditions, allowing the development of high compressive force which the beam fails to sustain.

The Cardington test results showed that local buckling had occurred in nearly all of the tests. As described in the report published by the British steel (1999), most of the buckling occurred around the area of the connection between beams and columns.

The SAFIR analyses were two dimensional, therefore the beam was assumed to be laterally restrained and the beam buckling was only possible about the strong axis. Local buckling is not an issue, as it is not modelled in the beam element analysis in SAFIR. It is only taken into account in a shell element analysis.

The axial force on the pin-pin and fix-fix beam experienced some alteration during the fire exposure due to subsequent events, and the investigation on whether or not buckling was one of the causes was considered necessary.

Using the Euler formula (Equation 2.28) with reduction in modulus of elasticity (Equation 2.14), the critical buckling load was obtained with respect to time showing the reduction in the beam capacity.

Figure 5.30 shows the comparison between the axial force induced in the pin-pin beam from the SAFIR analysis and the critical buckling load from the Euler formula. The upper curves are the axial force induced in the pin-pin and fix-fix beams obtained from the SAFIR output, with the negative sign indicating compression. The bottom line is the critical buckling load. It

is obvious that the axial force induced was nowhere near the critical buckling load until the end of the analysis and therefore member buckling did not occur in the beams analysed. This is a separate item to local flange buckling which may have occurred in the plastic hinge regions, due to large plastic rotations.

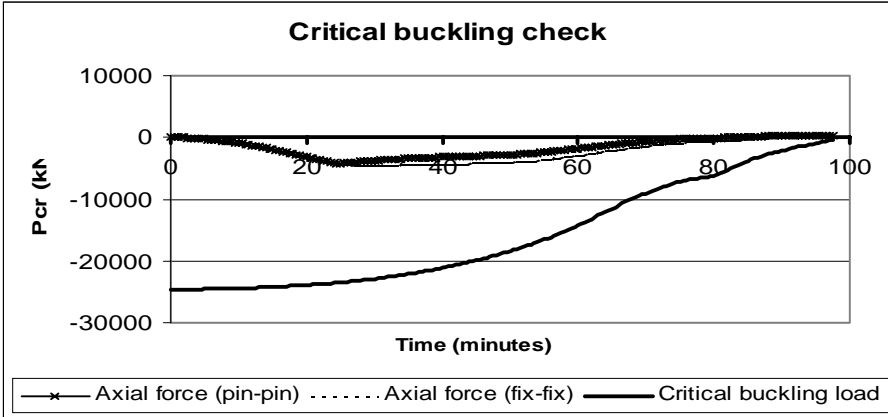


Figure 5.30 Comparison between the axial load and the critical buckling load

## **5.7 Conclusions**

Based on the above analyses, some important aspects can be concluded regarding the behaviour of beams with four different support conditions under a given loading and fire exposure.

### **5.7.1 Simply supported beams**

Simply supported beams are not restrained against rotation at the supports. At ambient conditions, the applied loading causes larger initial deflection compared with the moment resisted beams due to this end rotation. Elevated temperature causes the beam to lose its stiffness and elasticity resulting in the forming of one plastic hinge at the midspan and failure mechanism occurs.

#### **Pin-roller beam**

The ideal pin-roller beam is unrealistic. Real structural members have axial restraint to some degree. Upon heating, pin-roller beam is free to elongate and there is no axial force induced in the beam due to thermal expansion. The bending moment along the beam stays constant, being only due to the static load. Deflection of a pin-roller beam gradually increases due to the loss of strength in the steel. When the plastic hinge has developed, the beam has lost most of its strength and the deflection greatly increased, pulling the roller support closer to the pin support, known as the runaway failure. Compared with the other three beams with different supports investigated, a pin-roller beam fails the earliest.

#### **Pin-pin beam**

The axial restraint in the pin-pin beam prevents the beam from expanding. Thermal expansion causes large axial force along the beam resulting in greater deflection. The forming of the plastic hinge at the midspan causes reduction in the axial load as the deflection increases. Approaching failure, when the loss of stiffness overwhelms the beam performance, the load is supported by the catenary action as the whole beam is in tension.

### **5.7.2 Moment resisting supported beams**

A beam with moment resisting supports is not free to rotate at its ends. As a result, it has less initial deformation due to the applied loading. The forming of the plastic hinge at the midspan alone will not cause failure to beams with this type of supports. Additional plastic hinges at the ends of the span are required to form a failure mechanism.

#### **Fix-fix beam**

This beam is fully fixed at both ends. Thermal loading induces a great amount of axial force within the beam. This high compressive force soon brings the ends of the span to yield, the axial force slowly reduces and the deflection starts increasing. The behaviour of the fix-fix beam is found to be very sensitive to the stresses reaching the proportional limit or the yield stress.

Greater deflection eventually forms a plastic hinge at the midspan, which reduce the axial force considerably with increasing deflection. Fix-fix beam fails earlier than the pin-pin beam without as much deflection.

#### **Fix-slide beam**

In a fix-slide beam, thermal expansion has no significant effect, as the beam is free to expand. This fact, together with the moment resisting supports result in a minimum deflection for a considerable period of time into the fire. The moments at both midspan and ends of the span increase due to thermal bowing and then decrease as there is no more thermal gradient along the cross section at later time when the section temperature is roughly uniform.

As there is no  $P-\Delta$  effect in a fix-slide beam, the shape of the bending moment is constant throughout the fire exposure. Three plastic hinges form due to reduction in the steel strength leading to runaway failure shortly after the failure of the fix-fix beam.

## 6. Effect of a spring at the support

As mentioned earlier in section 4.3.4, the pin-roller and pin-pin supports are not common in real structures. Most of the members in steel frames are joined with some degree of axial restraint. A spring was introduced at one of the supports to model this situation, with the stiffness of the spring,  $k$  being a fraction of the stiffness of the steel beam. That means when  $k=1$ , the restraint provided from the spring to the beam is the same as if another beam with the same stiffness is placed right next to it.

### 6.1 Spring stiffness between 0 and 1

This section compares the beam behaviour when the spring introduced has stiffnesses between 0, which is equal to pin-roller condition, and 1, as if another beam with same stiffness is present. The results are set out in Figures 6.1 to 6.3.

Using the stiffness range from 0 to 1, it is observed that for  $k=0.1$ , the behaviour of the beam was very similar to the early stage of the pin-roller condition. A big jump was obvious in all graphs presented in that when  $k=0.2$  or higher, the reactions in the beam were almost exactly the same as in the pin-pin condition. However, when a spring was introduced, the beams failed at about 40 minutes irrespective of the value of  $k$ . This was considered to be a numerical problem in SAFIR analysis, rather than physical failure.

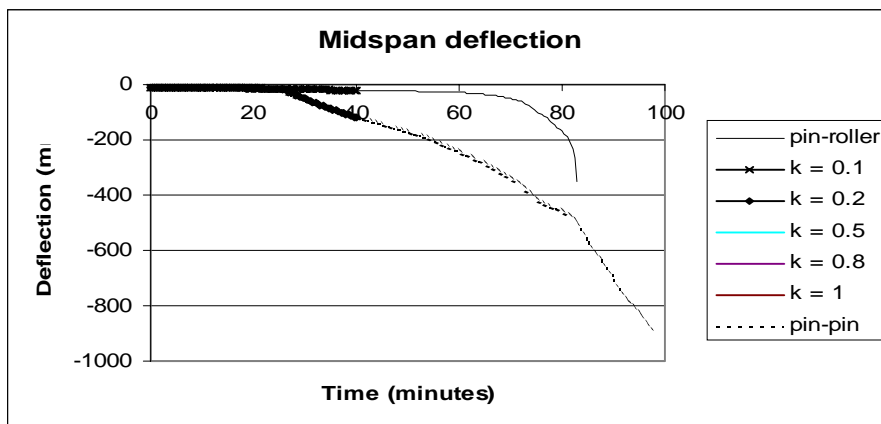


Figure 6.1 Midspan deflection with spring stiffness between 0 and 1

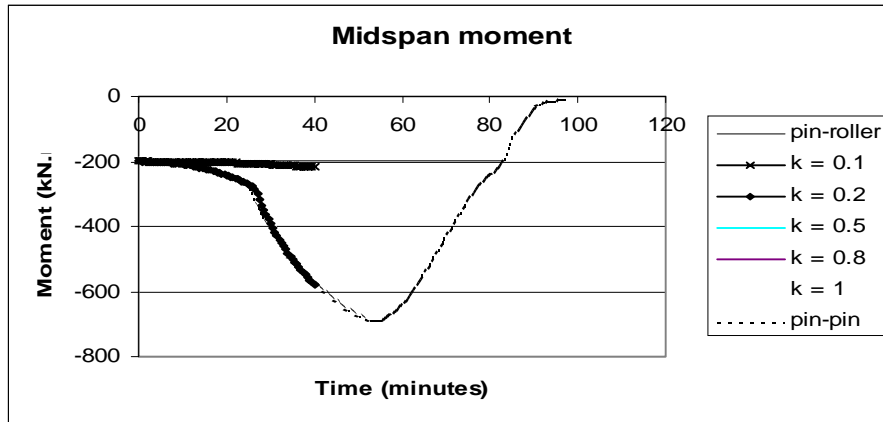


Figure 6.2 Midspan moment with spring stiffness between 0 and 1

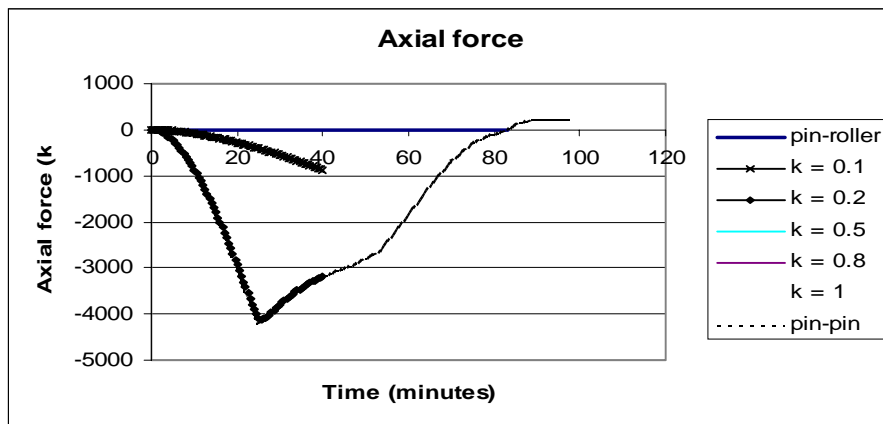


Figure 6.3 Axial force with spring stiffness between 0 and 1

## 6.2 Spring stiffness between 0 and 0.1

Considering only axial stiffness values between  $k=0$  and  $k=0.1$ , it can be seen that beams with various  $k$  values within this range have the same deflection pattern as the pin-roller support case although those with an axial spring fail sooner as discussed in the previous section.

The bending moment and the axial force however showed very even changes in proportion with the changes in  $k$  over this range, which was expected and self-explanatory.

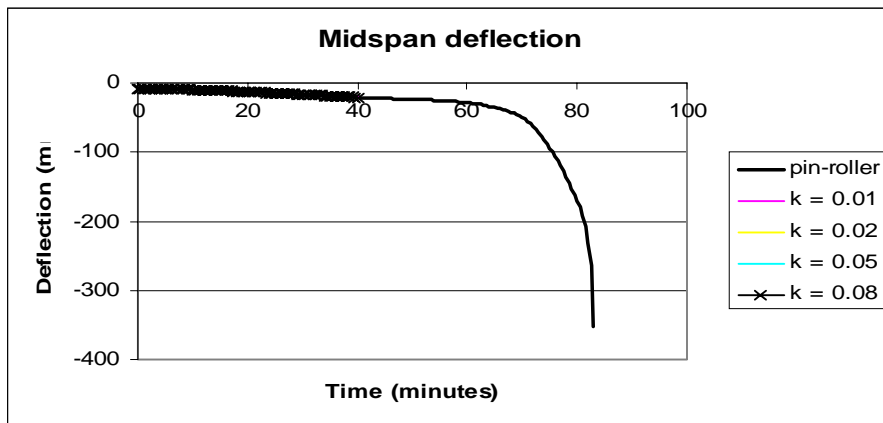


Figure 6.4 Midspan deflection with spring stiffness between 0 and 0.1

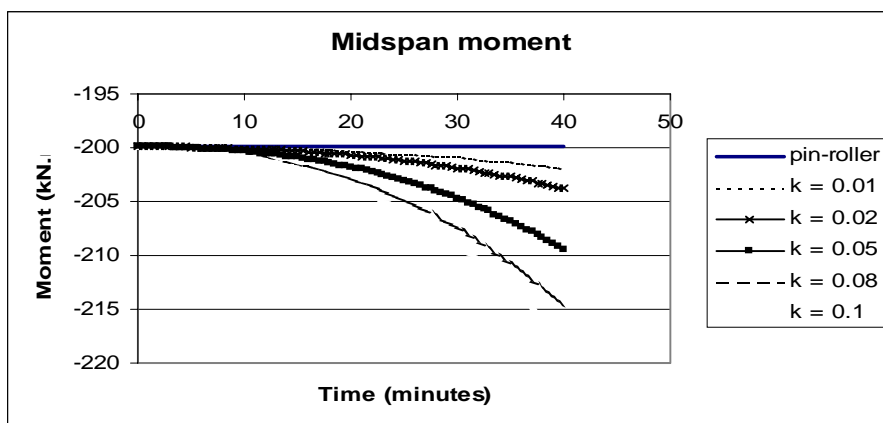


Figure 6.5 Midspan moment with spring stiffness between 0 and 0.1

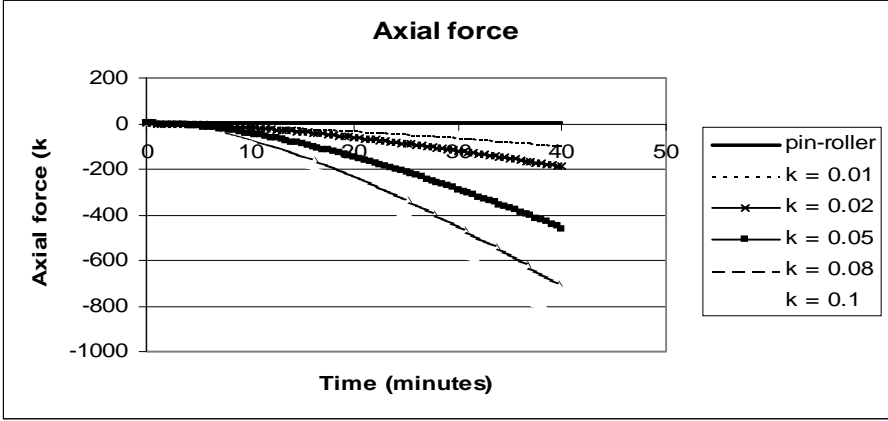


Figure 6.6 Axial force with spring stiffness between 0 and 0.1

### 6.3 Spring stiffness between 0.1 and 0.2

In this section, the effects of spring with  $k$  varying from 0.1 to 0.2 are investigated regarding the rather unusual behaviour observed in section 6.1. While the distribution was very even for  $k$  between 0 and 0.1, there seems to be a big change from  $k=0.1$  to 0.2 while there is no change in behaviour when  $k=0.2$  and higher.

The deflection plot in Figure 6.7 suggested the same pattern occurred for  $k=0.1$  up to 0.195. Figures 6.8 and 6.9 show an even distribution over this range, but the tiny increment from  $k=0.195$  to 0.2 showed otherwise.

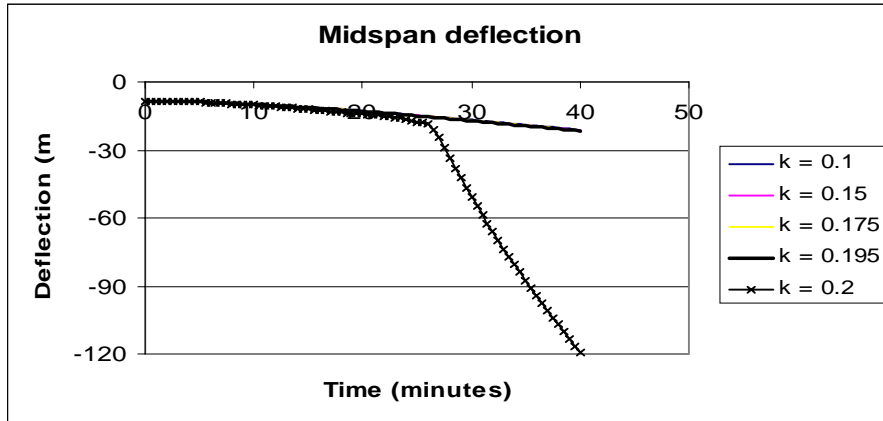


Figure 6.7 Midspan deflection with spring stiffness between 0.1 and 0.2

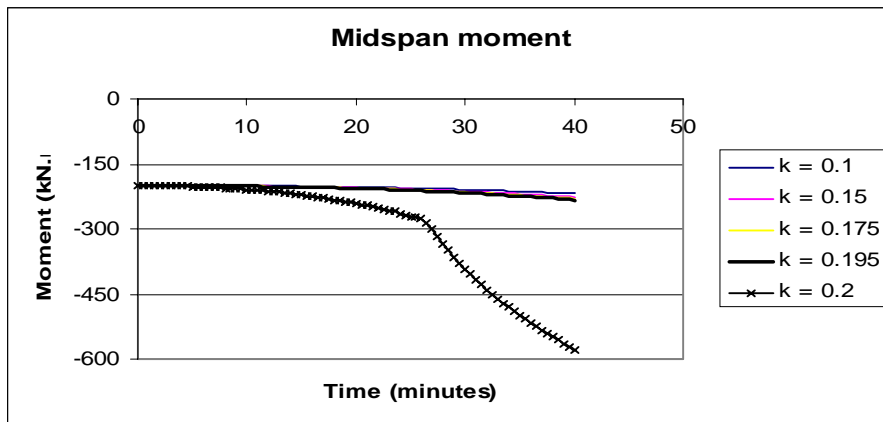


Figure 6.8 Midspan moment with spring stiffness between 0.1 and 0.2

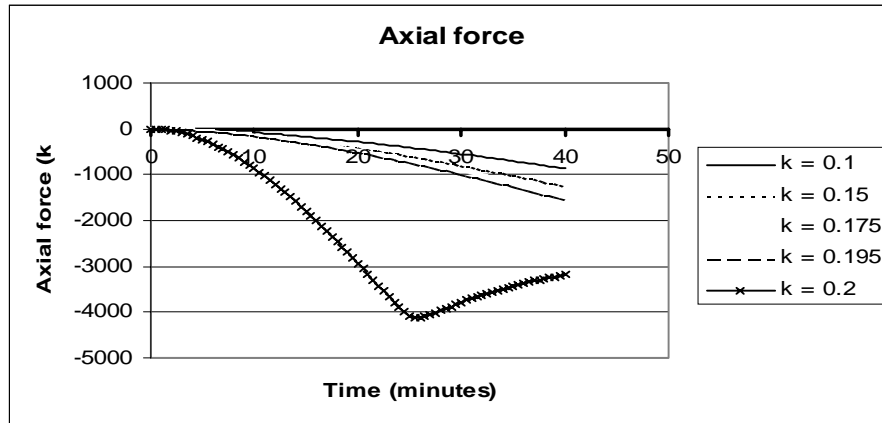


Figure 6.9 Axial force with spring stiffness between 0.1 and 0.2

The stress check proved the top flange has not yielded at time of failure and the bottom flange stress was nowhere near the proportional limit. The big jump at a stiffness of 0.2 is rather unexplainable and may well be due to compounding numerical error in the stiffness matrix. Welsh (2001) has also encountered similar problem for certain arrangements of the structure. The program was seen to terminate when both top and bottom stresses reach the proportional limit at the same time.

## **7. Comparison between different applied fires**

### **7.1 Linear heating rates**

Analyses of the beam responses using faster heating rates showed that the behaviour pattern of the four support conditions is very similar. The pin-pin case was chosen to illustrate the comparison.

It is observed in Figure 7.1 that the behaviour trend was very much the same for the 10, 20, and 30°C/minute heating rates with respect to temperature, taking the midspan deflection as an example. This shows that no matter how fast a beam is heated, it will fail at the same temperature when it loses its strength.

In respect to time, however, faster heating failed the beam sooner, as expected. Figures 7.2 to 7.4 illustrate the development of the deflection, bending moment, and axial force for the three different heating rates, with each one showing similar trends.

A faster heating rate caused higher thermal gradient along the cross section of the beam. This caused the beam to fail not only faster but also without as great a deflection. A slower rate allowed the temperature in the beam to be more uniform and hence better development of plastic hinges.

When the beam experienced plastic deformation, greater deflection but lower moment was found. Figure 7.4 shows that for 10 and 20°C/minute heating, the beam was in tension at time of failure, while the 30°C per minute heating failed the beam when it was still in compression, as a result of the plastic hinge not becoming fully developed.

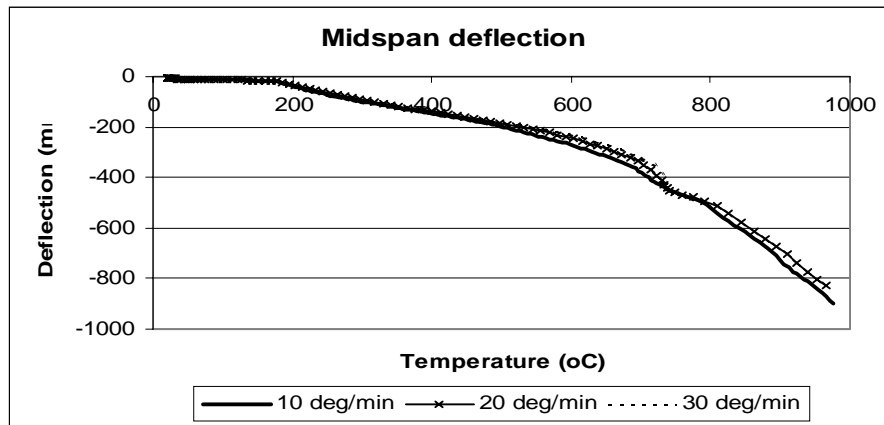


Figure 7.1 Midspan deflection of pin-pin beam with respect to temperature

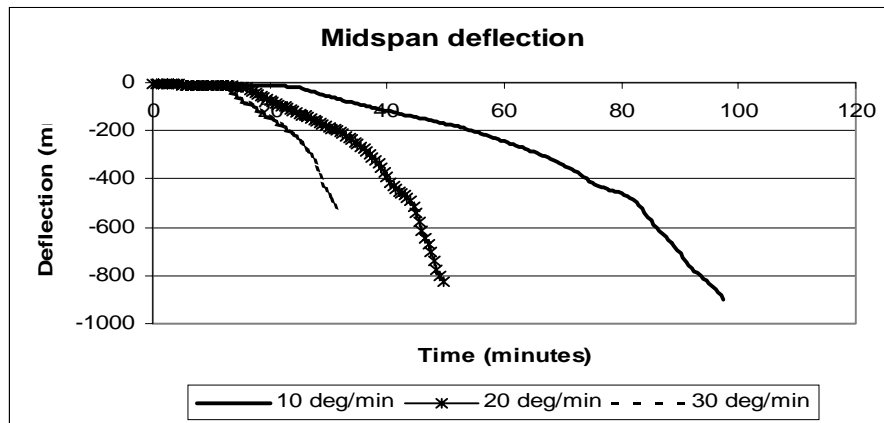


Figure 7.2 Midspan deflection of pin-pin beam under various linear heating rates

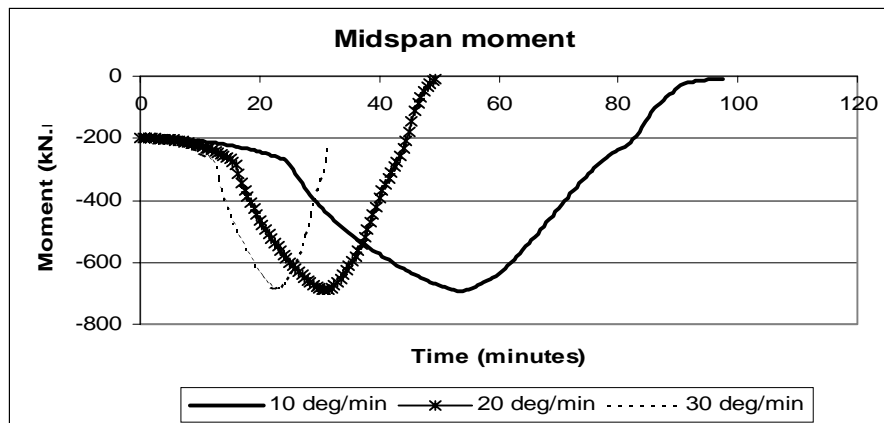


Figure 7.3 Midspan moment of pin-pin beam under various linear heating rates

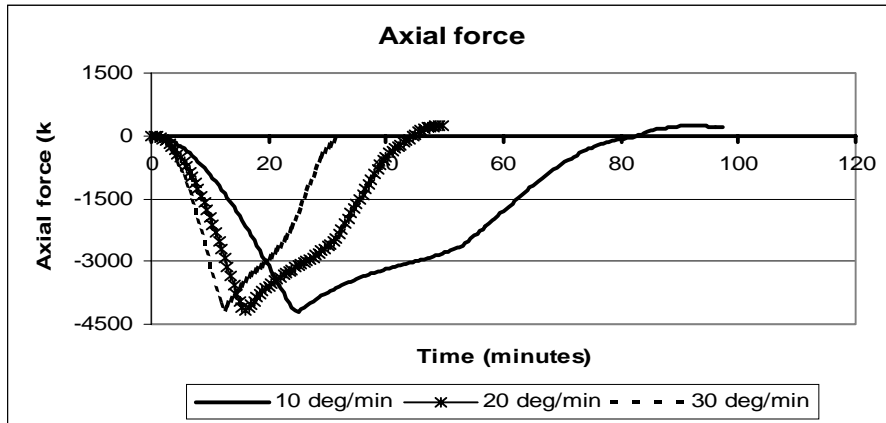


Figure 7.4 Axial force of pin-pin beam under various linear heating rates

## 7.2 ISO fire

The observation on the ISO fire exposure illustrated in Figure 7.5 shows very similar deflection patterns as the exposure to the 10°C/minute heating rate (refer to Figure 5.1). The beams in both cases were heated on three sides. From these two figures, it is shown that steel beams fail in a certain temperature range roughly around 800-900°C regardless of the type of the supports and the duration of the fire.

The ISO fire exposed beams, however, failed at slightly lower temperatures than those exposed to the slower 10°C/minute heating rate due to high thermal loading creating high thermal gradient and thermal bowing in the cross section.

The fix-slide beam lasted the longest as it could expand and form three plastic hinges in contrast with the pin-pin beam which soon developed large deflection and quickly lost its stiffness due to the rapid heating and failed on the forming of one plastic hinge.

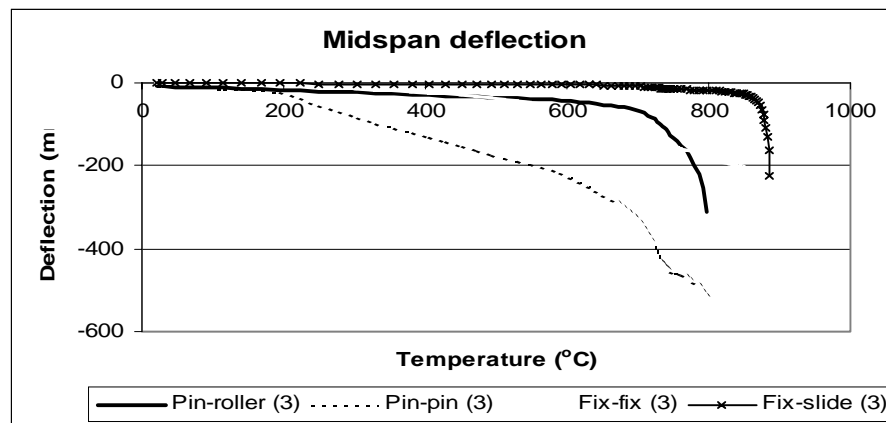


Figure 7.5 Midspan deflection of beams exposed to ISO fire

For the discussion in this section, the behaviour patterns of the pin-pin beam exposed to the ISO fire are compared to the ones exposed to the 10°C/minute heating rate. Figure 7.6 shows the deflection patterns with respect to temperature that are very close for both fires. The ISO fire exposed beam, however, failed sooner with less deflection due to high thermal gradient as explained above.

Figure 7.7 shows the same deflections but with respect to time. It is obvious that the ISO fire exposure caused the beam to fail much earlier with much less of a deflection due to the rapid forming of the plastic hinge at the midspan. There was not much catenary action observed in the beam prior to failure based on the bending moment plot in Figure 7.8. Slower heating rate allowed more catenary action towards failure when the beam was sagging like a rope and the whole length of the beam was in tension. Figure 7.9 shows the axial force in the beam heated with 10°C/minute rate ended up being in tension. The overall behaviour, however, is very similar for both exposures, only on different time scales.

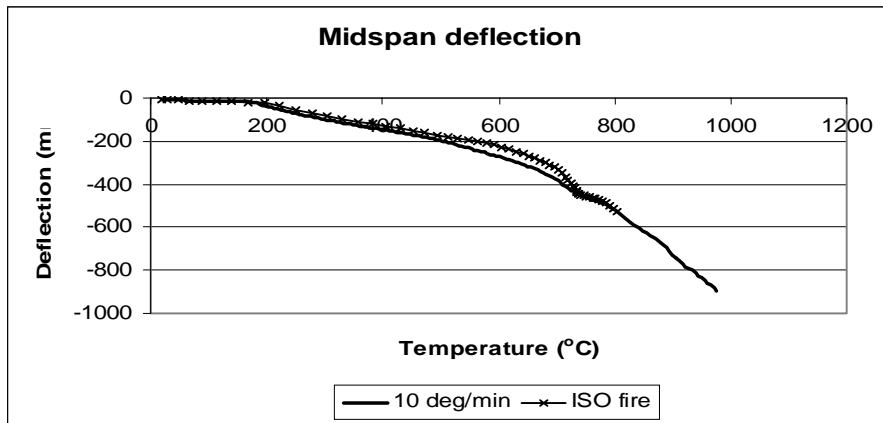


Figure 7.6 Comparison of midspan deflection of pin-pin beam

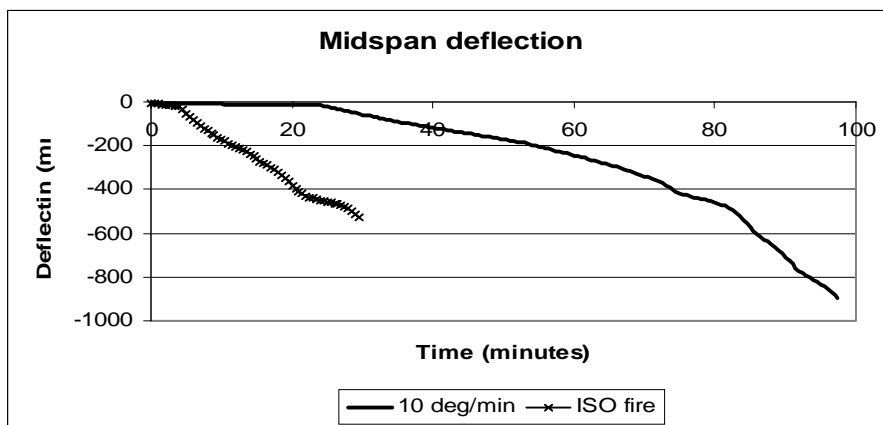


Figure 7.7 Midspan deflection of pin-pin beam exposed to 10°C/minute heating and ISO fire

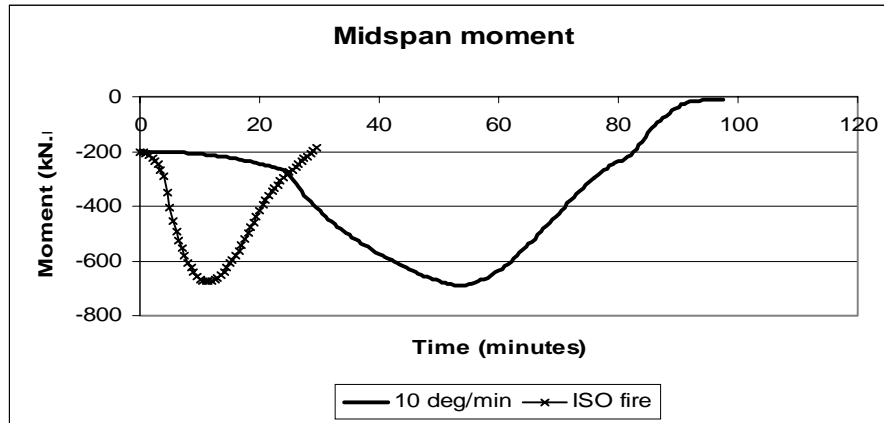


Figure 7.8 Midspan moment of pin-pin beam exposed to 10°C/minute heating and ISO fire

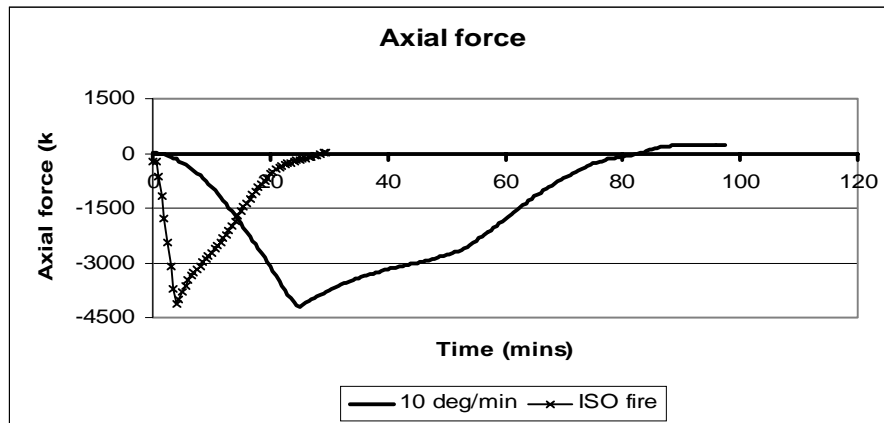


Figure 7.9 Axial force of pin-pin beam exposed to 10°C/minute heating and ISO fire

Figures 7.10 and 7.11 show the stresses at the midspan of the pin-pin beam exposed to the standard ISO fire. It can be seen that at roughly the first five minutes into the fire, the stress at the top flange had reached the proportional limit, very close to the yield envelope. Upon yielding it followed the yield line up to failure at about half an hour of exposure.

The bottom flange was in compression at the start of the fire and changed into tension when the top flange reached the proportional limit. The trend for the bottom flange stress was not very much affected by the proportional limit. The bottom flange yielded at about 20 minutes and then followed the yield envelope to failure.

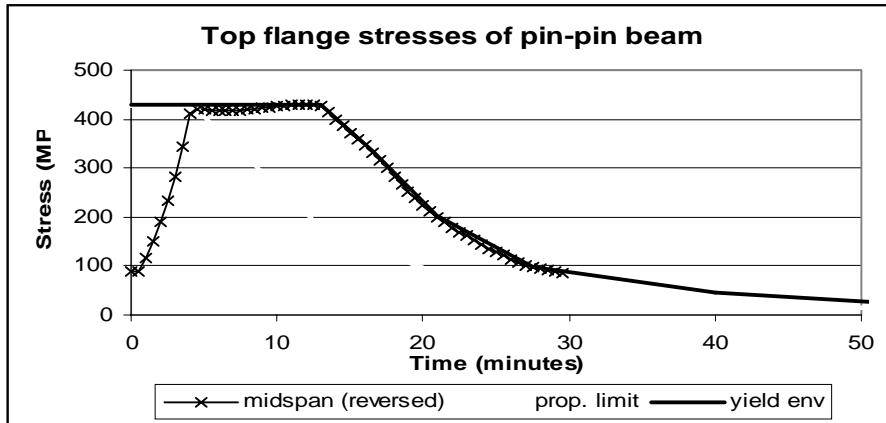


Figure 7.10 Top flange stresses of pin-pin beam exposed to ISO fire

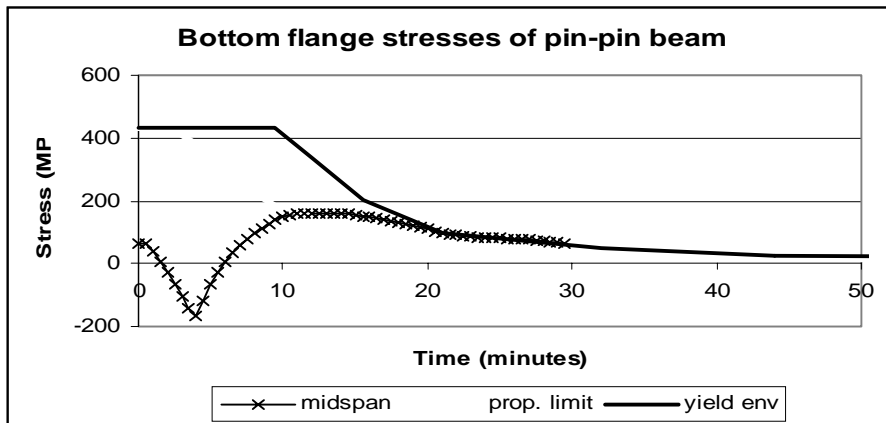


Figure 7.11 Bottom flange stresses of pin-pin beam exposed to ISO fire

### 7.3 Parametric fire

A more realistic fire with a decay phase was applied on three sides of the beam. The ISO fire analysis showed that the beams with different support conditions failed at different times after 25 minutes. It is important to understand what would happen to the beam if the fire started to decay before the beams fail as this is the case in most of the realistic fire situations.

For the chosen parametric fire as illustrated in Figure 4.5, a twenty minute burning period was adopted where the fire grew following the ISO fire curve and then decayed at  $625^{\circ}\text{C}$  per hour as defined according to the Eurocode reference decay rate (EC1, 1994) as shown in Figure 2.17.

Shown below in Figures 7.12 and 7.13 are the deflection and bending moment patterns of four beams with different support conditions subjected to this ISO fire with a decay phase. For the first 20 minutes, which represented the burning period following the ISO fire curve, the deflections were exactly the same as those in section 7.2.

When the fire decayed, the deflections recovered. The fix-slide beam that had very little deflection even after 20 minutes into the ISO fire, recovered completely to the deflection at ambient condition, because no plastic hinge had formed during the 20 minutes of burning.

The other three beams had permanent deformations because the stresses reached the proportional limit at the burning period and plastic hinges started to form. In the pin-pin case where there was no rotational restraint at the supports and the beam had large deformation and yielded fairly quickly, the permanent deformation was much more obvious.

The moment of the pin-roller beam stayed constant as expected, while the fix-fix and fix-slide moments varied due to yielding, compression by thermal elongation and tension during the cooling phase. The pin-pin case in particular is discussed below in more detail and compared with the failure of the beam exposed to the ISO fire as discussed in the previous section.

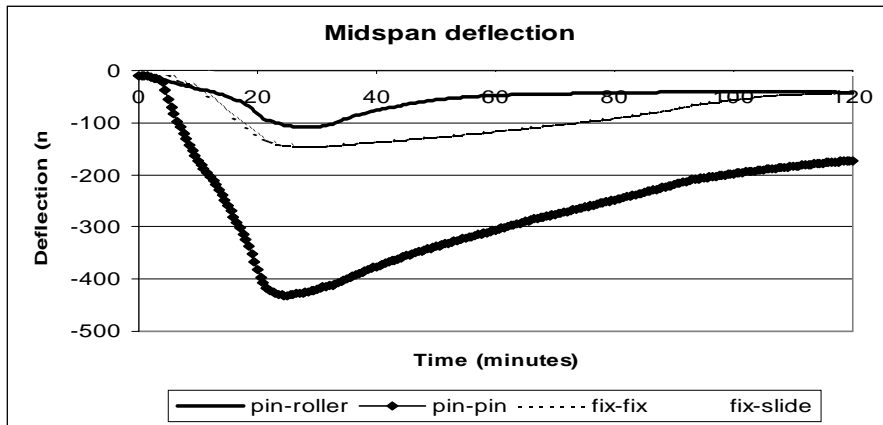


Figure 7.12 Midspan deflection of all beams subjected to a parametric fire

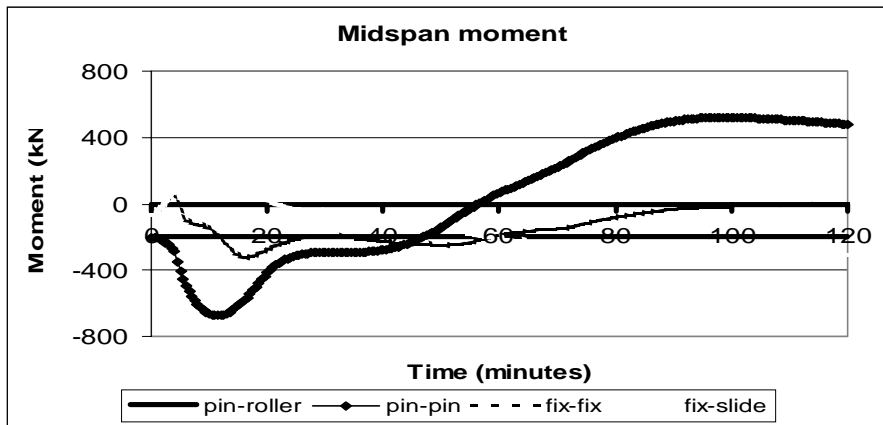


Figure 7.13 Midspan moment of all beams subjected to a parametric fire

It can be seen from Figure 7.14 that after 20 minutes when the fire temperature started to reduce, the beam deflection recovered to a certain permanent deformation. Figures 7.15 and 7.16 show bending moment diagram and the axial force. The analysis was terminated at 120 minutes, as what happened thereafter was not a matter of interest.

At the start of the cooling phase, the axial force stayed constant for a period of time, as there was no increase in temperature in the beam, therefore limiting the thermal expansion effect. This plateau indicated the thermal lag experienced by the steel beam. The cooling process in the beam did not occur straight away as the fire decayed. The P- $\Delta$  action was governed by the axial force causing the bending moment to stay constant up to about 40 minutes.

Upon cooling, the thermal expansion recovered and the beam was now in tension as it pulled back in due to shrinkage (Figure 7.16). This tension force was very large and it could be a big problem for the connections. This issue was discussed by Rotter et al. (1999) that plastification of the steel beam leads to very high tensile stresses that may cause rupture damage to the connections after cooling. The connections have to be strong in tension, or very ductile to avoid this failure, which is opposite to the common assumption that connection would be in compression due to thermal expansion.

The bending moment at the cooling phase followed the trend of the axial force resulting in very high hogging moment, shown in Figure 7.15.

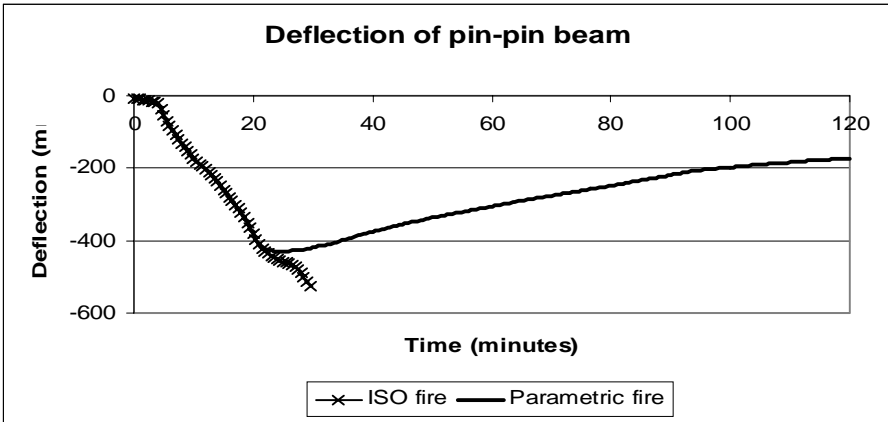


Figure 7.14 Deflection of pin-pin beam subjected to ISO and Parametric fires

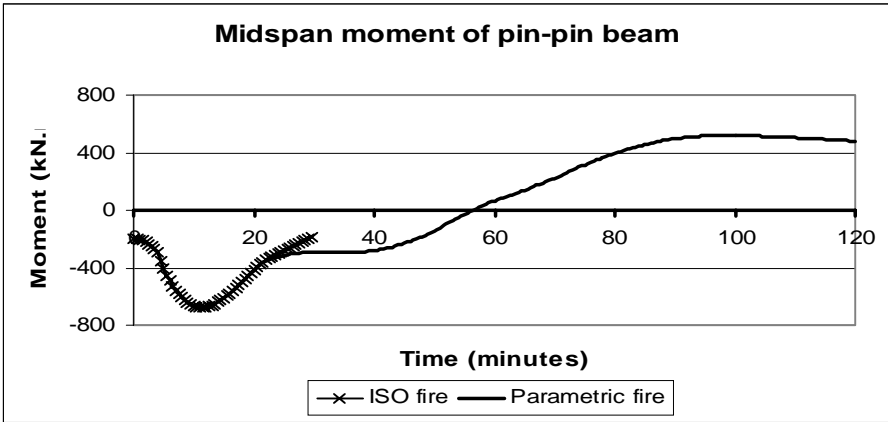


Figure 7.15 Midspan moment of pin-pin beam subjected to ISO and Parametric fires

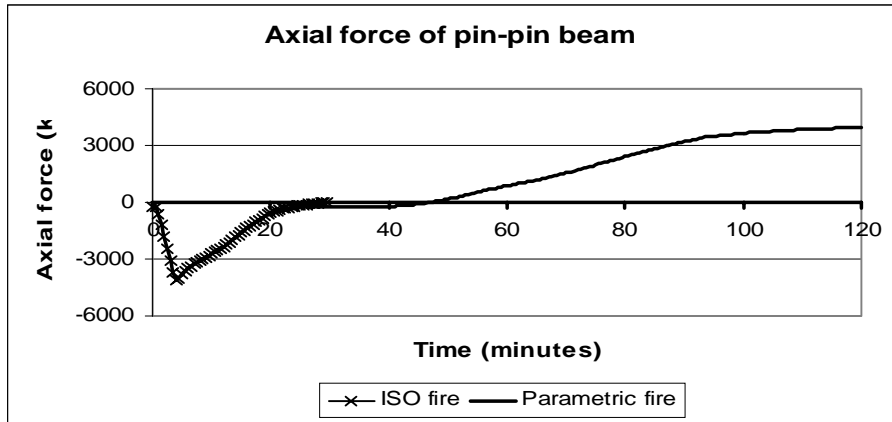


Figure 7.16 Axial force of pin-pin beam subjected to ISO and Parametric fires

### 7.4 Three and four sided heating

Using the exposure to the standard ISO fire, the behaviour of the same beams heated on four sides was compared to those heated on the three sides. Four sided heating provides more uniform temperature across the beam cross section in contrast with the three sided heating where there is thermal gradient across the cross section causing thermal bowing as the top flange will be relatively cooler than the rest of the section.

In real construction, a concrete slab is commonly attached to the steel beam, either simply supported or composite. Composite steel beam and concrete slab is one example of extreme three sided heating as concrete has very high heat sink, which keeps the top flange of the steel beam relatively cool and thus generates a high thermal gradient in the steel beam (Welsh, 2001).

In Figure 7.17, the midspan deflections of the beams with four different types of support condition were plotted, showing the comparison between the three and four sided heating. The patterns of the deflection evolution are very similar for the three and four sided heating for each case. The beams with pin-pin and fix-fix supports show a very similar trend in both cases. On the other hand, the pin-roller and fix-slide beams show earlier failure for the four sided heating.

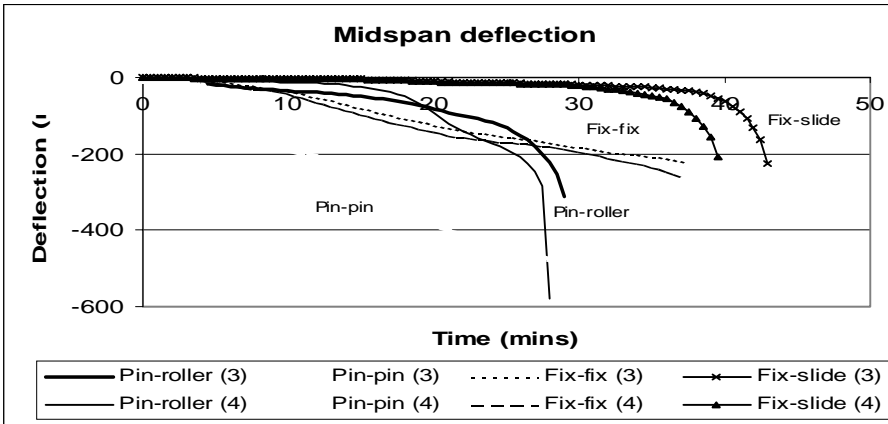


Figure 7.17 Midspan deflection of all beams exposed to ISO fire on 3 and 4 sides

For the beam with pin-roller supports, four sided heating caused less deflection at the start due to uniform heating and no thermal bowing, but at a later stage it caused larger deflections and earlier failure due to higher average temperature in the section. There is no certain explanation on the fact that this beam had much larger deflection at failure compared with the three sided case, most likely it was merely a computational effect.

For the pin-pin and fix-fix beams, there were only slight differences for three and four sided exposure due to the presence of axial restraint. There is no thermal bowing in the four sided case because of more uniform temperature along the cross section.

The bending moment of the pin-roller beam stayed constant regardless of the number of the fire exposed sides. The bending moment of the pin-pin beams are shown in Figure 7.18. Prior to yielding of the midspan, the trend of the bending moment was the same for both cases. Thereafter the four sided moment decreased more rapidly due to rapid reduction in the axial force illustrated in Figure 7.21. Higher average temperature in the cross section caused the section to lose its strength and stiffness faster.

In the fix-fix case, the four sided beam had much more uniform moment throughout the exposure as shown in figure 7.19. Given roughly the same amount of axial compression (Figure 7.22), the absence of thermal bowing effect led to the same elongation rate between the top and bottom flanges. The three sided one, on the other hand, experienced a series of moment alterations mainly due to the thermal gradient inducing high stresses. The moment changed rapidly upon yielding of the flanges as fix-fix beam was very sensitive to the stresses reaching the proportional limit.

From the deflection point of view, both the fix-slide beams behaved almost the same way, only the four sided beam failed sooner at about the same amount of deflection. The bending moment of the fix-slide beams shown in Figure 7.20 were very interesting to compare. The three sided beam developed large hogging moment due to thermal bowing as discussed in

section 5.5 that disappeared when the temperature in the beam was roughly uniform. The four sided beam had constant moment due to the absence of thermal bowing effect. The moment altered slightly towards failure to obtain moment balance between the midspan and the ends of the span of  $wL^2 / 16$ , which was the value reached by the three sided beam at failure.

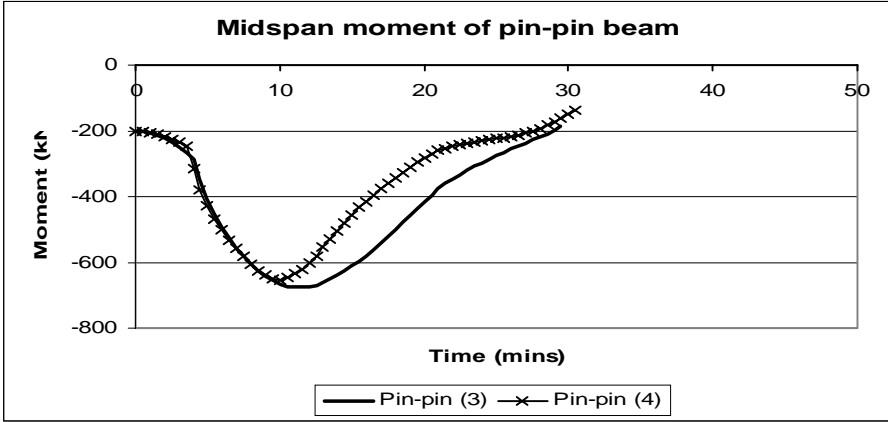


Figure 7.18 Midspan moment of pin-pin beam heated on 3 and 4 sides

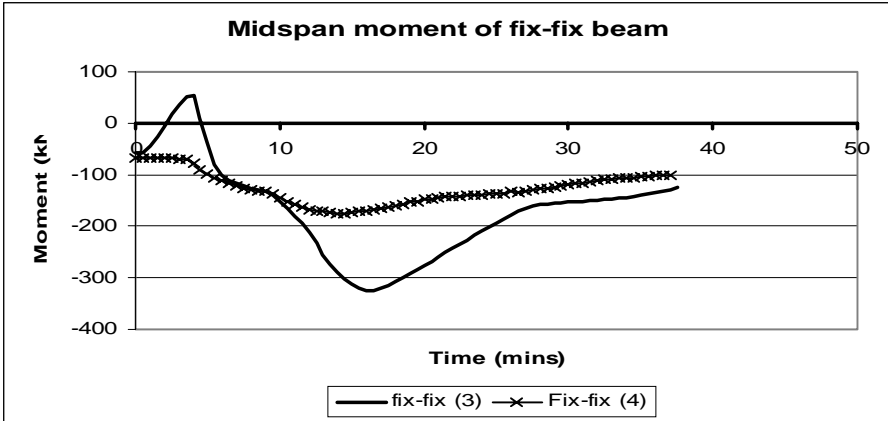


Figure 7.19 Midspan moment of fix-fix beam heated on 3 and 4 sides

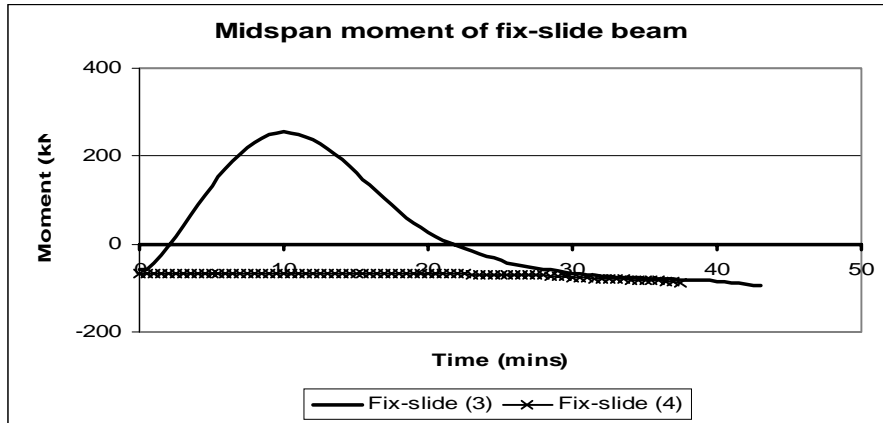


Figure 7.20 Midspan moment of fix-slide beam heated on 3 and 4 sides

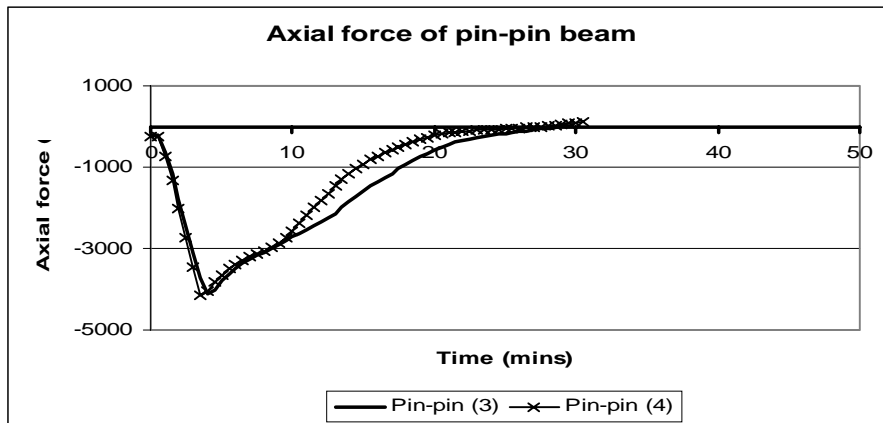


Figure 7.21 Axial force of pin-pin beams heated on 3 and 4 sides

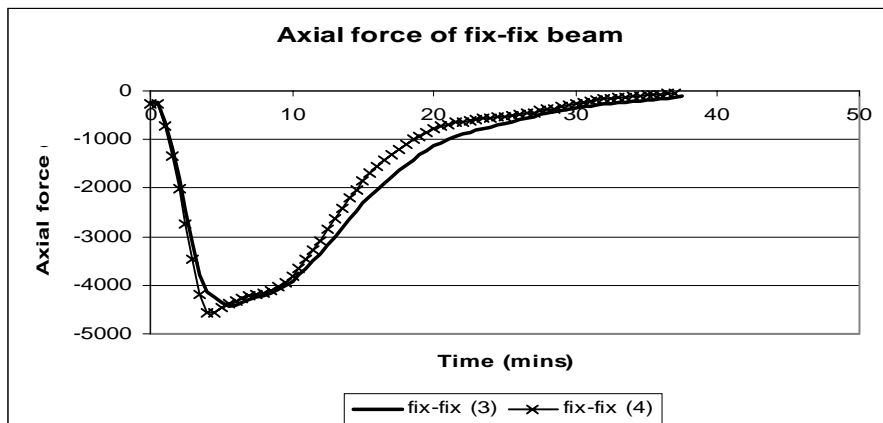


Figure 7.22 Axial force of fix-fix beams heated on 3 and 4 sides

## **8. Comparison of different applied loads**

The loading used as the base case for all the analyses above is the uniformly distributed load of 25 kN/m. In this chapter, the behaviour of the same beams with uniform loads of 12.5 and 50 kN/m are compared with that of the base case. The load ratios at cold condition are 0.08, 0.16 and 0.32 for 12.5, 25 and 50 kN/m applied loading respectively with the detailed calculation shown in the appendix. These ratios are low and the beams are expected to have high fire resistance capacity.

SAFIR analyses showed that when the load was halved or doubled, the trends of the deflections, moments, and the axial forces stayed the same as expected. The beam with the heavier load had greater deflections, especially towards failure, greater bending moments, both positive and negative, and greater axial load. It failed earlier as opposed to the one with the lighter load that failed later.

The case of the fix-fix beam are shown below in Figures 8.1 – 8.4 for comparison. The other beams with different support conditions had very similar behaviour, with the trends illustrated and discussed in chapter 5.

Greater deflection and bending moments on the beam with heavier loading were expected and very much self-explanatory. The axial force was induced in the beam due to thermal expansion as the beam was restrained, and therefore had nothing to do with the amount of loading on the beam. This applied up to the point where the first plastic hinge started to form, and from here on, the beam with heavier load would lose its stiffness faster and consequently had more rapid reduction in the axial force.

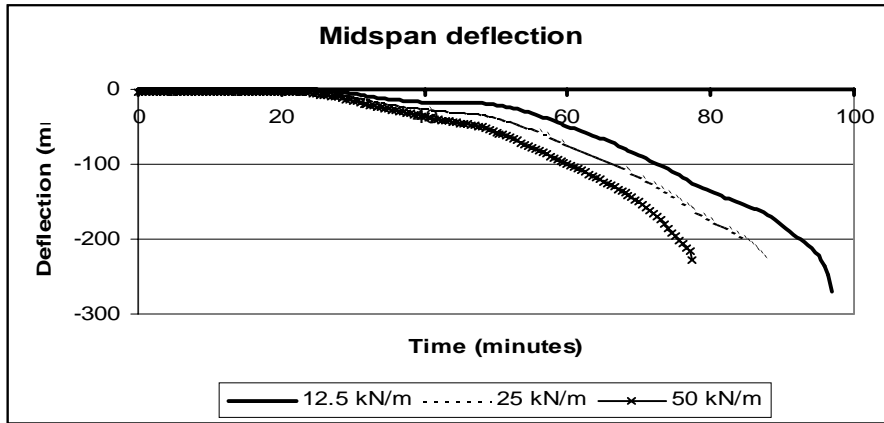


Figure 8.1 Midspan deflection of fix-fix beam under different loading

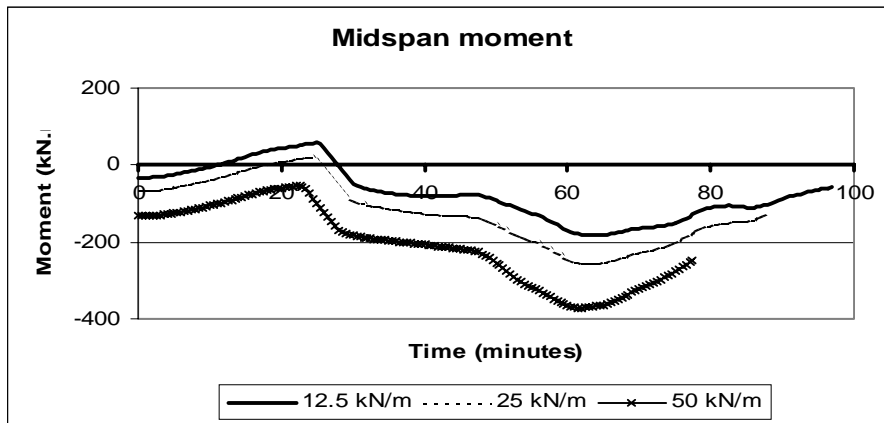


Figure 8.2 Midspan moment of fix-fix beam under different loading

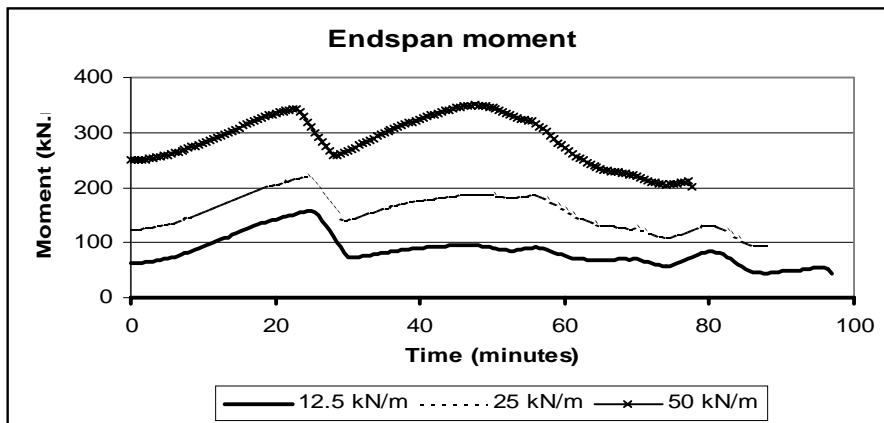


Figure 8.3 Endspan moment of fix-fix beam under different loading

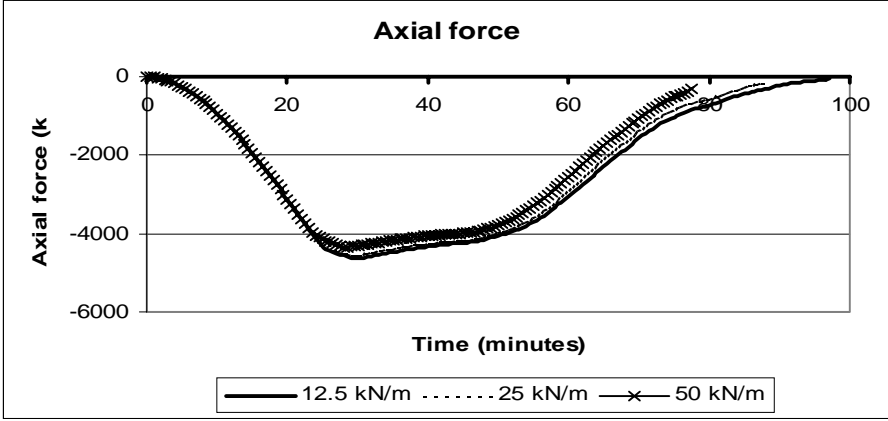


Figure 8.4 Axial load of fix-fix beam under different loading

## 9. Comparison of various line of thrust locations

All the above analyses discussed in chapter 5–8 considered that the steel beams were supported at the mid height of the section. However, different elements may have different location of supports, depending on how they are supported as described by Buchanan (2000) and illustrated in Figure 9.1.

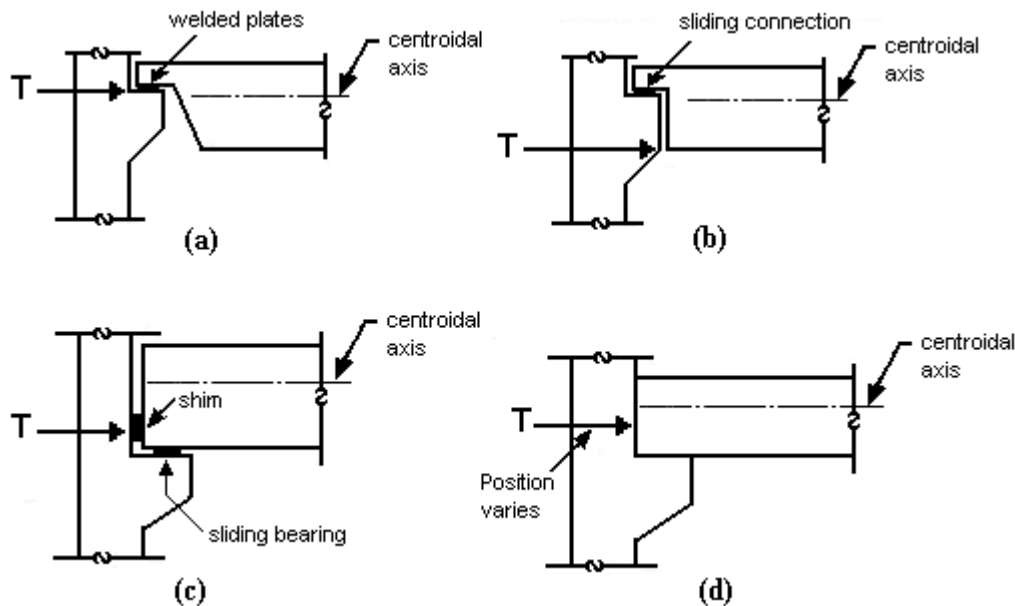


Figure 9.1 Lines of thrust for several support conditions (Buchanan, 2000)

The SAFIR pre-processor assumes the line of thrust to be at the mid height of the section by default. In this chapter the effect of the variation in the line of support is investigated. The same beams with four different end conditions subjected to linear heating of  $10^{\circ}\text{C}/\text{minute}$  were supported at a quarter up and a quarter down from the mid depth of the section. Typical results are illustrated in Figures 9.2 – 9.4, and the results were compared with the base case.

The analyses showed that the beams with pin-roller and fix-slide support conditions had exactly the same behaviour regardless of where they were supported because there was no axial force induced in the beams. Some variations were found in the pin-pin and fix-fix supported beams.

When the supports of a beam are fully fixed and the beam is loaded, there are several actions interacting within the beam. There is bending moment due to the applied loading to start with, and thermal expansion causes additional moment due to P- $\Delta$  effect. Fix-fix supports allow the beam to re-adjust its line of thrust to balance the internal forces. Fixing a certain line of thrust in fact only adds the complication in the internal actions and the behaviour of the beam becomes very difficult to analyse.

The effect of the line of thrust location on a fix-fix beam needs to be investigated further considering different components of the bending moment. This involves a broad range of analyses and could not be included in this project mainly due to the time constraint.

The deflection pattern, bending moment and axial force comparisons for the pin-pin beam are shown in Figures 9.2 – 9.4. The bottom curve in each graph shows the base case where the line of thrust was at the neutral axis of the section as discussed in section 5.3.

When the beam was supported at a quarter up the mid height of the section, some of the moment due to bending and axial compression cancelled each other out resulting in the deflection, bending moment and axial force being not as large as those of the base case. The axial force, as shown in Figure 9.4, started in tension due to the bending induced by the load. This beam had more deformation only at the earlier time into the fire as a result of less restraint at the bottom flange when subjected to thermal elongation.

Supported at a quarter down the mid height of the section, the beam showed different behaviour from the earlier cases. The thermal elongation caused the shift in bending moment to a hogging moment due to the P- $\Delta$  effect, because the line of thrust was below the neutral axis. The P- $\Delta$  effect governed the moment as soon as the deflection increased.

The thermal elongation and the axial restraint caused very large axial compression at the bottom flange. The stress of the bottom flange reached the proportional limit earlier and

lessened the axial force. The hogging moment, however, kept increasing and the beam was hogging up.

Upon yielding at the midspan, the axial force dropped even more causing the sagging moment to increase and the deflection recovered. The early loss of strength caused the beam to fail earlier in compared with the beam supported at the mid height or a quarter up the mid height of the cross section.

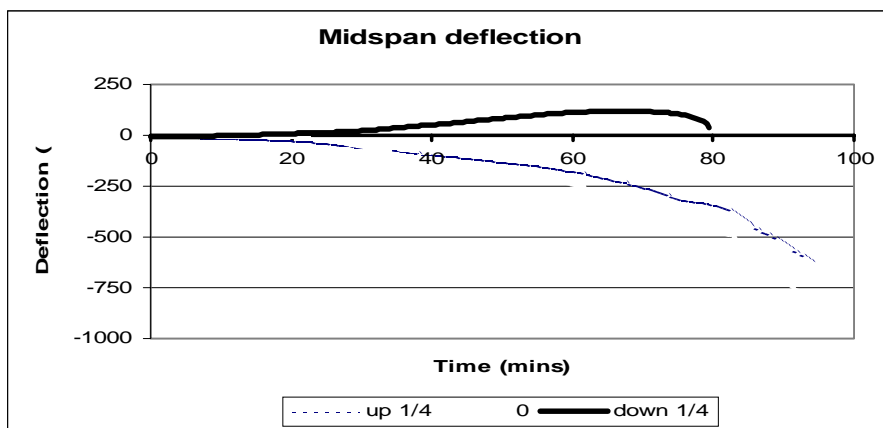


Figure 9.2 Midspan deflection of pin-pin beam with different lines of thrust

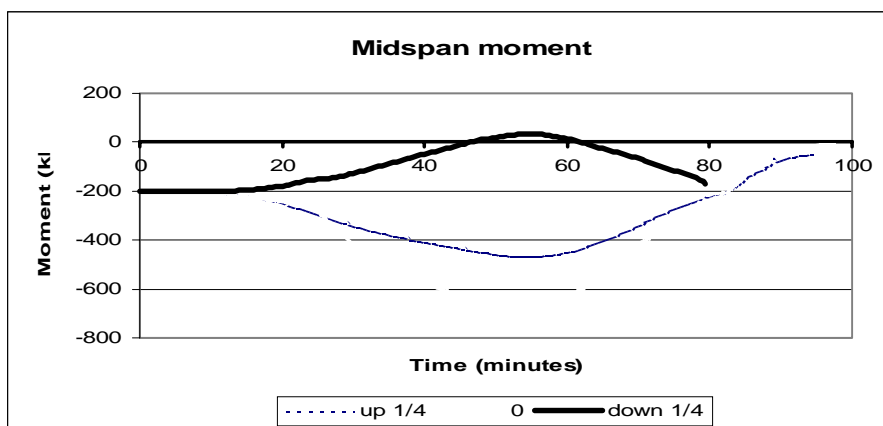


Figure 9.3 Midspan moment of pin-pin beam with different lines of thrust

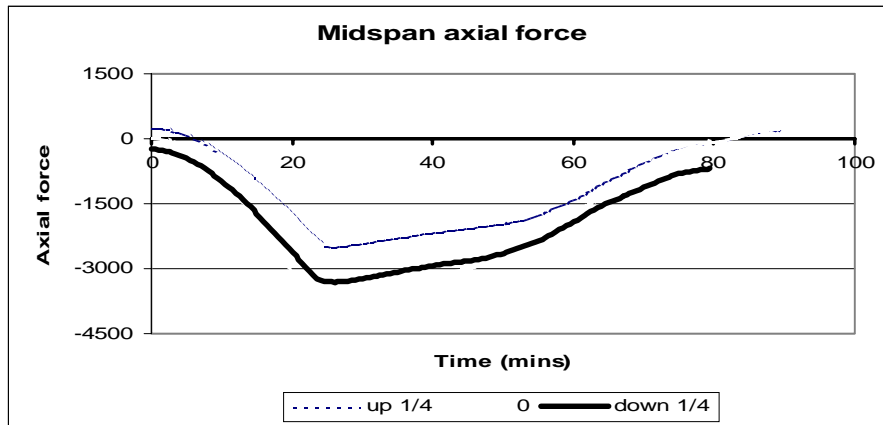


Figure 9.4 Axial force of pin-pin beam with different lines of thrust

Figures 9.5 and 9.6 show the stresses at the top and bottom flanges respectively for the above case. The bottom flange reached the proportional limit at 25 minutes and it never actually reached yield, but decreased parallel to the yield envelope. The top flange did not reach the proportional limit until 75 minutes and it nearly yielded when the analysis was terminated at 80 minutes, which was most likely due to some numerical instability in the program.

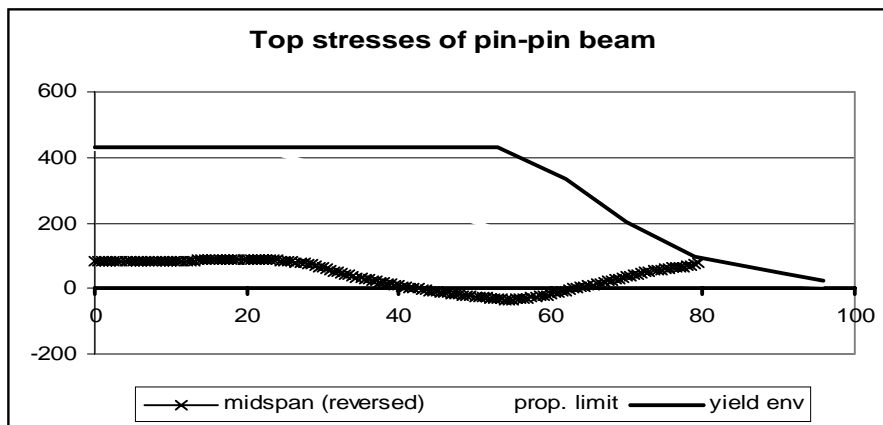


Figure 9.5 Top flange stresses of pin-pin beam supported  $\frac{1}{4}$  down from mid height

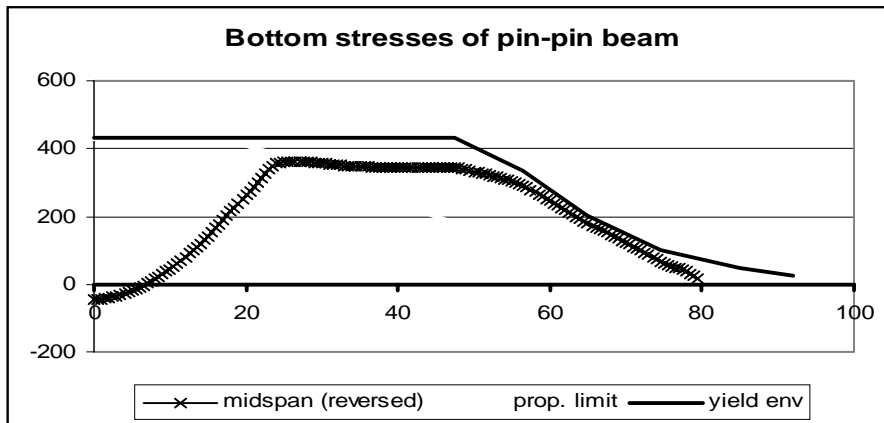


Figure 9.6 Bottom flange stresses of pin-pin beam supported  $\frac{1}{4}$  down from mid height

## 10. Problems

A few problems were encountered during the analyses using the SAFIR program:

1. The recorded output such as moments, axial forces, or stresses are on the integration points, which in case of coarser discretisation may not give the exact properties at a particular point of interest.
2. Diamond 2000 is unable to display the fibre stresses from the \*.OUT file, therefore Microsoft Excel spreadsheet was used to extract the required information.
3. Discontinuity was found in the spring model with stiffness of 20% of the beam stiffness that may be due to some numerical error in the stiffness matrix in the program. This requires further investigations in future research.
4. Premature terminations were encountered in some of the analyses that may be caused by some instability in the stiffness matrix.
5. The effect of the line of support locations, especially for the fix-fix beam, could not be thoroughly explained due to the complex behaviour and further analyses are needed to verify the detailed behaviour.
6. Some results showed great complications as so many actions were interacting and the trend behaviour of the beam became rather difficult to accurately analyse.

## 11. Conclusions and recommendations

The behaviour of a steel beam at elevated temperatures was found to be complex and very difficult to analyse accurately. Using the finite element program SAFIR, an unprotected steel beam was exposed to simulated fire conditions, with a number of parameters being varied:

- ♣ Pin-roller, pin-pin, fix-fix and fix-slide support conditions.
- ♣ A spring introduced at the roller end of the pin-roller beam to model an intermediate case between pin-roller and pin-pin beams.
- ♣ Various applied fires including linear heating rates of 10, 20 and 30°C / minute, the standard ISO fire and a parametric fire which is the ISO fire with a decay phase.
- ♣ Three and four sided heating.
- ♣ Applied loading of 12.5, 25 and 50 kN/m.
- ♣ Different locations of line of thrust, at mid height, at a quarter up and down the mid height.

### 11.1 General behaviour

The beam supported by pin-roller has no axial restraint, and therefore is not effected by the P- $\Delta$  action. The behaviour of this beam is predictable and runaway failure occurs when one plastic hinge is formed at the midspan. Pin-roller beam fails the earliest compared with the other supports.

The fix-slide beam also has no axial restraint and hence has no P- $\Delta$  effect. However, it has more complex behaviour because of the progressive formation of plastic hinges. The behaviour is sensitive to the reduction in proportional limit stress and yield stress of steel at elevated temperatures.

The pin-pin and fix-fix beams are axially restrained and axial force is induced along the beams due to thermal expansion. There is a complex interaction between the axial force, deflection and bending moment, all of which change during fire exposure. This behaviour could not be

predicted without a program like SAFIR. The times at which flange stresses reach the proportional limit have a significant effect on the sequence of these events during the fire. In fire conditions, the pin-pin beam shows very ductile behaviour and survives the longest in comparison with the other types of support. However, the pin-pin beam undergoes very large deformations which may be unacceptable.

## **11.2 Effect of spring**

When a spring is introduced, the beam becomes an intermediate case between the pin-roller and pin-pin beams. The behaviour of a beam with relative spring stiffness of 20% or less is somewhere in between that of the pin-roller and pin-pin beams.

Analysis of beam with axial spring restraint was difficult for two reasons, the SAFIR program was consistently terminated after 40 minutes, and the behaviour of very soft springs was similar to the pin-roller condition, while the behaviour of stiffer springs was similar to the pin-pin condition. There was a very sudden transition between the two behaviours at  $k=0.195$ . Further investigation is required to explain such discontinuity and other significant effect of the additional spring.

## **11.3 Effect of different applied fires**

When a steel beam is exposed to a hotter fire, it behaves in a similar way but fails earlier, as expected. Faster heating on three sided exposure also causes a higher thermal gradient across the section and the resulting thermal bowing produces a very high compressive force especially on the bottom flange.

If the fire decays before the beam fails, the deformation and the steel strength will recover. Permanent deformation occurs when part of the beam has been strained beyond its elastic limit. The cooling phase causes shortening in the beam, which can be dangerous in the pin-pin and fix-fix cases as it may cause tensile rupture of the end connections. It is recommended that

the design of steel connections for fire condition, especially those providing axial restraint, be sufficiently ductile to resist this large tension force.

#### **11.4 Effect of different applied loads**

At ambient conditions, there is no obvious physical difference when the load on the beam is changed except larger deflections. The bending moment is proportional to the load, and the load does not affect the thermal elongation of the beam. A beam with high loads tends to fail faster than with light loads due to higher stresses, as expected.

#### **11.5 Effect of the line of thrust location**

The change in the line of thrust location only affect beams with axial restraint, where  $P-\Delta$  effects are induced in the beam. For the pin-pin beam, an increase in support height causes less deflection, moment and axial force in the beam as the effect of the thermal elongation is cancelled out by the bending stresses. A lower support height causes increased axial compression stress in the bottom flange, as the effect of thermal expansion is enhanced by the stresses due to the loading. This beam fails earlier because of the very high stresses in the bottom flange.

## **12. Recommendations for future research**

It is recommended that the following aspects be taken into account in the future research:

1. The analyses of multi-span beams and frame structures.
2. Three dimensional analysis of the beams.
3. Various location of fire within the structure allowing investigation of neighbouring cooler elements.
4. More realistic fires taking account of different fuel loads and ventilation.
5. Intermediate cases between pin-pin and fix-fix support conditions by introducing some rotational springs.
6. Further investigation on the variation of the line of thrust locations, including the possibility of self-adjustment due to the elevated temperature, to explain the problems encountered in this project.
7. Comparisons with analyses of composite structures, observing the enhanced behaviour due to the composite actions.
8. Comparisons between the computer analysis and laboratory test results to validate the computer modelling.
9. Investigation of the validity of the current steel design based on the analysis results.

## 13. References

- BHP Co. Pty Ltd. *Hot Rolled and Structural Steel Products*. 98 ed. Australia.
- British Steel Plc. (1999) *The Behaviour of Multi-storey Steel Framed Buildings in Fire*. Swinden Technology Centre, South Yorkshire, United Kingdom.
- Buchanan, A.H.(2000) *Structural Design for Fire Safety*. School of Engineering, University of Canterbury, Christchurch, New Zealand.
- Buchanan, A.H.(Ed) (1994). *Fire Engineering Design Guide*. Centre for Advanced Engineering, University of Canterbury, Christchurch, New Zealand.
- Building Industry Authority (1992). *New Zealand Building Code Handbook and Approved Documents*. Building Industry Authority, Wellington, New Zealand.
- Clifton, C. (1999) Key Aspects of the Behaviour of a Multi-storey Steel Framed Building Subject to Fully Developed Natural Fires. *HERA Steel Design and Construction Bulletin*, No. 48, 3-13 pp.
- EC1 (1994). Eurocode 1: *Basis of Design and Design Actions on Structures*. ENV 1991-2-2 Part 2-2: *Actions on Structures Exposed to Fire*. European Committee for Standardization, Brussels.
- EC3 (1995). Eurocode 3: *Design of steel structures*. ENV 1993 Part 1-2: *General rules – structural fire design*. European Committee for Standardization, Brussels.
- Franssen, J.M. (2000) SAFIR Seminar Notes. University of Canterbury, Christchurch, New Zealand.

- Franssen, J.M., Kodur, V.K.R., Mason, J. (2000) User Manual for SAFIR98: A Computer Program for Analysis of Structures Submitted to the Fire. University of Liege, Belgium.
- Gorenc, B., Tinyou, R., Syam, A. (1996) *The Steel Designer's Handbook*. Sixth edition. UNSW Press, Kensington, New South Wales.
- Harmathy, T.Z. (1993) *Fire Safety Design and Concrete*. Concrete Design and Construction Series. Longman Scientific and Technical, United Kingdom.
- ISE (1978) *Design and Detailing of Concrete Structures for Fire Resistance*. The Institution of Structural Engineers, London.
- Kirby, B.R., Preston, R.R. (1988) High Temperature Properties of Hot-Rolled Structural Steels for Use in Fire Engineering Design Studies. *Fire Safety Journal*, Vol 13, 27-37 pp.
- Kodur, V.K.R., Nwosu, D.I., Sultan, M.A., Franssen, J.M. (1999) Application of the SAFIR Computer Program for Evaluating Fire Resistance. *Proc. Third International Conference on Fire Research Engineering (Chicago, USA)*. October 4-8. 287-298 pp.
- Mason, J.E. (2000) *Heat Transfer Programs for the Design of Structures Exposed to Fire*. Fire Engineering Research Report No. 00/9. School of Engineering, University of Canterbury, Christchurch, New Zealand.
- Nwosu, D.I., Kodur, V.K.R., Franssen, J.M., Hum, J.K. (1999) *User Manual for SAFIR: A Computer Program for Analysis of Structures at Elevated Temperature Conditions*. Internal Report 782. Institute for Research in Construction, National Research Council of Canada.

Rotter, J.M., Sanad, A.M., Usmani, A.S., Gillie, M. (1999). Structural Performance of Redundant Structures under Local Fires. *Interflam '99, Proceedings of the Eighth International Conference (Scotland, 29th June-1st July 1999)*, p.1069-1080.

Rotter, J.M., Usmani, A.S.(2000). Fundamental Principles of Structural Behaviour Under Thermal Effects. *First International Workshop on Structures in Fire (Copenhagen – June)* (as Report TM2).

Sanad, A.M., Rotter, J.M., Usmani, A.S., O'Connor, M.A. (1999) Finite Element Modelling of Fire Tests on the Cardington Composite Building. *Interflam '99, Proceedings of the Eighth International Conference*, p.1045-1056.

Welsh, R.D. (2001) *2-D Analysis of Composite Steel-Concrete Beams in Fire*. Fire Engineering Research Report. School of Engineering, University of Canterbury, Christchurch, New Zealand.

## Appendix

### Load ratio calculations

Uniformly distributed load, $w$	12.5 kN/m	25 kN/m	50 kN/m
Span length, $L$	8 m	8 m	8 m
Applied moment $M^* = w L^2 / 8$	100 kN.m	200 kN.m	400 kN.m
Moment capacity $M_n = S.f_y$	1247 kN.m	1247 kN.m	1247 kN.m
Load ratio $R = M^* / M_n$	0.08	0.16	0.32

## A typical \*.DAT input file for the thermal analysis

Profile type: User

Fire curve: FISO; Values of faces exposed:1 1 1 0

Protected with: 0 mm; 0 mm; 0 mm;

```

      NPTTOT      412
      NNODE      280
      NDIM       2
NDIMMATER      1
      NDDLMAX     1
      FROM      1   TO 280 STEP   1 NDDL   1

TEMPERAT
      TETA       0.9
      TINITIAL   20.0
      MAKE.TEM
LARGEUR11      40000
LARGEUR12      100
      NORENUM
FISO.str
FISO.tem
      PRECISION  1.E-3
      TIME
                10.    7200.

      ENDTIME
IMPRESSION
      TIMEPRINT  30.
```

## A typical \*.DAT file for the structural analysis

Profile type: 610UB101

Fire curve: 10deg.fct; Values of faces exposed:1 1 1 0

Protected with: 0 mm; 0 mm; 0 mm;

```

      NPTTOT      8240
      NNODE      41
      NDIM       2
NDIMMATER      1
      NDDLMAX     3
      FROM       1   TO   41 STEP   2 NDDL   3
      FROM       2   TO   40 STEP   2 NDDL   1

      STATIC
      NLOAD      1
      OBLIQUE    0
      COMEBACK   1.
NARCLENGTH     .02
      LARGEUR11  426
      LARGEUR12  10
      NORENUM
pinpin10.str
      PRECISION  1.E-3
      LOADS
      FUNCTION    F1
      DISTRBEAM   1      .      -25E3
      DISTRBEAM  20      .      -25E3   1

      TIME
           5.      3600.
          10.      7200.

      ENDTIME
LARGEDISPL
      EPSTH
IMPRESSION
      TIMEPRINT  30.
      PRINTMN
PRINTREACT
```

## A typical \*.STR file for the structural analysis

Profile type: 610UB101

```

      NMAT      1
ELEMENTS
      BEAM     20      1
      NG       2
      NFIBER   206

      NODES
      NODE      1      0.00000      0.00000
      NODE     41      8.00000      0.00000      1
FIXATIONS
      BLOCK      1              F0          F0
      BLOCK     41              F0          F0

      NODOFBEAM
10.tem
      TRANSLATE      1      1

      1      1      2      3      1
      20     39     40     41     1     2
MATERIALS
      STEELEC3
      210.E+9          .3      430.E+6
```